Welding Research

SPONSORED BY THE WELDING RESEARCH COUNCIL
OF THE ENGINEERING FOUNDATION

W. SPRARAGEN, DIRECTOR

SUPPLEMENT TO THE WELDING JOURNAL, FEBRUARY, 1956

THE BEHAVIOR OF SPOT WELDS UNDER STRESS

Relationship shown to exist between these four spot-welding parameters: failure system, weld strength, macro-geometry of cross section, and sectioned spot shear test observations

BY JOHN F. RUDY, ROY B. McCAULEY AND ROBERT S. GREEN

ABSTRACT. The purpose of this paper is to give evidence of the existence of a relationship between four spot-welding parameters. To accomplish this, spot weld joints were made in 11 gage Armco Iron. These four parameters are as follows:

1. The physical strength of the spot weld in tension shear (coupon is in tension —weld in shear).
2. The mechanism of weld failure when pulled in tension shear. Terms in the literature that are used to describe these failure mechanisms are shear, button, tear, etc. Only the three failure mechanisms which the authors have called shear, intermediate and tear were observed in this investigation.
3. The macro-geometry of the weld cross section, e.g., the size and shape of the cast nugget and of electrode indentation, the bond area in the faying plane that is not part of the nugget, etc.
4. "Sectioned Spot Shear Test" observations. These are observations of the exposed cross section of a spot weld as load is applied to the section in tension shear. Half of the spot cross section was exposed by longitudinally splitting the tension shear coupon. This allows the strain reaction to the application of loading to be traced through the section. The observation technique is explained in the paper.

The four-parameter relationship is established by showing individual correlations between several parameter pairs such that a general interdependence is shown to exist. The parameter pairs that were related for the purposes of this investigation are as follows:

1. The spot-weld mechanism of failure (Parameter No. 2) is shown to be related to strain reactions observed in the sectioned spot shear test (Parameter No. 4). That is to say, the occurrence of the various failure systems in whole welds can be explained in terms of the movement of plastic strain as it is traced in similar sectioned half welds. This validates the sectioned spot shear test as a useful tool for understanding the behavior of the spot weld joint under stress.
2. The failure system of a spot weld when loaded in tension shear (No. 2) is shown to be determined by the macro-geometry of the cross section (No. 3). This is established by noting that the system of failure changes when the cast nugget development reaches certain stages. A similarity was seen in this respect for all three welding runs studied. Also this relationship is explainable in terms of observations of the sectioned spot shear test.
3. Lastly, the physical strength of a spot weld (No. 1) is shown to be related to the weld failure system (No. 2) by observing the similarities of the dependence of each on welding heat for each of the three welding runs used.

John F. Rudy is USAF, Project Officer, Wright Air Development Center, Wright Patterson Air Force Base, Dayton, Ohio; **Roy B. McCauley** is Chairman, Department of Welding Engineering and **Robert S. Green,** Executive Director, Engineering Experiment Station, Ohio State University, Columbus, Ohio.

Presented at AWS 1955 National Fall Meeting held in Philadelphia, Pa., Oct. 17-21.

Introduction

Spot welding specifications of quality are probably expressed more often in terms of tension shear strength than all other parameters combined. The purpose of this paper is to indicate a relationship between weld strength and three other parameters: the system of failure, the macro-geometry of weld cross section, and the observations of a cut away weld cross section under stress. The establishment of these correlations will increase the value of each as a measure of spot weld quality. The mechanism of failure in tension shear (button or shear) has already found limited reference in the literature. Statements of desired cross section macro-geometry are even more common. In many specifications, the geometry of the cast nugget is controlled for acceptability. However, the fourth parameter which is introduced into this study is a new one. The observations of cut away cross sections under stress are shown to be valuable primarily as a tool for explaining other relationships and dependencies. These observations were accomplished by means of a "Sectioned Spot Shear Test" which was devised by the authors for the purposes of this investigation.

Experimental Procedure

Welding

In a sense, this investigation is a study of the change in weld properties which occur with a change in weld cross section geometry. Therefore, welding machine settings were chosen to produce a variety of weld cross-section shapes.

Table 1 Welding Variables

WELDING RUN	ELECTRODE FORCE (POUNDS)	PERCENT HEAT	WELDING CURRENT (CYCLES)	SQUEEZE TIME (CYCLES)	HOLD TIME (CYCLES)	ELECTRODE GEOMETRY
A	4000	100	16 - 60	80	60	5/8"
B	4000	100	8 - 48	80	60	5/16" 5/8"
C	1300	100	6 - 50	80	60	20°

It was found that the most effective method of obtaining a gradual continuous change in geometry was to vary the number of weld cycles from no weld to excessive heat. Table 1 presents the machine settings, pressures and electrode shapes used to produce the welds. Three welding runs were used. Each welding run consisted of a group of joints in which all machine variables were held constant except for the duration of current flow. The time in cycles was varied in small increments from a minimum which gave no weld to a maximum limited either by excessive indentation or electrode melting. Either electrode shape or welding force was changed from run to run as shown in Table 1.

The welding was accomplished on a 2-phase, 60-cycle, 150-kva, RWMA No. 2 spot welder. Current durations greater than the 30 cycle single pulse maximum were obtained in two pulses separated by one cycle of cool time. Just prior to welding, the inside (faying) and outside surfaces of the specimen were cleaned with a wire brush followed by fine emery cloth. Four to six tension shear coupons (single spot) and two specimens for metallographic examination were prepared at each machine setting combination at the same time. Care was taken to keep the electrode tips dressed and uniform for all similar weld sets.

Sectioned Spot Shear Test

When employing the "Sectioned Spot Shear Test" technique, a spot weld is sectioned, polished and etched. The grain structure thus exposed is observed as the weld is loaded in tension shear. In this manner microscopic evidences of plastic strain can be traced from grain to grain as the joint is subjected to increasing levels of stress. A sketch of this specimen is shown in Fig. 1. The sequence of fabrication of the specimen was as follows. Sheets 2 by 4 by 11 gage (0.125 in.) were spot welded in two places as shown. The first spot is the test weld and is identical to the group of whole welds with which it is to be compared. A center section of this test weld was then exposed by a saw cut running the entire 6-in. length of the coupon. This exposed section was then polished and etched to reveal the weld microstructure.

The purpose of the second weld was to balance the eccentricity of tensile machine loading and thus limit the stresses in the test weld to those which are due to tension shear. This second weld is weakened by a saw cut as shown so that both half welds will be of the same order of strength. However, if the test weld is to be observed at stresses up to weld failure, it must fracture before the second weld since the tension shear system of loading is destroyed as soon as either spot fails.

After the specimen was prepared, polished and etched, the cross section was observed at no load and three fine vertical lines were scribed on the polished surface. These scribed lines serve to trace subsequent deformation and to locate the cross section areas which are being observed. The specimen is then loaded to a low stress level, removed from the tensile machine, examined under a microscope, reloaded to a higher stress level, re-observed, etc. until failure occurs. Photographs of cross sections at various load levels are pictured in later figures.

Physical Testing

The physical testing which was performed as part of this program gave, first, the ultimate strength of each weld set in tension shear and, second, the characteristic system of failure for each weld. Attempts to obtain a measure of joint ductility with the "cross-tension test" were abandoned because of the insensitivity of the material to the circumferential notch. Results of this test were merely a measure of spot diameter in most cases.

The ultimate strength of each weld group was taken as the average of four to six coupons pulled to failure in the tension shear test. The coupons used are shown in Fig. 2 and are the RWMA recommended standard for 11-gage material. A hydraulic tensile testing machine was used with a loading speed of 0.2 ipm. No yield point was observed.

The characteristic system of failure was recorded for each test. These systems are shear, intermediate and tear as shown in Figs. 4, 9 and 14. Although all failures fit into one of these three categories, there were variations within each group as is to be expected. These differences are described below.

Macro Cross-Section Geometry Measurements

One of the four parameters being

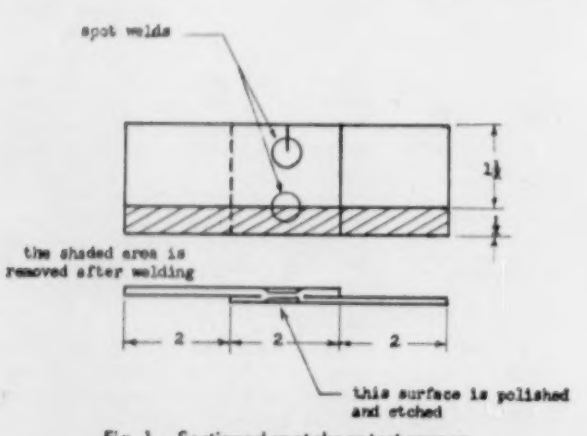

Fig. 1 Sectioned spot shear test coupon

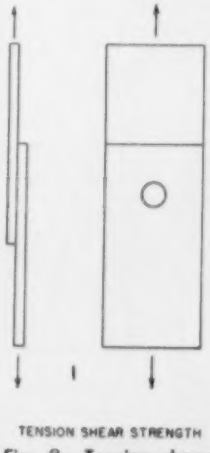

Fig. 2 Tension shear coupon

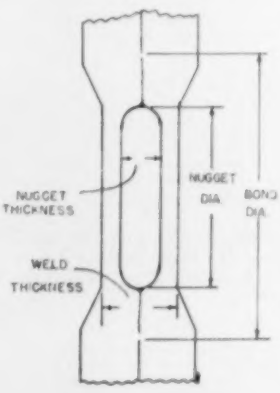

Fig. 3 Macro-geometry of cross section

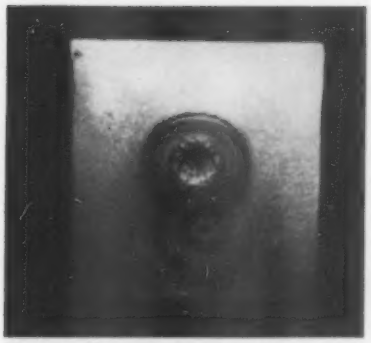

Fig. 4 Photograph of a shear fracture in the tension shear test. Center area shows deformation while surrounding area does not

studied is the geometry of the weld cross section. The sizes and shapes of zones in each cross-section weld set were determined. The actual measurements recorded were: weld bond diameter, cast nugget diameter, cast nugget height, and weld thickness as shown in Fig. 3.

A single joint from each weld setting was sectioned, polished, etched and observed microscopically. The dimensions were then determined with a micrometer eyepiece mounted on a metallograph. It is felt that the use of measurements taken from a single sample for each weld setting combination is justified because of the relatively small increment of welding heat between adjacent sets within each welding run. Each section geometry as it was measured, was compared with its nearest neighbors in the welding run. In instances where the shapes and sizes seemed out of line with adjacent welds, the dimensions were checked by preparing a second specimen that had been welded at the same time. The accuracy of these measurements is dependent primarily on the ability of the technician to expose a section of the weld which is a diametrical plane. The results of these measurements are recorded graphically in Figs. 21, 22 and 23.

Discussion of Results

Sectioned Spot Test Observations

The discussion of sectioned spot shear test observations is divided into three parts according to the three characteristic systems of failure in the tension shear test. These systems are:

1. Shear failure (Fig. 4) in which the fracture plane is the faying plane.
2. Intermediate failure (Fig. 9) in which the fracture occurs partly along the faying plane and then veers off to pull a button.
3. Tear failure (Fig. 14) in which the fracture occurs perpendicular to the faying plane in an area removed from the nugget itself.

Since both intermediate and tear failures may sometimes be classed as button failures, the latter term has been avoided.

In each of the failure mechanisms previously mentioned, it can be seen that the fracture patterns of whole welds can be explained by the strain evidences observed in exposed half sections of similar welds as both coupons are loaded in tension shear.

Shear System of Failure

A typical shear type failure of a spot weld loaded in tension shear is shown in Fig. 4. The irregular or nonplanar surface in the center of the fracture circle shows that some base metal deformation did occur. This is in contrast to a weaker group of shear failures in which the whole fracture circle was a smooth plane similar to the area surrounding the deformed circle as shown. The weld bond in both of these cases was a solid phase heat and pressure type as shown in Fig. 7. In the first case, however, this solid phase bond is strong enough to withstand the applied load and the path of fracture is in the parent metal. In the weaker case the solid phase bond in the faying plane is not completely formed and fracture occurs along the plane of bonding.

To observe the cross section of a shear failure, a weld that had been failing thus was incorporated as the test weld in the sectioned spot shear test. This weld was then prepared and studied under load as previously described. Figure 5 is a macrograph of this weld section before load was applied. Three vertical lines have been scribed for location purposes for the subsequent photomicrographs. Note that solid phase grain growth across the faying plane is more complete in the center of the weld which reached a higher temperature. The extent of this growth determines the strength of the bond itself. Figure 6 is a macrograph after maximum load but before complete fracture. The displacement of the scribed lines shows that weld failure has occurred in shear slippage along the faying plane.

Figure 7 is a micrograph of the area including the right-hand scribed line at no load. This shows the solid phase bond and surrounding microstructure. Figure 8 is a similar area on the other side of the weld after the application of some load. The plastic slippage has not occurred in the bond or faying plane but is removed slightly into the parent metal. This explains the appearance of nonplanar nature of some of the shear system fractures. Slightly lower heat welds fractured along the bond itself with little or no deformation.

Intermediate System of Failure

One half of a typical intermediate type failure mechanism is pictured in Fig. 9. This fracture shows the metal button pulled from the other plate. This button is surrounded by a plane fracture area similar in appearance to the corresponding area in a shear fracture (Fig. 4). Some of the spot welds which fracture within the intermediate classification exhibit a large planar area in relation to the area of the pulled button. These intermediate type failures are said to resemble shear, while the opposite extremes resemble tear type system of failure.

A weld that was found to fail with an intermediate type fracture was incorporated into the sectioned spot shear test as previously described. Three

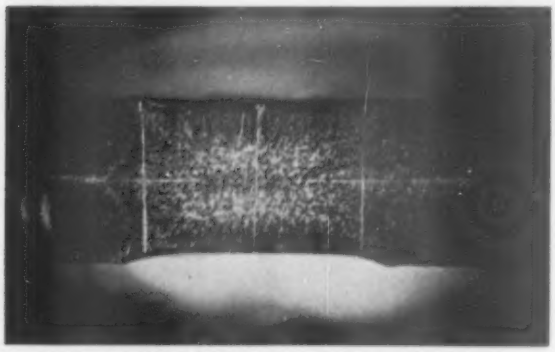

Fig. 5 Unstressed solid phase bond spot weld

Fig. 6 Same weld (Fig. 5) after application of maximum load. Note displacement of three scribed lines

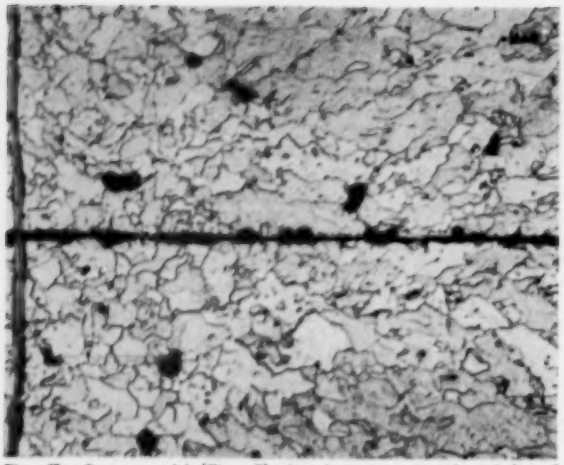

Fig. 7 Same weld (Fig. 5) showing area to the right of right-hand scribed line at no load

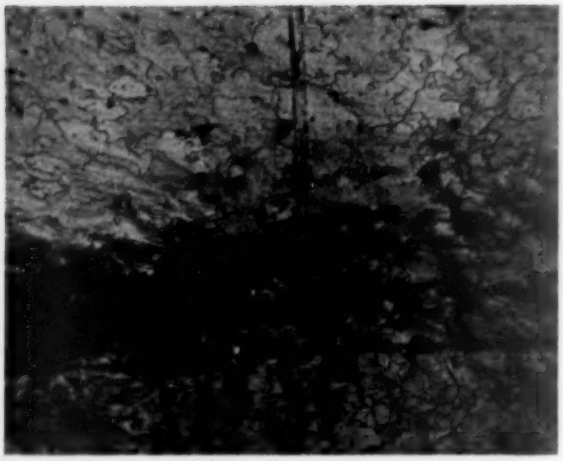

Fig. 8 Same weld (Fig. 5) showing area of left-hand scribed line after application of 3500 lb stress. Note that metal flow has not occurred along the faying plane

vertical lines were scribed as before, the centerline through the cast nugget and the two outside lines through the solid phase bonded areas of the weld.

The four photomicrographs of Figs. 10, 11, 12, and 13 show the area of solid phase bonding at four stress levels. Figure 10 shows this area at no load. The applied stress will be to the right in the upper half of the joint. The next figure (11) shows the same area after a load of 3500 lb had been applied to the sectioned spot specimen. Plastic strain has moved in from the right edge of the weld bond, starting at the notch caused by the weld joint. Figure 12 shows approximately the same area (note scribed line) after the application of 5000 lb stress to the coupon. As strain has moved left from the notch, it has shown no apparent preference for the faying plane over the parent metal. The smaller grained area to the left is the beginning of the cast nugget structure. The last figure of this series (Fig. 13) shows the area just to the left of the scribed line which is visible at the right lower margin. This micrograph shows how the more strain-resistant cast nugget structure impedes the movement of strain. In this area, plastic strain can no longer occur near the faying plane as would be expected from the shear system of weld loading. Therefore slippage occurs around the nugget, causing a button to pull away from one of the joined sheets. This explains the whole weld fracture appearance of an intermediate type failure.

Fig. 9 Photograph of intermediate fracture. Shows center button surrounded by sheared surface

Tear System of Failure

A typical tear failure is pictured in Fig. 14. In this system of failure, no part of the fracture path is parallel to the faying plane. The failures observed were tears either around the spot as pictured or across one of the sheets. In both cases the fracture is tensile rather than shear or slip as in the other failure systems.

A weld that had been found to fail by tearing was incorporated into the sectioned spot shear test for study of its cross section under stress. Figures 15 and 16 show macrographs of this sectioned weld at no load and at failure.

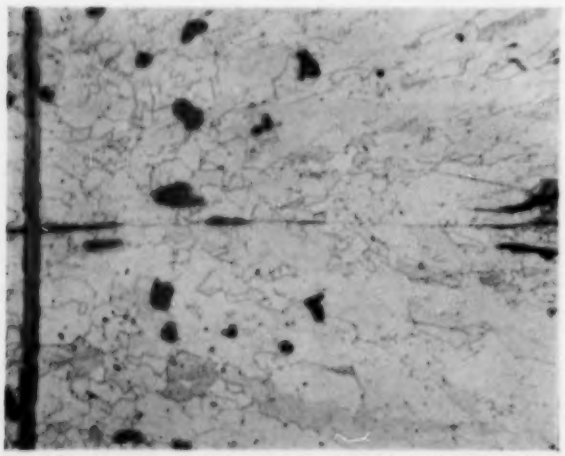

Fig. 10 Area just inside notch showing solid phase bonding at no load

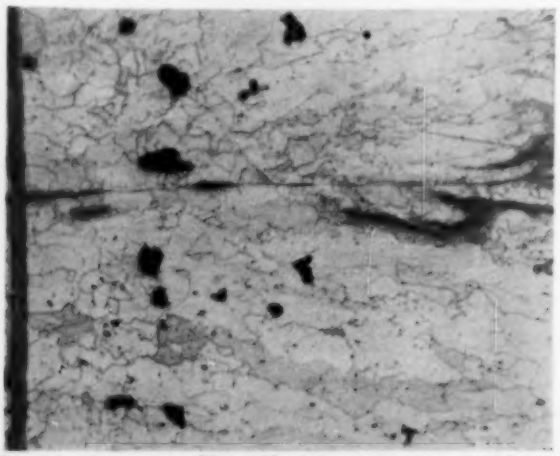

Fig. 11 Same area (Fig. 10) after application of 3500 lb load to the right in the top sheet

Fig. 12 Approximately same area (Fig. 10) after 5000 lb load. Cast nugget is to the left

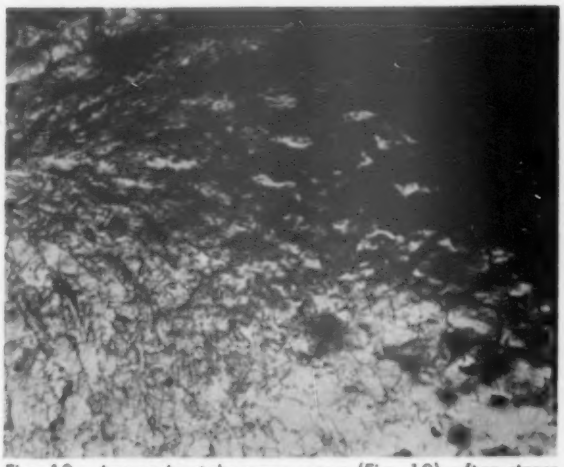

Fig. 13 Approximately same area (Fig. 10) after stress just under failure. Cast nugget has resisted strain. Note the roughly 45-deg line dividing strained and unstrained areas

The fracture is almost perpendicular to the direction of loading and has the appearance of a tensile fracture in the welded sheet slightly removed from the nugget. The scribed lines are bent on either end of the cast nugget but the centerline is only slightly deformed if at all. This suggests that defects in the center of the nugget might not be too important in this instance.

Photomicrographs of this cross section at various stress levels are shown in Figs. 17 to 20. Figure 17 shows the area between the weld edge and the cast nugget at no load. Note the relative shortness of this distance compared to cross sections exhibiting the tendency to fail by shearing. Figure 18 shows the same area after application of 3500 lb of stress to the composite specimen. The loading is to the right in the upper sheet. Evidence of strain is apparent between the edge of the weld and the cast structure. Figure 19 shows the same area at a test specimen load of 6000 lb which was just below failure stress. The plastic strain is still confined to the same small area instead of progressing away from the notch as it did in the intermediate system of failure. Of note is the fact that the rough dividing line between strained and unstrained metal is more nearly vertical than in Fig. 13 (intermediate failure). Evidently the small distance between notch and nugget combined with the height of the nugget above the faying plane resulted in a geometry of spot weld which protected the 45-deg plane which is susceptible to slip. Once failure by shear in this direction is effectively blocked, the sheet itself fails in tension initiated at the notch at the edge of the weld. The last figure in this series (Fig. 20) shows the almost completely unstrained cast nugget structure.

Fig. 14 Photograph of a tear fracture. Failure plane is normal to the faying plane

Failure System vs. Weld Strength

The foregoing discussion of the sectioned spot shear test was divided into three sections corresponding to the shear, intermediate and tear failure systems studied. These failure sys-

Fig. 15 Unstressed weld showing cast nugget

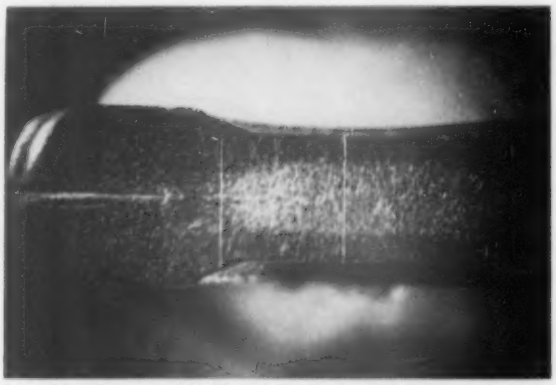

Fig. 16 Same weld (Fig. 15) showing failure on the left removed from the spot. Note scribed lines

Fig. 17 Same weld (Fig. 15) showing notch and cast nugget at no load

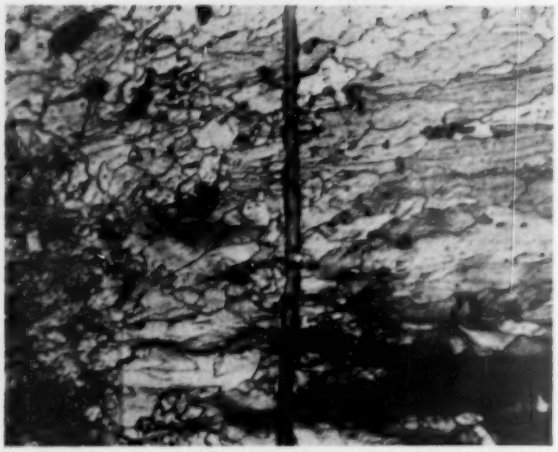

Fig. 18 Same area (Fig. 17) after application of 3500 lb load to the right in the top sheet

tems were seen to be separate and distinct from each other according to observed behavior of the weld sections under stress. It is to be expected that such marked differences in strain behavior will be reflected in the ultimate strength of the weld in tension shear. The initial strain reaction to stress is the same in each system. That is, evidence of strain first appears at the weld edge and progresses along the faying plane toward the center of the weld. The difference between the three systems is the manner in which this movement along the faying plane is blocked. In the shear system of failure this movement is allowed to continue through the spot. The intermediate system of failure produced a change in the slippage path after considerable progression along the faying plane; while failure by tearing resulted from almost immediate interference with faying plane slip. Therefore, reasoning that strength increases with interference to strain, the order of strength should be shear, intermediate and tear systems, from weak to strong. Figures 21, 22 and 23 show this to be generally true for Welding Runs A, B and C, respectively.

Figure 21 is a plot of percent indentation, and ultimate strength as functions of cycles of welding current for Welding Run A in Table 1. Notice that the weld strength plot exhibits a rapid increase between 36 and 44 cycles. This is also the weld heat at which the system of failure changes from shear to intermediate. Figure 22 is a plot of spot weld strength, percent indentation, and the percent of the weld bond that is cast nugget all plotted as functions of cycles of welding current for Welding Run B, Table 1. Figure 23 shows the same parameters for Welding Run C. In both of these figures the weld strength is again increased at the heat (10 cycles) at which the failure system changes from shear to intermediate. Therefore Welding Runs A, B and C all show a strength increase of the intermediate over the shear failure system.

Figure 21 does not include any welds which failed by tearing. Larger electrodes were used for this run and the distribution of heat caused excessive indentation and electrode melting before an appreciable cast nugget structure was formed. Figures 22 and 23, however, have welds that failed by the tear system at their upper heat values. Welding currents of 28 or more cycles in both of these runs produced welds that failed by tearing. In Fig. 22, Welding Run B, there is no marked increase in weld strength at this point. However, there is a gradual strengthening at higher heats. Figure 23, Run C, however, shows a definite step increase in weld strength on failure by tearing. This is as expected from observations of the sectioned spot shear test. The strength is seen to drop off again at the higher heat tear failures but this is due

Fig. 19 Same area (Fig. 17) after application of 6000 lb load. Note the roughly vertical line dividing the unstrained and the strained areas

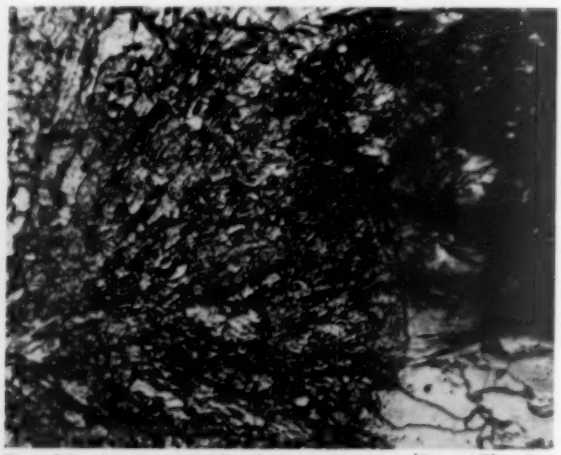

Fig. 20 Approximately the same area (Fig. 17) after failure showing unstrained cast nugget

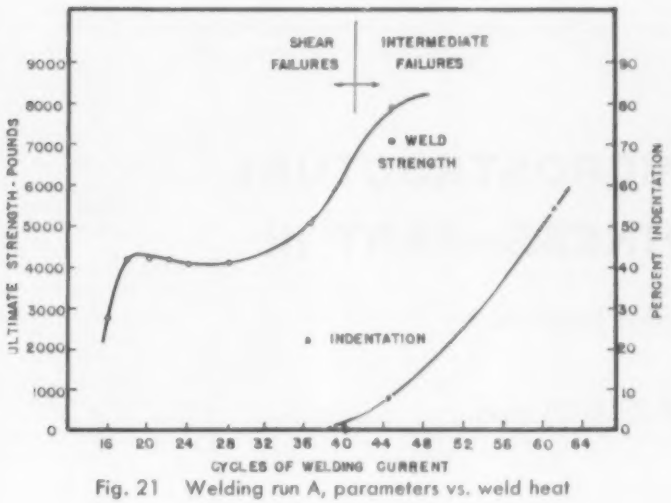

Fig. 21 Welding run A, parameters vs. weld heat

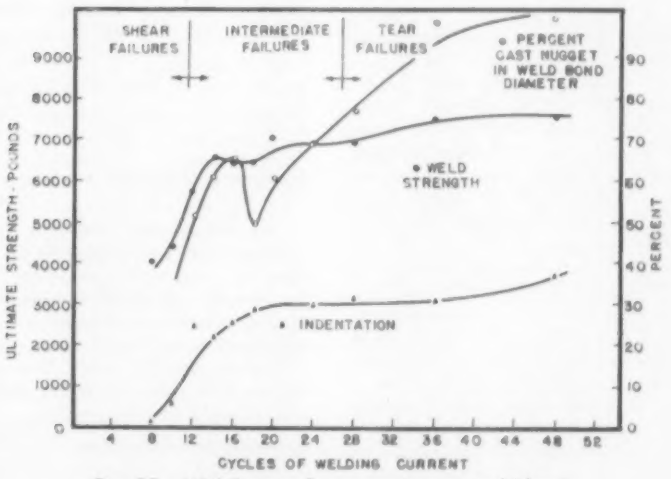

Fig. 22 Welding run B, parameters vs. weld heat

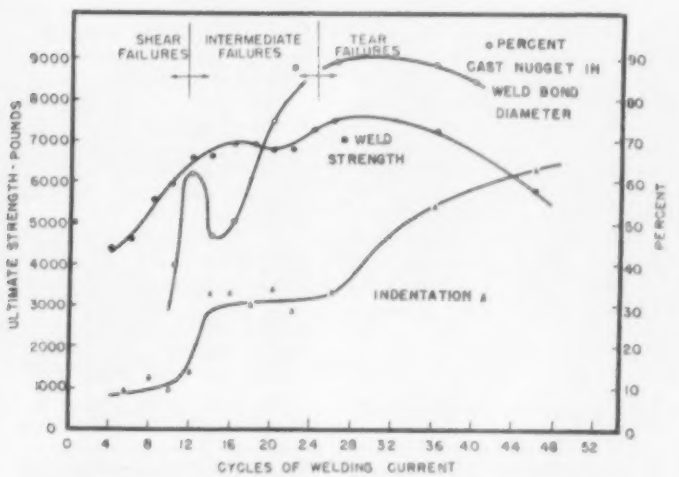

Fig. 23 Welding run C, parameters vs. weld heat

to the weakening of the joint by excessive indentation. More electrode pressure was used for Run B than for Run C. It is not established why this difference would cause the strength increase to be more gradual.

Macro-Geometry vs. Failure System

In the preceding discussion on the observations of the sectioned spot shear test, the various strain patterns obtained by loading the sectioned spot were described for each failure system. From these observations it is apparent that the development of a cast nugget plays an important part in the distribution of stress and in the failure system of the weld. For this reason the plot, "percent of the weld bond that is cast nugget," was included in Figs. 22 and 23 to give a measure of nugget development. In Figs. 21, 22 and 23 it is apparent that shear failure is prevented at that heat at which a cast nugget first begins to form. Figures 22 and 23 show that intermediate failure is prevented when the cast nugget structure occupies roughly 80% of the weld bond. These correlations are as expected from sectioned spot shear test observations.

Conclusions

The following conclusions are indicated by the data presented in this paper. These conclusions are limited to spot welds in 11 gage Armco Iron which is relatively soft and ductile.

1. Observations of the exposed spot weld cross section under stress by means of the "sectioned spot shear test" give valid indications of the reaction of a similar whole weld to applied stress.

2. Spot welds fail by either a shear, intermediate or tear system of failure as defined.

3. The macro-geometry of the weld cross section determines the system of failure. The most important factor is the extent of development of the cast nugget.

4. Welds that fail by shear are considerably weaker than welds that fail by the intermediate system of failure, size considered.

5. Welds that fail by tearing are slightly stronger than intermediate failures.

6. The four parameters, failure system, weld strength, macro-geometry of cross section and sectioned spot shear test observations are related.

THE EFFECT OF MICROSTRUCTURE ON NOTCH TOUGHNESS—PART III

Lehigh investigation covers the notch toughness of pearlite and ferrite aggregates in a fine-grained plain-carbon (0.32% C) steel

BY J. H. GROSS AND R. D. STOUT

Introduction

It has been well established by previous investigations that the microstructure of a steel has a strong influence on its notch toughness. In quenched and tempered steels the relation of notch toughness to microstructure has been demonstrated particularly for mixed structures. The harmful effects of small amounts of ferrite and pearlite have been clearly shown. Relatively little quantitative work has been published on unhardened steels, including the structural steels which are used for engineering structures subject to environmental conditions conducive to brittle failures. It is known that the factors of importance to notch toughness in unhardened steel include austenitic and ferritic grain size, the amount and distribution of the ferrite and pearlite, and possibly inclusions. A complete understanding of the interplay of these microstructural variables is essential because of the complexity of microstructures produced by fabrication operations such as welding, cold forming and heat treatment. Thus a study of the effects of the usual base metal microstructures on notch toughness is insufficient. Microstructures capable of resisting the initiation of brittle fracture may nevertheless propagate a fracture initiated in less resistant microstructures. While special combinations of microstructures have been synthesized and tested for notch toughness, a thorough understanding of the problem will not be achieved until the effect on notch toughness of each micro-constituent, singly and in combination, is known.

The initial investigations of the problem were confined to the simpler case of eutectoid steel. In the first investigation[1] it was observed that increasing austenitic grain size and decreasing pearlite spacing may result in a substantial reduction in the notch toughness of plain carbon eutectoid steels. Subsequent results reported by Rinebolt[2] did not agree with these findings. Additional investigation[3] confirmed the original findings with the added observation that commercial steels are highly susceptible to spheroidization of pearlite during transformation and that a uniformly lamellar pearlite is the exception rather than the rule. Spheroidization, which favors notch toughness, was more prevalent in the fine-grained steel than in the coarse-grained steel.[3] Thus it might be better stated that increasing fineness of the lamellar pearlite produced at the lower subcritical transformation temperatures results in a loss of notch toughness in plain carbon, eutectoid steels. A corrollary investigation[4] conducted at Lehigh University on the micro-mechanism of deformation and fracture provided added confirmation to these findings.

The results reported here are concerned with the more complex hypoeutectoid problem. It is quite reasonable to believe that the behavior of pearlite might be substantially modified by the surrounding ferrite matrix. Grossman[5] reported an improvement in the notch toughness of a hypo-eutectoid steel with decreasing subcritical transformation temperature. The improvement was attributed in large part to an increase in the fineness of the pearlite. Since no attempt was made to separate the contribution of the attendant decreasing ferrite grain size, no evaluation of the independent effect of pearlite fineness can be made.

Rinebolt[2] confirmed the notch toughness effect reported by Grossman but observed that the simultaneous variation in the ferrite grain size and pearlite spacing precluded conclusions for other than the aggregate behavior. Thus the specific effect of the individual microstructural variables on the notch toughness of plain carbon, hypo-eutectoid steels is not known. The following results are intended to provide additional insight into this problem.

Table 1—Chemical Analysis of C 1032 Steel

C, %	0.32
Mn, %	0.61
P, %	0.016
S, %	0.029
Si, %	0.18

Experimental Procedure

The steel investigated was a fine-grained C 1032 steel of chemical analysis shown in Table 1. It was obtained as $^{7}/_{16}$-in. square bars. After cutting to length, specimens were normalized at 1650° F prior to final heat treatment. After heat treatment the specimens were machined to final V-notch Charpy or tension test dimensions.

Three types of heat treatment were performed as follows:

1. Continuous cooling: austenitizing at 1600° F followed by direct transformation in lead at 1270, 1000, 700° F, or oil quenching.
2. Pot cooling in lead from 1600 to 1270° F followed by transformation in lead at 1270 or 700° F.
3. Furnace annealing from 1600 or 2000° F followed by reaustenitizing in lead at 1350° F and transformation in lead at 1270, 1000 or 700° F.

Specimens were treated in batches of sixteen—14 V-notch Charpy specimens and 2 tension specimens. After testing, two Charpy specimens were microscopically examined and quanti-

J. H. Gross is Assistant Professor and R. D. Stout is Professor of Metallurgy at Lehigh University, Bethlehem, Pa.

Presented at AWS 1955 National Fall Meeting held in Philadelphia, Pa., Oct. 17–21.

Table 2—Summary of Transition Temperatures and Microstructural Variations in Heat Series in C 1032 Steel

Specimen	Heat treatment*	Charpy V 15 ft-lb T. T., ° F	Ferrite, %	Ferrite G. S.	Pearlite G. S.
Q-1	1600-quench 1270	+35	63	9.5	9.2
P-1	1600-quench 1000	−55	0–64	11.8	...
T-1	1600quench 700	−70	..	12	...
R-1	1600-oil quench	+30	5	(19% martensite)	...
B-1	1600-pot cool 1270	+95	61	7.6	6.7
A-1	1600-pot cool to 1270-quench 700	+60	56	7.9	6.1
H-1	1600-FC reheat 1350 quench 1270	+60	60	8.2	8.1
I-1	1600-FC-reheat 1350 quench 1000	+45	63	8.2	8.5
G-1	1600-FC-reheat 1350 quench 700	+40	60	8.0	7.5
K-1	2000-FC-reheat 1350 quench 1270	+90	55	6.0	4.7
L-1	2000-FC-reheat 1350 quench 700	+75	51	6.0	5.3

* Figure at right indicates bath temperature at which specimens were isothermally transformed.

tatively evaluated by a method of lineal analysis[6] employing the experimental setup shown in Fig. 1.

Experimental Results and Discussion

The results of the experimental work are presented in Table 2.

Continuous Cooling Results

As previously mentioned, an appreciable improvement in notch toughness has been reported in hypo-eutectoid steels with increased rates of cooling. This effect was verified in the continuous cooling experiments. However, the conclusion that decreased pearlite spacing contributes substantially to this improvement is misleading. Examination of Fig. 2 demonstrates the marked change in microstructure as the cooling rate increases. Figure 2*A* represents a typical equilibrium type microstructure of coarse pearlite surrounded by large amounts of pro-eutectoid ferrite. Transformation at 1000° F (Fig. 2*B*) not only produces a substantially finer ferrite grain size and pearlite spacing and island size but also introduces appreciable areas of massive pearlite, essentially free of pro-eutectoid ferrite. This massive pearlite extended irregularly into the specimen to depths varying from a few thousandths to a tenth of an inch. Therefore the notch, located 0.079 in. below the surface, traversed a highly inhomogeneous microstructure. Extremely erratic impact values resulted. A further increase in the cooling rate produced continuous massive pearlite to depths greater than the notch root (Fig. 2*C*). Oil quenching resulted in massive pearlite almost to the center of specimen with almost no pro-eutectoid ferrite but with the formation of approximately 20% martensite.

The marked improvement in notch toughness produced by the increased cooling of lead at 1000 and 700° F is noted in the reduction of the 15 ft-lb transition temperature from +35 to −70° F.

However the microstructural variation responsible for this improvement is quite complex. The reduction in ferrite grain size from about No. 10 at 1270° F to No. 12 at 1000° F is contributory. Since pro-eutectoid ferrite is absent in the notch region of the 700° F specimens, the improvement must be associated with the pearlite. The pearlite spacing in the massive pearlite is finer than in the 1270° F transformation, in fact, it is not resolvable by ordinary optical techniques. It is also true that the carbon content of the pearlite must be substantially reduced from the equilibrium value of 0.80%. The pro-eutectoid ferrite, formerly present as the matrix, is now present in the pearlite proper, diluting it, in the absence of any pro-eutectoid ferrite, to the carbon content of the steel as a whole—0.32%. Thus four inextricable variables may be operating to affect notch toughness—ferrite grain size, pearlite island size, pearlite spacing, and the amount of pro-eutectoid ferrite, i.e., pearlite carbon content.

It should be emphasized that the bath temperatures of 1000 and 700° F do not represent the true reaction temperature at which the pearlite is formed. Actual measurements of recalescence indicated continuous cooling in lead at 1000° F produced transformation at 1225 and 700° F at 1210° F. Lead at 1270° F produced transformation also at 1270° F

It was apparent from examination of the complex continuous cooling structures that no conclusions regarding the specific effect of the individual microstructural variables could be drawn. Therefore heat treating cycles were devised by which it was expected to maintain all of the variables constant except for the pearlite spacing. Two separate techniques were employed. The first consisted of cooling the specimens in the austenitizing lead bath from 1600 to 1270° F in approximately one hour. This treatment was intended to precipitate out all of the pro-eutectoid ferrite without formation of pearlite. Since it represented the lowest subcritical temperature to which the specimen could be cooled, at the cooling rate employed, without danger of pearlite formation, 1270° F was chosen. The untransformed austenite was then transformed by means of lead baths at a series of temperatures to pearlites of widely different spacing without change in the previously precipitated ferrite. Complete control of ferrite precipitation was not possible by this technique.

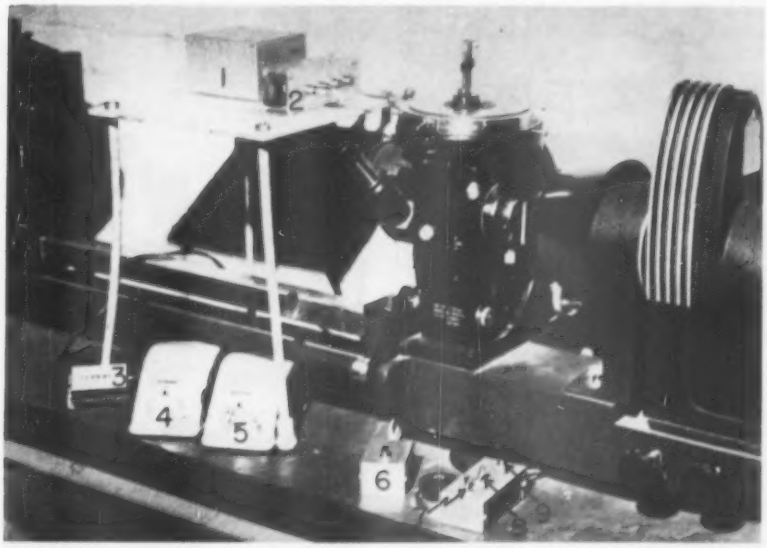

1, 0.65 rpm synchronous motor; 2, gear reduction unit; 3, grain counter; 4, totalizing timer; 5, proportioning timer; 6, grain counter switch; 7, start and reverse motor switch; 8, totalizing timer switch; 9, proportioning timer switch.

Fig. 1 Experimental apparatus for quantitative evaluation of microstructures by lineal analysis

Therefore, a second method involving furnace annealing and re-austenitizing just above the lower critical was used. This treatment was designed to produce complete precipitation of the ferrite after annealing. Subsequent austenitizing at the lower critical was to be limited to the pearlite areas, which austenite could then be transformed by appropriate subcritical treatment to pearlites of varying spacing without changing the ferrite. A re-austenitizing temperature of 1350° F, 20° F above the lower critical, was necessary to insure complete solution of the pearlite.

Pot Cooling Results

The microstructures resulting from the lead pot cooling are shown in Fig. 3. Although some variation in the pro-eutectoid ferrite occurred, the results are informative. The finely spaced pearlite microstructure (Fig. 3*B*) exhibited notch toughness slightly superior to the coarsely spaced pearlite (Fig. 3*A*). The 35° F improvement in transition temperature is probably not the exclusive contribution of the finer pearlite. A decrease in the quantity of pro-eutectoid ferrite equivalent to a reduction of approximately 0.10% in the carbon content of the pearlite and a slightly finer ferrite grain size also improved the notch toughness of the specimen containing finely spaced pearlite. It may be concluded therefore that the maximum improvement in notch toughness to be expected from a reduction of pearlite spacing to be of the order of 35° F.

Furnace Annealing Results

Results of the furnace annealing and re-austenitizing technique are shown in Fig. 4 for the 1600° F annealing treatment and in Fig. 5 for the 2000° F annealing treatment. It will be noted from Fig. 4 that the improvement in notch toughness due to increasing fineness of the pearlite is only 20° F. The resulting microstructures showed satisfactory uniformity in the quantity and grain size of the pro-eutectoid ferrite as well as the size of the pearlite islands. This observation is confirmed in Fig. 5 for a substantially coarser ferrite grain size. In this instance the improvement in notch toughness resulting from a marked reduction in the pearlite spacing is only 15° F. The loss of notch toughness due to austenitizing at 2000° F instead of 1600° F is small in view of the coarsened ferrite grain size. A possible explanation is the reduction in the quantity of the pro-eutectoid ferrite which in turn reduces the pearlite carbon content of the 1270° F transformation to 0.73% and the 700° F transformation to 0.65% from the equilibrium value of 0.80%. Such behavior would be consistent with the exceptional notch toughness exhibited by the 0.32% C pearlite produced by continuously cooling to 700° F.

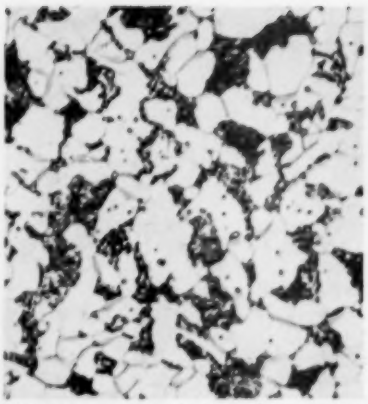

(a) Transformed in lead at 1270° F; transition temperature, 35° F; pro-eutectoid ferrite, 63%; ferrite grain size no., 9.5; pearlite island size no., 9.2.

(b) Transformed in lead at 1000° F; transition temperature, −55° F; pro-eutectoid ferrite, 0–64%; ferrite grain size no., 11.8.

(c) Transformed in lead at 700° F; transition temperature, −70° F; ferrite grain size no., 12.

(d) Oil quenched; transition temperature, 30° F; pro-eutectoid ferrite, 5%; martensite, 19%.

Fig. 2 Microstructures resulting from continuous cooling into quenching baths at indicated temperatures (picral etch, X 500)

(a) Transformed in lead at 1270° F; transition temperature, 95° F; pro-eutectoid ferrite, 61%; ferrite grain size no., 7.6; pearlite island size no., 6.7.

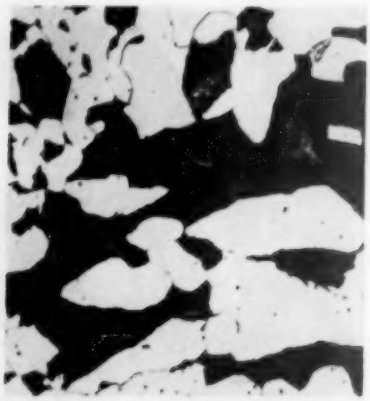

(b) Transformed in lead at 700° F; transition temperature, 60° F; pro-eutectoid ferrite, 56%; ferrite grain size no., 7.9; pearlite island size no., 6.1.

Fig. 3 Microstructures resulting from pot cooling from 1600 to 1270° F followed by indicated transformation (picral etch, X 500)

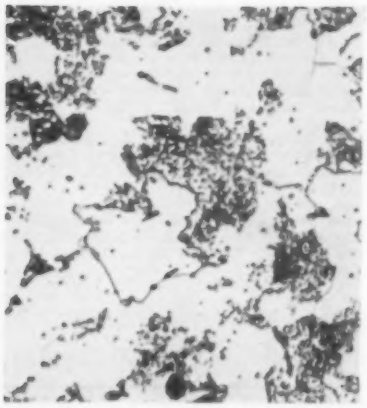

(a) Transformed in lead at 1270° F; transition temperature, 60° F; pro-eutectoid ferrite, 60%; ferrite grain size no., 8.2; pearlite island size no. 8.1.

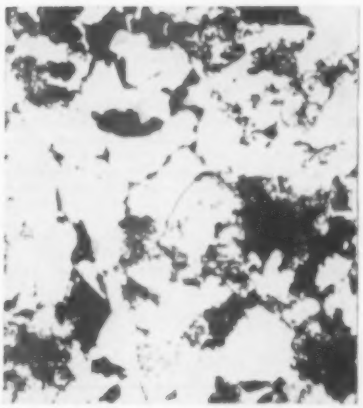

(b) Transformed in lead at 1000° F; transition temperature, 45° F; pro-eutectoid ferrite, 63%; ferrite grain size no., 8.2; Pearlite island size no., 8.5.

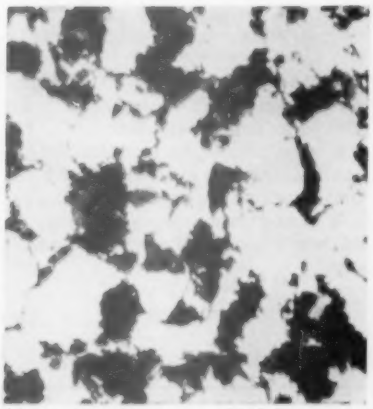

(c) Transformed in lead at 700° F; transition temperature, 40° F; pro-eutectoid ferrite, 60%; ferrite grain size no., 8.0; pearlite island size no., 7.5.

Fig. 4 Microstructures resulting from furnace annealing from 1600° F followed by austenitizing at 1350° F and transformation as indicated (picral etch, X 500)

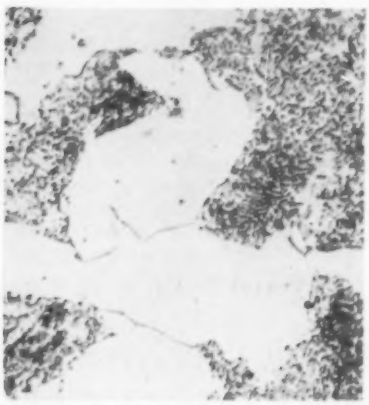

(a) Transformed in lead at 1270° F; transition temperature, 90° F; pro-eutectoid ferrite, 55%; ferrite grain size no., 6.0; pearlite island size no., 4.7.

(b) Transformed in lead at 700° F; transition temperature, 75° F; pro-eutectoid ferrite, 51%; ferrite grain size no., 6.0; pearlite island size no., 5.3.

Fig. 5 Microstructures resulting from furnace annealing from 2000° F followed by austenitizing at 1350° F and transformation as indicated (picral etch, X 500)

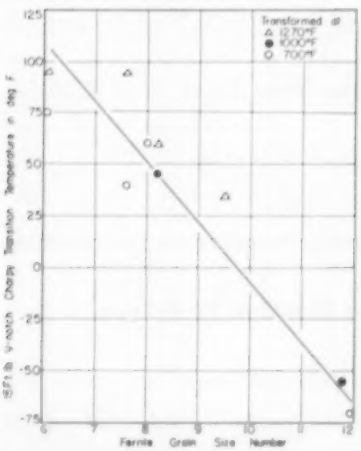

Fig. 6 Effect of ferrite grain size on transition temperature

General Discussion

It must be concluded from these observations that variation in pearlite spacing can account for only a minor portion of the total improvement in notch toughness observed to occur with increased cooling rate. Of the possible contributing factors—ferrite grain size, pearlite island size, pearlite spacing, and quantity of pro-eutectoid ferrite—only the ferrite grain size yielded any degree of correlation with transition temperature as shown in Fig. 6. The scatter is indicative of the influence exerted by the other variables. The fact that correlation exists in spite of the influence of known additional variables emphasizes the importance of ferrite grain size. It is interesting to note that the ferrite grain size effect is 30° F per grain size number which confirms the value obtained in a previous investigation[7] on ingot iron. It is also noted that the finely spaced pearlite transition temperature values are consistently lower than the coarsely spaced values implying a small influence of pearlite spacing. The effect is not sufficient, however, to produce any correlation at all with transition temperature when no correction for ferrite grain is made. This is not necessarily inconsistent with previous observations on eutectoid steels which indicated coarsely lamellar pearlite to possess superior notch toughness. In a companion investigation[8] on the micromechanism of plastic deformation and fracture, it was observed that pearlite does not participate appreciably in the deformation of a hypo-eutectoid steel. Moreover the cracks leading to failure initiate in the ferrite or at the ferrite-pearlite interface and propagate initially through the ferrite.

Although the ferrite grain size, subject to some scatter, is apparently capable of accounting for most of the improvement in notch toughness observed in these experiments the importance of the quantity of pro-eutectoid ferrite cannot be overlooked. The exceptional notch toughness of the 100% pearlite structure attests to the marked change in behavior that may be expected from pearlite as its carbon content is reduced by dilution with ferrite. Insufficient data were available to permit a satisfactory analysis of this effect. Experiments are now underway to attempt to evaluate the change in notch toughness of pearlite with decreasing carbon content.

Conclusions

In the fine-grained, plain carbon (0.32% C) steel investigated:

1. Notch toughness is substantially improved as the cooling rate during transformation is increased.

2. The spacing of the pearlite is of secondary importance to notch toughness.

3. In ferrite-pearlite aggregates, the ferrite grain size is the principal factor controlling notch toughness.

4. Pearlite of low-carbon content resulting from dilution with ferrite exhibits unusually good notch toughness.

5. Small amounts of untempered martensite markedly reduce notch toughness.

References

1. Gross, J. H., and Stout, R. D., "The Effect of Microstructure on Notch Toughness—Part I," THE WELDING JOURNAL, 30 (10), Research Suppl., 481-s to 485-s (1951).

2. Rinebolt, J. A., "Effect of Pearlite Spacing on Transition Temperature of Steel at Four Carbon Levels," *Trans. Am. Soc. Metals*, 46, 1527–1537 (1954).

3. Gross, J. H., and Stout, R. D., "The Effect of Microstructure on Notch Toughness—Part II," THE WELDING JOURNAL, 34 (3), Research Suppl., 117-s to 122-s (1955).

4. Danko, J. C., and Stout, R. D., "The Effect of Microstructure on the Morphology of Fracture," *Ibid.*, 34 (3), Research Suppl., 113-s to 116-s (1955).

5. Grossman, N., "Pearlitic Structure Effect on Brittle Transition Temperature," *Ibid.*, 28 (6), Research Suppl., 265-s to 269-s (1949).

6. Howard, R. T., and Cohen, M., "Quantitative Metallography by Point Counting and Lineal Analysis," *Trans. AIME*, 172, 413–426 (1947).

7. Hodge, J. M., Manning, R. D., and Reichhold, H. M., "The Effect of Ferrite Grain Size on Notch Toughness," *J. Metals*, 1 (3), 233–240 (1949).

8. Danko, J. C., and Stout, R. D., "The Effect of Microstructure on Fracture Morphology—Part II." Presented at the Annual Meeting of the AMERICAN WELDING SOCIETY, Philadelphia, October 1955.

BULLETIN SERIES

Requests for single copies should be sent to the
AMERICAN WELDING SOCIETY, *29 W. 39th St., New York 18, N. Y.*

Requests for bulk lots ten or more, should be sent to the
WELDING RESEARCH COUNCIL, *29 W. 39th St., New York 18, N. Y.*

No. 10 **Thermal Fatigue and Thermal Shock,** *by Helmut Thielsch, April 1952. $1.00.*

No. 11 **Investigations of Effect of Fabrication Operations Upon Pressure Vessel Steels,** *by S. S. Tör and Robert D. Stout, May 1952. $1.00.*

No. 12 **An Analytical Study of Aluminum Welding,** *by C. O. Smith, E. R. Funk and H. Udin, June 1952. $1.00.*

No. 13 **A New High-Yield Strength Alloy Steel for Welded Structures,** *by L. C. Bibber, J. M. Hodge, R. C. Altman and W. D. Doty, July 1952. $1.00.*

No. 14 **Welding Processes and Procedures Employed in Joining Stainless Steels,** *by Helmut Thielsch, September 1952. $2.00.*

No. 15 **Slag-Metal Interaction in Arc Welding,** *by Nils Christensen and John Chipman, January 1953. $1.00.*

No. 16 **Ship Structure Research, Part I—The Third Technical Report of the Ship Structure Committee; Part II—Research Under the Ship Structure Committee,** *by Capt. E. A. Wright, Finn Jonassen and H. G. Acker, November 1953. $2.00.*

No. 17 **A Critical Survey of Brittle Failure in Carbon Steel Structure Other Than Ships,** *by M. E. Shank, January 1954. $2.00.*

No. 18 **Testing of Stainless-Steel Weldments,** *by Helmut Thielsch, September 1954. $1.00.*

No. 19 **Review of Welded Ship Failures,** *by Harold G. Acker, November 1954. $1.00.*

No. 20 **High-Strength, Low-Alloy Steels; Analytical Chemistry Fosters Progress in Steelmaking; Steel Quality;** *by Charles M. Parker, January 1955. $1.00.*

No. 21 **Coating Moisture Investigations of Austenitic Electrodes of the Modified 18–8 Type,** *by K. P. Johannes, D. C. Smith and W. G. Rinehart, February 1955. $1.00.*

No. 22 **Welded Tee Connections,** *by A. G. Barkow and R. A. Huseby, May 1955. $1.00.*

No. 23 **Cracking of Simple Structural Geometries,** *by S. T. Carpenter and R. F. Linsenmeyer, July 1955. $1.00.*

No. 24 **Nickel and High-Nickel Alloys for Pressure Vessels,** *by R. M. Wilson, Jr., and W. F. Burchfield, January 1956. $1.00.*

THE EFFECT OF MICROSTRUCTURE ON THE MORPHOLOGY OF FRACTURE—PART II

Fracture morphology investigation of a 1025 steel that fracture is associated with ferrite grain boundaries and the pearlite-ferrite interfaces which are subjected to large amounts of plastic deformation

BY J. C. DANKO AND R. D. STOUT

Introduction

The effect of microstructure on the notch toughness of steel has been clearly demonstrated by many investigators. Hollomon, et al,[1] for example, have shown the variation in impact properties of tempered martensite, tempered bainite and tempered pearlite of the same hardness level. An appreciable change in transition temperature for a normalized microstructure and spheroidite microstructures produced by quench and temper treatments and spheroidization of pearlite was reported by Rinebolt.[2] Grossmann[3] has shown that small amounts of ferrite in the prior austenitic grain boundaries of hardened steels have a very significant effect on the notch toughness. The effect of pearlite spacing on the transition temperature of a plain carbon eutectoid steel was investigated by Rinebolt,[4] and Gross and Stout.[5, 6] Rinebolt reported a decrease in transition temperature with decreasing interlamellar spacing whereas the data of Gross and Stout revealed the opposite trend. Although the investigations cited provided quantitative data on the effect of structure on notch toughness, little or no emphasis was placed on the aspects of fracture morphology, i.e., the effect of microstructure on the initiation and propagation of fracture.

A few investigations on the fracture characteristics of impact specimens have been reported. Bruckner[7, 8] has investigated the micromechanism of fracture of low-carbon steels and ingot iron in the tension impact test. The results of the investigation provided a wealth of data on the initiation of fracture as related to the microstructure.

A similar metallographic investigation of fracture in impact specimens of a structural steel was conducted by Baeyertz, *et al.*[9] However, the fracture studies by Bruckner and Baeyertz, *et al.*, were confined to ingot iron and low-carbon steels in which a limited variety of microstructures was attained. Therefore, an investigation was undertaken to determine the fracture morphology of various microstructures in ingot iron and carbon steels of several carbon contents. Simultaneous studies[10] on the effect of microstructure on notch toughness are being made in this laboratory. The ultimate objective is to establish, if possible, a parameter relating microstructure to notch toughness. The effect of pearlitic structures on the notch toughness[6] and fracture morphology[11] has already been reported. This investigation was made on a microstructure of ferrite and pearlite in a plain carbon steel of approximately 0.25% carbon.

Experimental Procedure

The material selected for this investigation was a plain carbon steel of 0.25% carbon. The chemical analysis of the steel is reported in Table 1. The steel was silicon killed. Specimen blanks $^3/_8$ x $^1/_2$ x 3 in. were cut from a $^3/_8$-in. rolled plate. Since a coarse-grained microstructure facilitates micrographic and fractographic observations, the specimen blanks were austenitized at 2400° F (1316° C) and furnace cooled to produce pearlite of intermediate spacing. Isothermal transformation studies at 1300° F (704° C) revealed that in the coarse-grained structure the pearlite rapidly spheroidized. Thus, furnace cooling was employed to produce a laminated microstructure. The resultant structure had a grain size of approximately ASTM No. 3. A representative area of the heat-treated steel is shown in Fig. 1.

Table 1—Chemical Analysis of Steel

C, %	0.25
Mn, %	0.66
P, %	0.020
S, %	0.022
Si, %	0.19

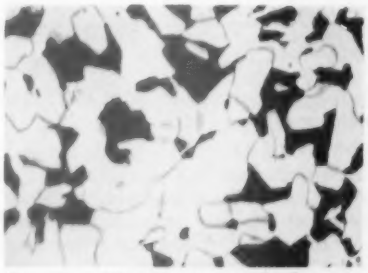

Fig. 1 Microstructure of furnace-cooled 1025 steel. (Picral-nital etch; X 100, reduced by 50% upon reproduction)

Subsized Charpy V-notch bars with a breadth of 0.197 in. and 0.394 in. height were machined from the heat-treated specimen blanks. The notch was cut perpendicular to the longitudinal direction of rolling. The subsized bars were tested in a standard impact testing machine. In addition, repeated blow experiments were made in an impact tester of 1 and 16 ft-lb capacity. After the transition temperature curve was obtained, prepolished and etched Charpy bars were tested above, within and below the transition temperature range. Prepolished and etched bars were used to detect the presence of microcracks and to observe the mode of deformation. After the detailed surface observations were completed on the fractured prepolished and etched sections, they were nickel plated and mounted in bakelite. Further metallographic observations were then made of areas below the surface. The proportion of fracture through the ferrite and through

J. C. Danko is Instructor and R. D. Stout is Professor of Metallurgy at Lehigh University, Bethlehem, Pa.

Presented at AWS 1955 National Fall Meeting held in Philadelphia, Pa., Oct. 17-21.

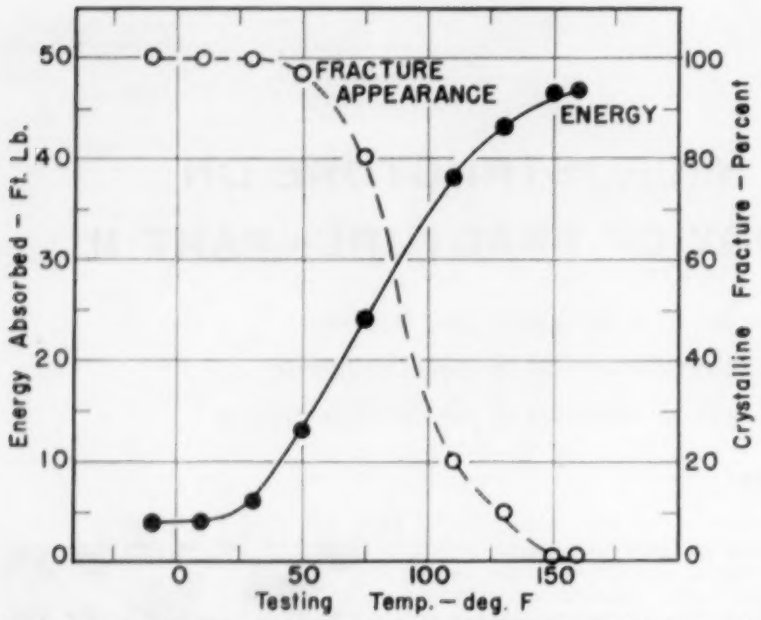

Fig. 2 Impact properties of 1025 steel for subsized (0.197 breadth) Charpy V-notch specimens

the pearlite for the specimens tested above, in and below the transition temperature range was determined by tracing the fractured edge on a piece of onion skin paper and marking the areas of pearlite and ferrite. A map recorder was used to determine the total fracture length and the amount of fracture that passed through the pearlite. Duplicate measurements were made at different levels below the fractured surface.

Supplementary information on the deformation of the pearlite-ferrite aggregate was obtained by slow bend test at low temperatures on unnotched Charpy bars. The strain hardening of the pearlite and ferrite was measured by microhardness tests in individual areas of the pearlite and ferrite of specimens strained to various amounts in compression. This technique was also used to study the strain hardening of a 100% pearlite of a eutectoid steel possessing pearlite comparable in spacing to that of the 1025 steel.

Results and Discussion

The transition temperature curve for the coarse-grained ferrite-pearlite aggregate is shown in Fig. 2. Metallographic observations made on the prepolished and etched Charpy bar tested below the transition temperature (−100° F) revealed cleavage behavior of the ferrite and pearlite. In many areas of the cleaved ferrite grains, mechanical twins were observed to lie parallel to the cleavage plane on the surface and a typical area is illustrated in Fig. 3. The observations of the mechanical twin-cleavage relationship do not necessarily imply that cleavage occurs along the twin plane (112), rather than the cleavage plane (100) in ferrite since the mechanical twin may intersect the cleavage plane below the surface. Other surface observations revealed that the primary and secondary fracture path was often interrupted by the pearlite areas. Similar results were reported by Baeyertz, *et al.*,[1] in their investigation on a structural steel (0.17% C).

After nickel plating the −100° F specimen, further metallographic observations were made in the interior, at several different depths below the surface. Secondary cracks were found at the ferrite grain boundaries in many different areas that were adjacent to the primary fracture. A grain boundary crack is illustrated in Fig. 4. If it is assumed that the advancing fracture front represents the narrowest part of the crack, then the secondary crack shown in Fig. 4 was probably initiated at the grain boundary. The crack is arrested by the pearlite area which showed no evidence of microcracking. That the ferrite grain boundaries act as sites for the initiation of cleavage cracks is not surprising, for Petch[12] has shown

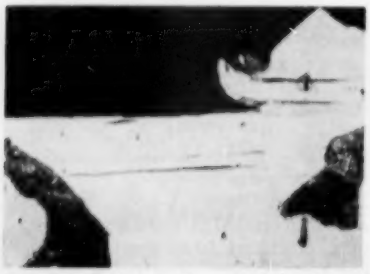

Fig. 3 Surface of prepolished and etched Charpy bar tested at −100° F. (Picral-nital etch; X 100, reduced by 50% upon reproduction)

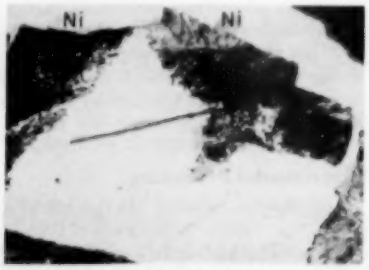

Fig. 5 Microcrack in interior of the specimen tested at −100° F. (Picral-nital etch; X 1000, reduced by 50% upon reproduction)

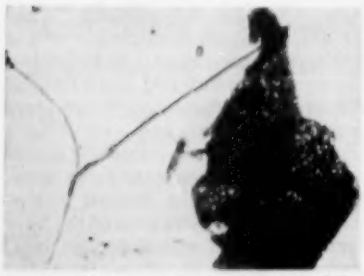

Fig. 4 Microcrack in the interior of the specimen tested at −100° F. (Picral-nital etch; X 1000, reduced by 50% upon reproduction)

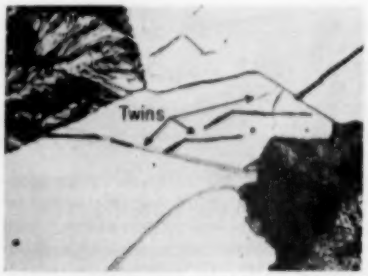

Fig. 6 Microcracks and mechanical twins in specimen tested at −100° F. (Picral-nital etch; X 1000, reduced by 50% upon reproduction)

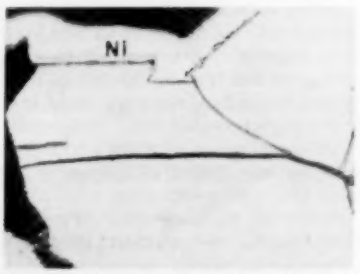

Fig. 7 Microcrack initiating in grain boundary in the specimen tested at −10° F. (Picral-nital etch; X 500, reduced by 50% upon reproduction)

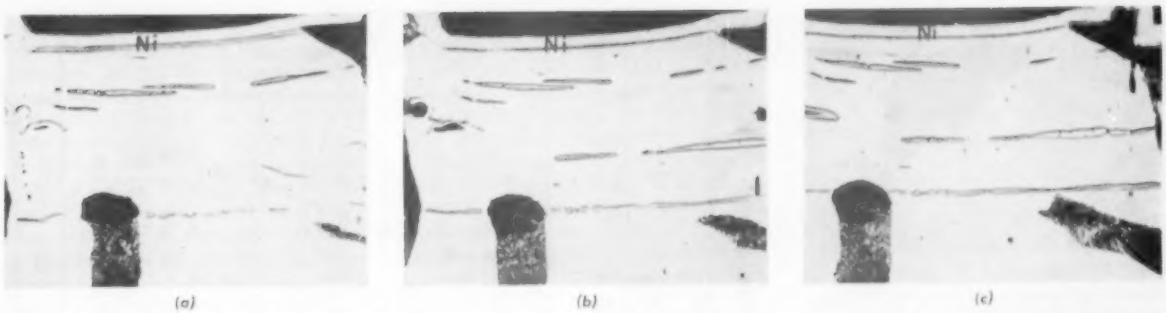

(a) (b) (c)

Fig. 8 (a) Twins parallel to cleavage. (b) same area as (a) at 0.0005 in. in depth; (c) same area as (a) but at 0.001 in. in depth. (Picral-nital etch; X 500, reduced by 50% upon reproduction)

that the cleavage strength of polycrystals is governed by the cleavage strength in the vicinity of the grain boundaries. Failure at the ferrite grain boundaries results from the action of the tensile stresses created by the dislocation array on a glide plane when it strikes an obstacle such as a grain boundary. This explanation may be extended to account for the many microcracks that initiated at the pearlite-ferrite interfaces. The microcrack illustrated in Fig. 5 originates at the pearlite-ferrite interface, and the crack did not extend into the pearlite area. Although microcracks were observed in some of the pearlite areas, in general, these cracks seldom extended into the ferrite.

Initiation of micro-cracks may not be entirely confined to the ferrite grain boundaries and the ferrite-pearlite interfaces, for many microcracks were intimately associated with the mechanical twins. Many of the microcracks observed had a tendency to follow the mechanical twin-matrix interface for appreciable lengths of the twins. The tendency for some microcracks to follow the mechanical twins is illustrated in Fig. 6, for the specimen tested at $-100°$ F. On the basis of the extensive metallographic observation made on the Charpy bars tested within and below the transition range, microcracks, in general, had their origin either at the ferrite grain boundaries and/or the pearlite interfaces. Therefore, some of the microcracks shown in Fig. 6 may possibly be related to the presence of the mechanical twins since most of the cracks were not associated with either the ferrite grain boundaries or pearlite-ferrite interface. The results of the investigations conducted by Low and Feustel,[13] Tipper and Sullivan[14] and Geil and Corwile[15] indicate that mechanical twins are not responsible for initiating cleavage failure. Therefore, further studies are being made to determine if the mechanical twins are related to the formation of microcracks.

From observations on the surface of a Charpy bar tested at $-10°$ F, below the transition range, cleavage behavior of both the ferrite and pearlite areas was evident. The pearlite-ferrite interfaces and the ferrite grain boundaries appeared to initiate microcracks. A large microcrack that initiated at a ferrite grain boundary and caused cleavage of the ferrite is shown in Fig. 7, a photomicrograph taken in the interior of the specimen. The pearlite area prevented further propagation of the microcrack. Metallographic observations on the surface and in the interior of the specimen revealed that cleavage in the ferrite was parallel to mechanical twins in many of the ferrite grains. Klier[16] has shown that cleavage may occur along the twin plane, the (112) plane. Therefore, in an attempt to determine if some of the cleavage planes were parallel to the mechanical twins, an area in which the parallel relationship was evident on the surface was photographed at several different levels by repolishing and etching. Approximately 0.0005 in. were removed by each repolishing and etching procedure. The original area is shown in Fig. 8 (*a*), Fig. 8 (*b*) illustrates the same area at a depth of approximately 0.0005 in. and Fig. 8 (*c*) is approximately 0.001 of an inch below the original area. This sequence of photomicrographs illustrates that the mechanical twins are slightly inclined to the cleavage plane. Although this evidence is not conclusive, it does suggest that the mechanical twins may intersect the cleavage plane at some higher or lower level in the many regions in which the mechanical twins were observed to be parallel to the cleavage plane on the surface.

Direct surface observations could not be made on the specimen tested at 72° F, in the transition range, since appreciable plastic deformation resulted. Observations in the interior of the specimen revealed that the ferrite grain boundaries and the pearlite-ferrite interfaces were the sites of the initiation of microcracks. A microcrack that apparently initiated at the pearlite-ferrite interface is shown in Fig. 9 and Fig. 10 illustrates a ferrite grain boundary locus of initiation. The grain boundary is actually sheared at both ends of the microcrack shown in Fig. 10. The large inclusion apparently prevented further extension of the microcrack. The areas of pearlite had a tendency to arrest both primary

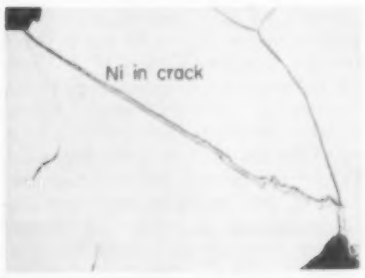

Fig. 9 Microcrack in interior of specimen tested at 72° F. (Picral-nital etch; X 1000, reduced by 50% upon reproduction)

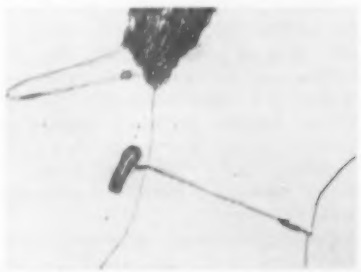

Fig. 10 Microcrack at ferrite grain boundaries in interior of specimen tested at 72° F. (Picral-nital etch; X 1000, reduced by 50% upon reproduction)

Fig. 11 Slow-bend specimen tested at $-100°$ F. (Picral-nital etch; X 500, reduced by 50% upon reproduction)

Fig. 12 Fracture of nonmetallic inclusion on surface of slow-bend specimen tested at −100° F. (Picral-nital etch; X 500, reduced by 50% upon reproduction)

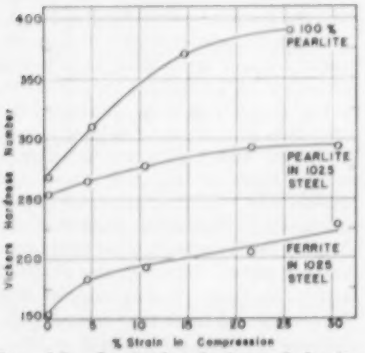

Fig. 13 Strain hardening of ferrite and pearlite in 1025 steel and pearlite in eutectoid steel that is comparable to pearlite in 1025 steel

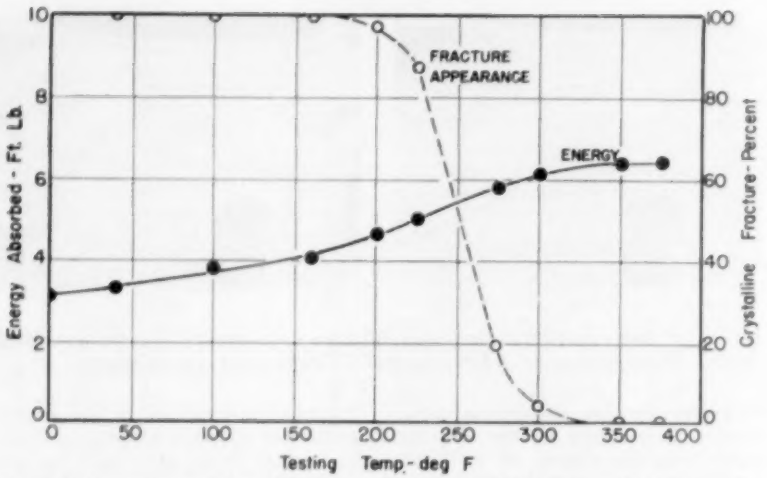

Fig. 14 Impact properties of pearlite for subsized (0.197 breadth) Charpy V-notch specimens

fracture and secondary cracks (microcracks). Near the fractured edge of the specimen the pearlite, in general, exhibited ductile type behavior.

Since pronounced deformation occurred in the specimen tested at 160° F, above the transition range, metallographic observations were confined to the interior of the specimen. Nonmetallic inclusions were observed to be the source of many secondary cracks. These cracks apparently originated at the inclusion-ferrite interface when the cohesive strength of the interface was exceeded. Likewise, secondary cracks occurred when the cohesive strength of the pearlite-ferrite interface was exceeded. The behavior of the pearlite-ferrite interface and also a ferrite grain boundary is illustrated in Fig. 11 obtained from the surface of a prepolished and etched bar that was subjected to a slow bend test at −100° F. This specimen also provided evidence that slip lines can fracture brittle constituents such as the nonmetallic inclusion shown in Fig. 12. This behavior supports the micromechanism theory of fracture proposed by Zener.[17]

Further metallographic studies made at the fractured edge of the specimen tested at 160° F showed that the fracture in general avoided the pearlite patches. Therefore, fracture length measurements were made to determine what percentage of the fracture length passed through the pearlite and ferrite. The results are tabulated in Table 2. Above the transition range, the fracture path was predominantly ferritic. The amount of fracture that passed through the pearlite in specimens tested within, and below the transition region is fairly constant but approximately double that for the specimen tested above the transition region and approximately 10% less than the amount of pearlite measured on a straight line through the microstructure. This behavior would indicate that even at low temperatures there is some tendency for the fracture path to avoid the pearlite. This tendency may be explained on the basis of the effect of the orientation of the pearlite to cleavage type behavior. Studies on eutectoid pearlite disclosed that cleavage appears to be limited to directions which intersect the lamellae at fairly high angles. Consequently, cleavage behavior of the pearlite appears highly dependent on orientation and the energy requirements for fracture to proceed along planes that do not exhibit cleavage behavior may be greater than the energy necessary to divert the brittle fracture to the adjoining ferrite. In addition, the orientation effect of pearlite on the cleavage behavior could account for the tendency of pearlite to arrest fracture. The significant increase in the proportion of fracture through the ferrite above the transition region may be explained by the low strength of the ferrite compared to the pearlite.

The metallographic observations on the various specimens revealed that the pearlite provided very little contribution to the over-all deformation of the microstructure. This viewpoint was confirmed by microhardness measurements made in the pearlite and ferrite

Table 2—Fracture Measurements

Testing temperature, ° F.	*Energy absorbed, ft-lb*	*Fracture pearlite, %*	*Through ferrite*
160	47	12	88
75	24	24	76
−10	4	21	79
−100	3	23	77

Proportion of pearlite and ferrite measured in the microstructure along straight lines that were selected at random: pearlite, 33.5%; ferrite, 66.5%.

regions in specimens of 0.25% carbon steel that were strained to various percentages in compression. The ferrite strain-hardened very rapidly as shown by the sharp rise in hardness in Fig. 13. Pearlite, on the other hand, showed a gradual rise in hardness that tended to level off. In comparison to the strain hardening shown for a pearlite of eutectoid steel that had approximately the same pearlite spacing as that in the 1025 steel, the pearlite in the 1025 steel was evidently subjected to small amounts of deformation relative to the total strain imposed upon the specimen. For example, at 25% over-all strain, the pearlite of the 1025 steel was actually strained to approximately 5%, according to the strain hardening curve for the pearlite of eutectoid steel. Consequently, the ferrite provided the majority of the deformation in the 1025 steel. Petch[12] has pointed out that the presence of pearlite increases the strain-hardening rate of ferrite and thereby reduces the amount of plastic strain required to raise the stress from the yield point to the cleavage strength.

Since the ferrite retards the strain hardening of the pearlite as shown in Fig. 13, the fracture behavior of the

pearlite may also be altered by the presence of the ferrite. For subsized specimens of pearlite of a eutectoid steel that had similar pearlite spacing as that of the 1025 steel, the transition to shear failure required very high temperatures. The Charpy transition curve is illustrated in Fig. 14. In the 1025 steel, the pearlite exhibited shear behavior at 160° F, above the transition range for that steel whereas the 100% pearlite specimen revealed a 100% cleavage type behavior at the same temperature. For the specimen of 1025 steel tested in the transition region, 72° F, most of the pearlite showed a shear type fracture while for the 100% pearlite 72° F corresponded to the lower end of the transition range. The pearlite of the 1025 steel showed cleavage behavior throughout the fractured surface in the specimens tested at −10 and −100° F. In view of these observations, it becomes apparent that prior knowledge of the fracture characteristics of microstructures consisting of 100% pearlite cannot be used to predict fully the fracture behavior of pearlite in the presence of massive ferrite.

Summary

In the coarse-grained ferrite-pearlite microstructure of a 1025 steel, the initiation of cleavage failure occurred at the ferrite grain boundaries and the ferrite-pearlite interface. Microcracks at the mechanical twin boundaries and the tendency for many cleavage cracks to follow the twin interface suggest the possibility that the mechanical twins may also initiate cleavage failure. Shear failures apparently occurred at the ferrite grain boundaries and the ferrite-pearlite interfaces and the ferrite-inclusion interfaces. When the cohesive strength is exceeded at the various interfaces shear failure occurs. In the region of 100% shear behavior, the shear path was predominantly ferritic, i.e., the fracture had a tendency to avoid the pearlite areas. In and below the transition temperature range, there was still a tendency for fracture to avoid the pearlite regions, but to a lesser extent. The areas of pearlite had a tendency to arrest fracture since the cleavage behavior of pearlite appears highly dependent on orientation. Pearlite apparently undergoes only small amounts of deformation compared to that of the ferrite in the pearlite-ferrite microstructures. With prior knowledge of the fracture behavior of 100% pearlite microstructures, the behavior of the pearlite in the presence of the massive ferrite of the 1025 steel could not be predicted since the behavior of the pearlite was appreciably altered by the presence of the ferrite.

Acknowledgments

This investigation was made possible by a grant-in-aid from the University Research Committee of the Welding Research Council, for which the authors are deeply grateful.

References

1. Hollomon, J. H., Jaffe, L. D., McCarthy, D. E., and Norton, M. R., "The Effect of Microstructure on the Mechanical Properties of Steel," *Trans. ASM*, **38**, 807–844 (1947).

2. Rinebolt, J. A., "Effect of Metallurgical Structures on the Impact Properties of Steels," Symposium on Effect of Temperature on the Brittle Behavior of Metals with Particular Reference to Low Temperatures, ASTM Tech. Pub. No. 158, 203–214 (1945).

3. Grossmann, M. A., "Toughness and Fracture of Hardened Steels," *Trans. AIME*, **167**, 39–79 (1946).

4. Rinebolt, J. A., "The Effect of Pearlite Spacing on Transition Temperature of Steel at Four Carbon Levels," *Trans. ASM*, **46**, 1527–1537 (1954).

5. Gross, J. H., and Stout, R. D., "The Effect of Microstructure on Notch Toughness—Part I," The Welding Journal, **30** (10), Research Suppl., 481-s to 485-s (1951).

6. Gross, J. H., and Stout, R. D., "The Effect of Microstructure on Notch Toughness—Part II," *Ibid.*, 34 (3), Research Suppl., 117-s to 122-s (1955).

7. Bruckner, W. H., "The Micro-Mechanism of Fracture in the Tension Impact Test," *Ibid.*, **29** (9), Research Suppl., 467-s to 477-s (1950).

8. Bruckner, W. H., "The Micro-Mechanism of Fracture in the Tension Impact Test" (Suppl. Report), *Ibid.*, **26** (9), 459–469 (1951).

9. Baeyertz, M., Craig, W. F., Jr., and Bumps, E. S., "A Metallographic Description of Fracture in Impact Specimens of a Structural Steel," *Trans. AIME*, **185**, 481–490 (1949).

10. Gross, J. H., and Stout, R. D., "The Effect of Microstructure on Notch Toughness—Part III," Paper to be presented at the National Meeting (1955) of The American Welding Society.

11. Danko, J. C., and Stout, R. D., "The Effect of Microstructure on the Morphology of Fracture—Part I," The Welding Journal, **34** (3), Research Suppl., 113-s to 116-s (1955).

12. Petch, N. J., "The Cleavage Strength of Polycrystals," *Jnl. Iron & Steel Inst.* **174**, 25–28 (1953).

13. Low, J. R., Jr., and Feustel, R. G., "Inter-Crystalline Fracture and Twinning of Iron at Low Temperatures," *Acta Metallurgica*, **1** (2), 185–192 (1953).

14. Tipper, C. F., and Sullivan, A. M., "Fracturing of Silicon-Ferrite Crystals," *Trans. ASM*, **43**, 906–929 (1951).

15. Geil, G. W., and Corwile, N. L., "Deformation Twinning in Charpy V-notch Specimens of Ingot Iron," The Welding Journal, **32** (6), Research Suppl., 273-s to 282-s (1953).

16. Klier, E. P., "A Study of Cleavage Surfaces in Ferrite," *Trans. ASM*, **43**, 935–957 (1951).

17. Zener, C., "The Micro-Mechanism of Fracture," ASM, Cleveland, Ohio (1948).

Welding Research Council Bulletin No. 24

"Nickel and High-Nickel Alloys for Pressure Vessels"

The Welding Research Council has just issued Bulletin No. 24 covering characteristics of nickel and high-nickel alloys for pressure vessel use. The report discusses in detail the analysis, physical and mechanical properties, method of determining ASME code design stresses, embrittlement by sulphur and lead, hot and cold forming, thermal treatments, cleaning, pickling, welding, brazing, joining of dissimilar metals and inspection. A discussion of the special characteristics of age hardenable alloys is also included.

This Bulletin consists of twenty-seven pages and is priced at $1 per copy (limited edition). Copies may be ordered through the American Welding Society, 33 West 39th Street, New York 18, New York.

DEPENDENCE OF STEEL WELD PROPERTIES ON LATTICE STRUCTURE

Temperature dependence found to be different for plain low-carbon and austenitic Cr-Ni steel weld metals, being primarily influenced by the inherent lattice structure

BY J. HEUSCHKEL

ABSTRACT. Unnotched tensile specimen data for plain low-carbon and austenitic Cr-Ni steel weld metals, deposited with the several arc processes, were examined with respect to temperature dependence. For each steel type the relative temperature dependence was independent of process. That dependence was different for the two steels, being primarily influenced by the inherent lattice structure. Interstitial impurities and gas and slag voids also influence the physical properties, particularly the ductility.

The differences between true fracture stress and yield stress from the tensile tests and the energy absorbed in the impact tests were simultaneously related to test temperature to show that the low temperature ductile-to-brittle transition temperature exists with either type of test. The transition with the tensile test is suppressed 350° F below that for the Charpy V-notch impact test for sound welds of low nitrogen content, probably reflecting differences in strain rate. Increased nitrogen contents raise the transition temperature for both test methods and decrease the differential between the two. For the Cr-Ni steel welds the low-temperature true fracture and yield stresses are divergent and for such metals the transition temperature is below that usually explored.

Introduction

The fact that the tensile strengths and ductilities of commercially pure metals are temperature dependent has been known for many years.[1] More recently it has been observed that one of the outstanding tensile characteristics of body-centered-cubic structure metals, such as iron, molybdenum and tungsten, is that the yield stress increases more rapidly than either the nominal ultimate or the fracture stresses when the temperature decreases below the ambient.[2] Brittle fracture occurs for these metals in the unnotched tensile test at low temperatures when the yield stress becomes equal to the true fracture stress.[3] On the other hand, the tensile yield stress of face-centered-cubic metals, such as aluminum, copper and nickel, increases less rapidly at the low temperatures than either the nominal ultimate or the true fracture stresses and brittle low-temperature fractures in simple tension do not ordinarily occur.

As temperatures are increased above ambient, the nominal ultimate strength of commercially pure iron first increases and then decreases as the combined result of strain and precipitation hardening, the strain-aging phenomena,[4] while the yield and true fracture stresses continuously decrease. For such metals as aluminum, copper and nickel, under similar conditions all three stresses tend to continuously decrease, at rates which are dependent upon the amount of prior cold work.[5]

Two previous papers described the temperature dependence of the tensile properties for metal-arc deposited unalloyed low-carbon and austenitic chromium-nickel steel welds.[6, 7] The present paper correlates the temperature dependence of those and other welds with normal lattice structure effects. At low temperatures variations are caused by the presence of interstitial impurities, such as nitrogen, oxygen and carbon. At high temperatures nonconformance to the normal pattern of the initial structure may occur as the result of local component phase changes or grain boundary weaknesses.

The tensile properties of sound unalloyed low-carbon steel weld metals are also influenced by other components of their composition and by initial cooling rate, both of which are influenced by detailed process techniques. However, the relative effect of temperature on the tensile properties, for all three commercially available shielded-arc processes (argon, flux and covered wire shieldings), is determined by the fact that the metal is inherently of a body-centered-cubic structure at and below 1400° F.[8] At and above 1600° F the low-carbon steels are face-centered-cubic,[8] and at that temperature range lower weld metal ductilities are found.

The temperature dependence of the chromium-nickel steel weld metals at subambient temperatures is determined by the predominant existence of the face-centered-cubic structure of the matrix.[7] At high temperatures the occurrence of different metallurgical phases sometimes completely disrupts the inherent plastic flow capacity pattern, although all the applicable stress-temperature relations of face-centered-cubic metals continue to prevail. The phase changes which occur in the chromium-nickel steel weld metals are not readily described and are the subject of continuing research. The problem of securing high ductilities at high temperatures, and therefore crack free welds under rigidly restrained conditions, reduces to that of control of composition and thermal conditions so that undesirable alloy concentrations and phase changes cannot occur at those temperatures on either a short or a long-time basis.

For all welds studied deposit soundness is a major consideration in securing high true-fracture-stress to yield-stress ratios or high impact values. The problem of securing sound welds is therefore as important as securing low-nitrogen and oxygen contents, although there are some recognized interrelations between the two problems.[6, 9]

Procedure

All tensile data involved were secured from 0.357-in. diam specimens as previously described.[6, 7] Comparisons were made by using, in turn, the several individual weld tensile properties of interest for all temperatures studied, −300 to +2200° F, and expressing that property

J. Heuschkel is Manager of Metals Joining Section, Westinghouse Research Laboratories, Pittsburgh, Pa.

Presented at AWS 1955 National Fall Meeting held in Philadelphia, Pa., Oct. 17-21.

as a ratio of the corresponding room temperature value as unity. The average and the maximum and minimum limits being shown for six low-carbon steel welds include those made with the argon shielded, flux shielded and covered electrode shielded processes. For some of the low-carbon steel weld comparisons the relative values calculated from previously published data for iron were superimposed on the same graphs.[10, 11] The same procedure was followed for Cr-Ni steel welds made with the argon shielded and the covered electrode shielded processes. Here appropriate comparisons can be made from data for nickel.[12]

For the low-carbon steel welds the ratio of the true fracture stress to the 0.2% yield stress was related to test temperature to show that this offered an excellent means for grading weld quality. By projecting the low temperature portions of such curves down to a value of unity the estimated temperature of fully brittle fracture in the unnotched tensile test was readily secured. This extrapolated fully brittle temperature determination for the unnotched tensile test was then used as an anchor point in drawing comparative transition temperature curves for the unnotched tensile and the Charpy V-notch impact tests. These were made by simultaneously relating both the arithmetical difference between the unnotched tensile test true fracture and 0.2% yield stresses and the Charpy V-notch impact values to test temperature for each weld to show that, by this means, a distinct ductile-to-brittle transition temperature exists for both test methods and that a definite relation exists between the two evaluation techniques.

The chemical composition of the welds used for this study are shown in Tables 1 and 2.

Ferritic Low-Carbon Steel Welds

The room temperature values for tensile properties, which were used as basic units of comparison, are listed in Table 3. For any one property relatively minor variations exist, at room temperature, between the several selected test welds made with the three processes. At room temperature these properties may be changed at will by alterations in electrode, flux and base metal compositions. The strength-ductility values resulting from such variations are inversely related.

The relative temperature dependence of the 0.2% yield strength values, Fig. 1, shows the striking similarity of performance for all the shielded-arc low-carbon steel welds. This relative temperature dependence was found for all conditions wherein at least 0.2% elongation was secured before fracture. The exception was at −300° F for a 0.043%

Table 1—Compositions of Carbon-Steel Weld Metals

Shielding process	*Element weight, %* C	Mn	Si	N_2	O_2
Covered wire	0.065	0.32	0.09	0.019	0.087
Covered wire	0.050	0.31	0.15	0.043	0.069
Flux	0.053	0.90	0.21	0.003	0.12
Argon	0.084	0.86	0.21	0.012	0.005
Argon	0.089	1.28	0.29	0.011	0.012
None (Air)	0.03	0.18	0.04	0.14	0.15

Table 2—Compositions of Cr-Ni Steel Weld Metals

Shielding process	*AISI comp. type*	*%* Cr	Ni	C	Mn	Si	N_2	O_2	*Other*
Covered wire	307	19.9	9.6	0.11	3.69	0.40	0.048	0.028	0.95 Mo
Covered wire	308	20.2	10.0	0.05	1.45	0.44	0.048	0.05	...
Covered wire	316	19.6	12.4	0.06	1.26	0.31	0.029	0.054	1.99 Mo
Covered wire	330	17.1	33.0	0.16	1.64	0.52	0.019	0.028	...
Covered wire	347	19.9	9.9	0.05	1.56	0.69	0.046	0.05	0.81 Nb
Argon	321	17.3	9.6	0.07	1.49	0.74	0.013	0.013	0.34 Ti
Argon	308	20.4	10.6	0.034	1.73	0.75	0.061	0.011	...

Table 3—Reference C-Fe Steel Weld Tensile Properties (+80° F)

Shielding process	*Metal condition*	*0.2% yield stress psi*	*Nominal ultimate stress, psi*	*True fracture stress, psi*	*Total elongation, %*	*Area reduction, %*
Covered wire						
0.019 N	As deposited	58,200	68,150	133,400	28.0	60.0
	1200° F ann.	53,300	65,400	143,400	34.2	66.8
0.043 N	As deposited	67,000	77,600	104,800	18.7	30.8
	1200° F ann.	61,000	72,100	127,800	24.7	55.6
Flux, 0.003 N	As deposited	48,500	61,400	139,000	36.7	69.5
Argon	As deposited	63,700	78,300	149,000	23.2	60.2
	As deposited	72,900	82,200	123,600	5.4	33.9
Bare (Air)	As deposited	48,400	62,000	74,400	5.2	17.3

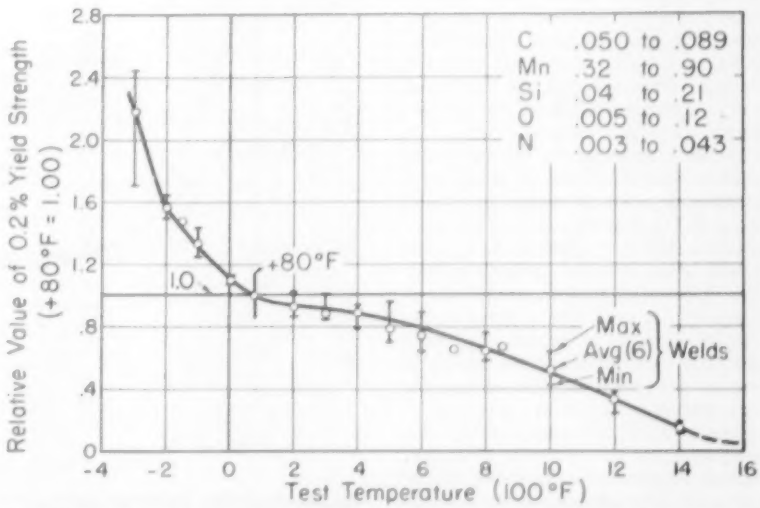

Fig. 1 Relations between temperature and relative magnitudes of yield stress for low-carbon steel shielded metal-arc welds (argon, flux and covered wire processes)

N content weld which also contained gas porosity voids and which failed before that amount of deformation was achieved in both the as-deposited and the stress-relief-annealed conditions.[8] Relatively, the yield stress in iron increases more rapidly per unit of temperature at the low temperatures than was found for the weld metals. This condition occurs because the stress increase per degree of temperature is about the same and the yield stress of iron at normal temperatures[10] is only about one-third that of the low-carbon steel chill-cast weld metal. The ratio of low temperature to ambient temperature values is therefore higher although the behavior pattern is the same.

The relative temperature dependence of the nominal ultimate strength values, Fig. 2, also shows a close similarity between the several processes and iron. The strain aging hump at +400° F was present for all welds tested, as it is for commercial, rolled and annealed iron. For all welds tested the plastic load-strain curves showed the presence of continuous sharp serrations at 300° F and for the early stages of plastic strain at 400° F.[8] These are considered to be typical of precipitation phenomenon.[12] The fact that the phenomenon was observed with nitrogen contents as low as 0.003% for the argon and for the flux shielded arc welds places some doubt upon the observation that this irregularity is caused by nitrides alone. Electron micrographs do reveal that the presence of cubic-shaped particles are more pronounced in the 0.043 N weld metals strained to rupture at 300 and 400° F.

The relative temperature dependence of the true fracture stress values, Fig. 3, shows the complete absence of the abrupt reversals of slope found in the ultimate stress curve of Fig. 2 and in this sense they are similar to the yield stress curve of Fig. 1. The reduced slope of the fracture-stress vs. temperature curve below ambient temperatures is the major item of contrast with the average yield stress curve of Fig. 1 and is of fundamental significance in the production of brittle fractures.

By superimposing the relative yield, ultimate and true fracture stress temperature dependence curves upon each other, Fig. 4, it is clear that at low temperatures the yield stress increases more rapidly than either the ultimate or fracture stresses and that the lowest rate of increase is in the fracture stress curve. The narrower the initial spread between the yield and fracture stress curves at normal temperatures, the sooner the temperature of brittle fracture will be reached. Large reductions of area before fracture are therefore desirable. As temperature increases above 800° F the relative decreasing change is about the same for all stresses. These phenomena are, within the limits shown, the

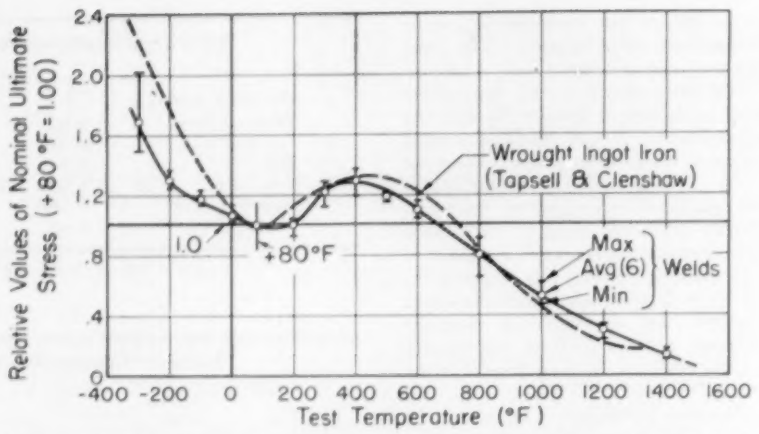

Fig. 2 Relations between temperature and relative magnitude of nominal ultimate stress for low-carbon steel shielded metal-arc welds (argon, flux and covered wire processes)

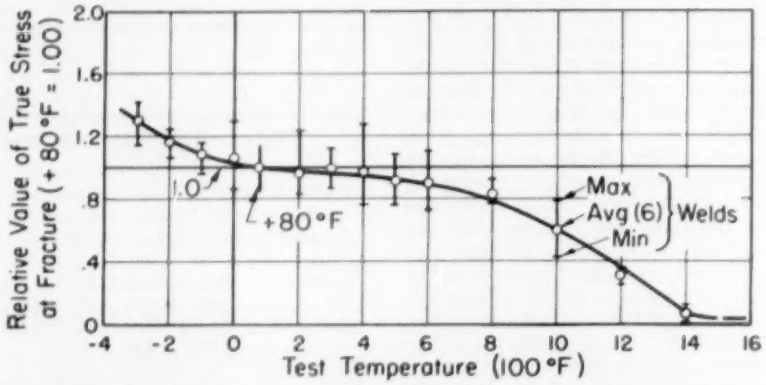

Fig. 3 Relations between temperature and relative magnitudes of fracture stress for low-carbon steel shielded metal-arc welds (argon, flux and covered wire processes)

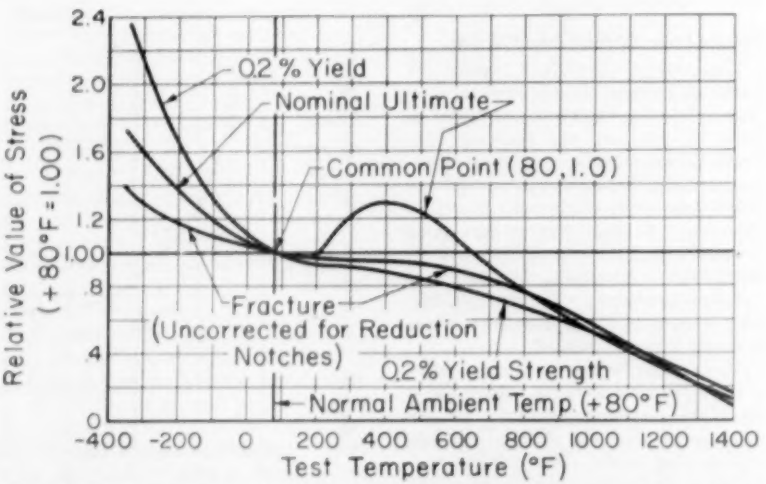

Fig. 4 Relations between temperature and relative magnitudes of strength for sound, low-carbon steel shielded metal-arc welds (argon, flux and covered wire processes)

same for all of the shielded-arc welding processes. Unshielded bare wire welds were found to fail at and below −110° F in a brittle manner, i.e., without measurable elongation or reduction in area and with low fracture stresses.

The two common criteria of tensile ductility, area reduction and elongation for the shielded-arc welds also follow the temperature-dependence pattern of iron, Figs. 5 and 6. Both the high and the low region humps and dips correspond closely with those found in iron. The reason for the elongation dip at 1000–1100° F has not been clearly revealed. Above 1500° F the ductility of iron (wrought or cast) decreases rapidly[11] as the metal structure undergoes the change from body to face centered.[5] Shielded arc welds also changed ductility at that temperature range, Fig. 7. It is not believed that the 1800° F dip is caused wholly by the fact that welds are "cast metal," as other investigations have concluded.[14] The body-centered-cubic to face-centered-cubic transformation need not and does not always occur at the same temperature-time conditions for all compositions and structures.

By comparisons of the low temperature ductility data, it has been concluded that the sound weld metals made with effective arc shieldings exhibit toughness characteristics which are superior to those of rolled pearlitic structural steels,[15] and in fact act much like tempered martensitic structures.[16]

The detail tensile property temperature dependence of the argon and flux shielded and for the unshielded arc welds, which entered in part into the preceding comparisons, is shown in Figs. 8, 9 and 10.

Several interesting criteria are available for judging the quality of metals in tension at any one temperature. Among these are: (*a*) specific values of selected tensile properties, (*b*) the ratio of true fracture stress to yield stress, (*c*) the arithmetical difference between true fracture stress and yield stress, (*d*) the energy absorbed to the point of achievement of maximum load, and (*e*) the total energy absorbed to rupture.

Since fully brittle rupture occurs when the true-fracture-stress to yield-stress ratio is reduced to unity, i.e., when the difference approaches zero, these ratios for unalloyed carbon steel welds made by the three shielded and the bare wire unshielded arc processes were calculated for each temperature, Fig. 11. The lowest values were secured, at any given temperature, with welds of the highest nitrogen and oxygen contents and for those welds containing mechanical or gas voids, even when the oxygen-nitrogen contents were low. This means that in so far as margin of safety from fracture is concerned, the problem of weld soundness becomes as or more important than that of arc shielding efficiency, although in certain instances these two factors are interrelated.[9]

Comparisons based upon useful energy absorption to maximum load or upon fracture-to-yield stress ratio both lead to the conclusion that the best operating range for low-carbon steel welds under short-time low strain rate tensile loading is between +600 and −150° F.

Higher and lower values of nitrogen and oxygen occur together in arc welds, Fig. 12. Charpy V-notch impact data

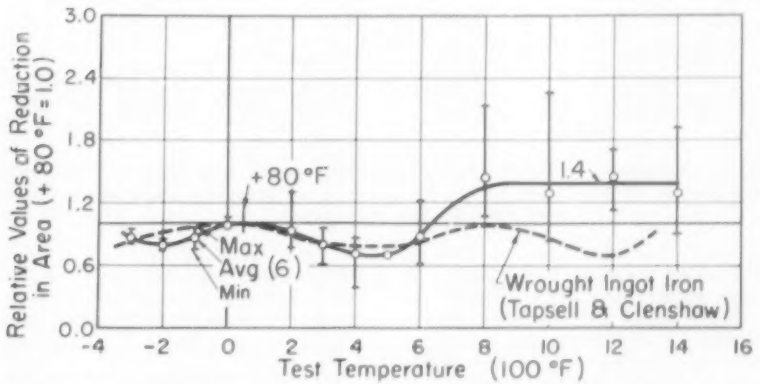

Fig. 5 Relations between temperature and relative magnitudes of reduction in area for low-carbon steel shielded metal-arc welds (argon, flux and covered wire processes)

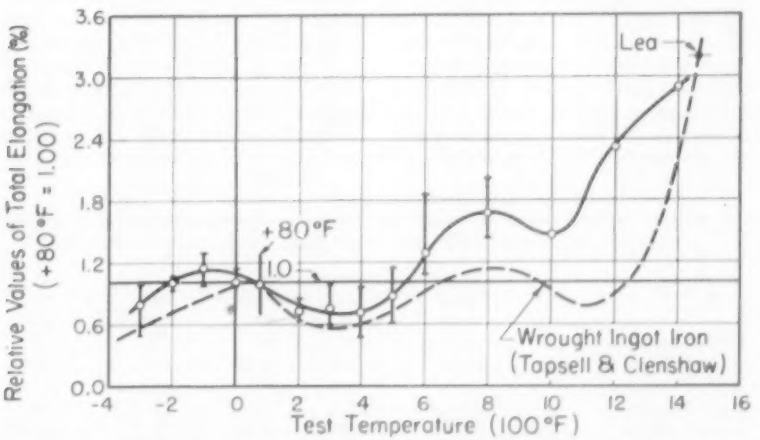

Fig. 6 Relations between temperature and relative magnitude of total elongation for low-carbon steel shielded metal-arc welds (argon, flux and covered wire processes)

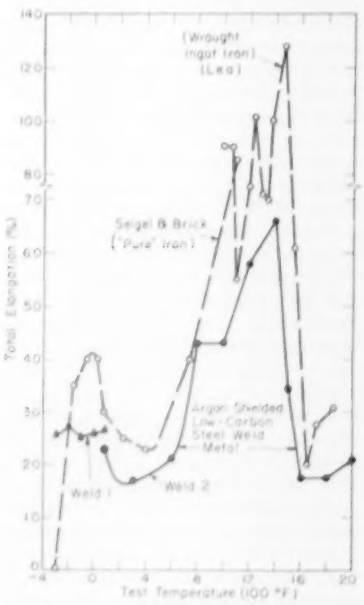

Fig. 7 Temperature-elongation relations for low-carbon steel weld metals and ingot iron (extended detail of portion of Fig. 6)

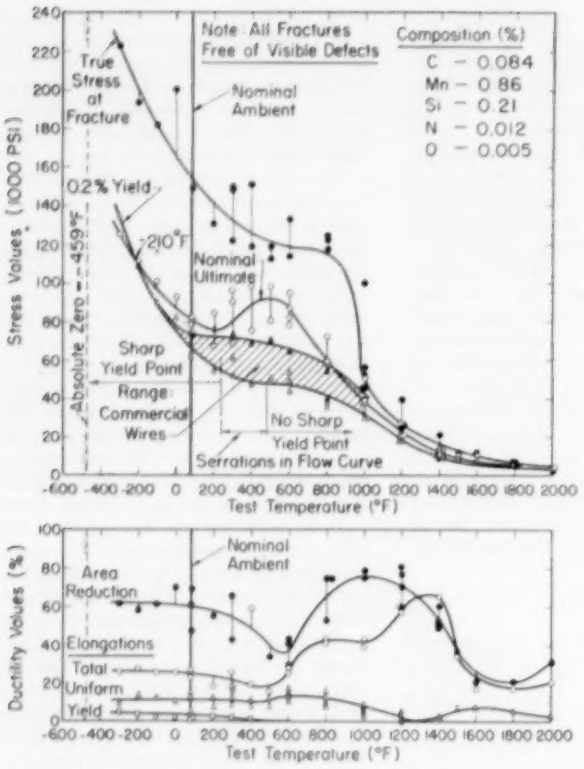

Fig. 8 Relations between tensile properties and temperature for as-deposited argon shielded low-carbon steel metal-arc weld metals

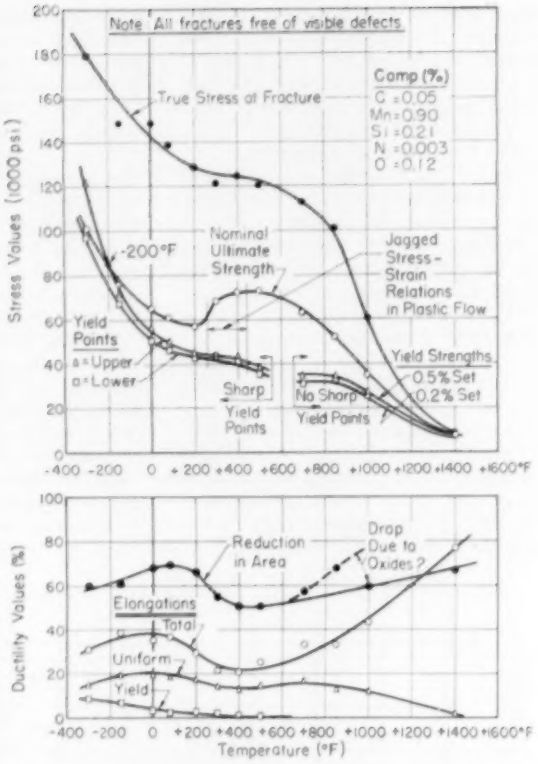

Fig. 9 Relations between tensile properties and temperature for as-deposited granulated flux shielded metal-arc weld metal in low-carbon steel

showing the relation of impact values to weld metal nitrogen contents are presented in Figs. 13 and 14. In the flux-shielded process impact values are further influenced by weld silicon and manganese contents. More than 15 ft-lb of energy can be absorbed down to −100° F with both the covered electrode and argon shielded processes, provided in both cases that the welds are sound. Both the tensile and impact values of low-carbon steel shielded-arc weld metals are therefore equal to or superior to those of structural and low carbon pearlitic steels and irons.[15, 17]

The relative merit of using the tensile and the impact types of test specimen for the evaluation of weld metals has been a subject of controversy for many years. Actually, the same conclusions can be reached from the use of both specimens provided proper interpretations are made. The unalloyed low-carbon steel welds of Tables 1 and 3 were used in the cross-evaluations shown in Figs. 15 to 19, inclusive. Overall the tensile test provides more revealing data.[6, 7] The impact test is simpler and cheaper. The essential requirement for the avoidance of low energy absorption brittle fractures in the impact test at low temperatures is that a high differential be maintained between true fracture stress and yield stress in the tensile test down to a temperature as much as 350° F below the level for which the high impact values are required. A superior method of securing high impact energy absorption is to provide increasing differentials between fracture stress and yield stress. It will be shown that this is the mode followed in austenitic matrix weld metals.

The preceding data also provided the basis for showing the relation between ductile-to-brittle transition temperature and weld metal nitrogen contents, for the oxygen, carbon, manganese and silicon content levels used, Table 1. While the weld nitrogen and oxygen contents are somewhat related, Fig. 12, the flux shielded welds, Fig. 9, contained low amounts of nitrogen (0.003%) and high amounts of oxygen (0.12%) and had about the same low-temperature tensile characteristics as the argon shielded welds (0.003% N, 0.005% O), Fig. 8. This tends to demonstrate that while higher nitrogen contents are more critical than oxygen contents in steel welds at low temperatures both interstitial elements exert a detrimental influence. The obsolete type bare wire unshielded arc welds, Fig. 10, were unsatisfactory not only because of their high nitrogen and oxygen contents but also because of their high void and inclusion contents. The influence of weld metal nitrogen content, with variable oxygen contents, upon the transition temperatures is summarized in Fig. 20.

Table 4—Reference Cr-Ni Steel Weld Tensile Properties (+80° F)

Shielding process	*AISI comp. type*	*0.5% yield stress, psi*	*Nominal ultimate stress, psi*	*True fracture stress, psi,*	*Total elongation, %*	*Area reduction, %*
Covered electrode	307	62,600	89,400	159,500	36.1	46.9
Covered electrode	308	59,000	80,800	184,800	45.1	62.3
Covered electrode	316	57,500	80,700	147,500	38.1	48.5
Covered electrode	330	47,500	79,600	164,000	41.3	60.9
Covered electrode	347	69,800	91,300	184,300	38.7	57.4
Argon	321	42,200	80,300	160,500	52.2	55.5
Argon	308	54,900	81,600	187,200	40.7	65.2

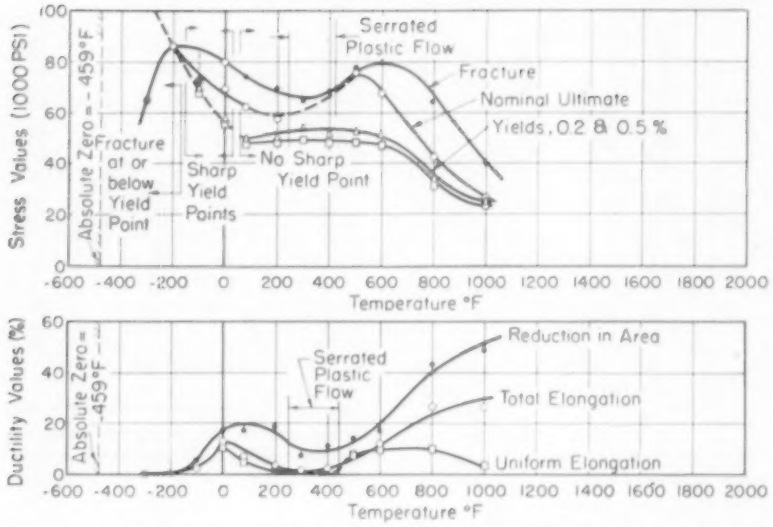

Fig. 10 Relations between tensile properties and temperature for as-deposited unshielded bare wire low-carbon steel metal-arc weld metals

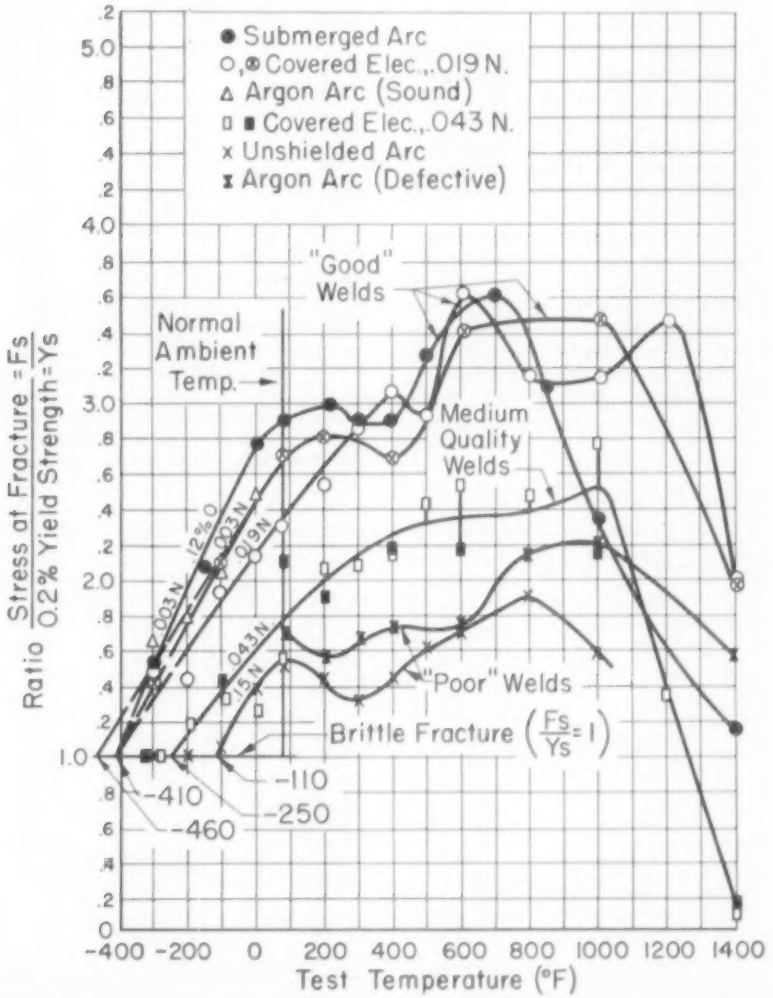

Fig. 11 Relation between test temperature and ratio of the stress at fracture to the 0.2% yield strength for low-carbon steel metal-arc weld metals

A related characteristic for high levels of performance in a weld metal appears to be that it must have the potential for strain hardening. For all welds tested high energy absorption was not obtained unless accompanied by an increase in hardness. Illustrative data are shown in Figs. 21 to 23, inclusive. Whenever the strain involved to reach maximum load was low, the increase in hardness was low, and the total energy absorbed up to that amount of deformation was also low.

Austenitic Matrix Chromium-Nickel Steel Welds

The room temperature tensile properties for seven AISI 300 series chromium-nickel steel welds of Table 2 are listed in Table 4. The tensile properties of four of these welds were discussed in detail in a previous paper.[7] Differences between the tensile properties at ambient temperature for the seven compositions of this study are not too striking.

All welds of this type at all temperatures being reported have gradual transitions from elastic to plastic flow in tension, that is, there are no sharp yield points. The relative 0.5% yield strengths, Fig. 24, show that all welds respond to temperature in about the same manner. There is no sharp rise in yield strength as temperatures are lowered to that of liquid nitrogen as was found in the unalloyed low-carbon steel welds, Fig. 1. At low temperatures the rate of change of yield stress is about the same as that for other face-centered-cubic metals.

The relative nominal tensile strength vs. temperature curves are similar for all welds, Fig. 25. There were no precipitation hardening increases at or near +300–500° F and no sharp serration irregularities in plastic flow were observed at any test temperature on any of the welds.

The relative true fracture stress vs. temperature curves, Fig. 26, are similar to those for the yield stresses except that the rate of rise at lower temperatures is steeper, a fundamentally significant fact. Superimposed, the yield, ultimate and fracture stress curves show the typical characteristics of austenitic, face-centered-cubic, metals. The divergence of the yield and fracture stresses at low temperatures, together with the strong strain hardening capacity of these metals at low temperatures results in high capacities to absorb energy at those temperatures. The capacity to absorb energy at high temperatures is much less. The impact characteristics of these weld metals have been previously described.[18]

The relative values of elongation follow no common pattern with respect to temperature, Fig. 27, particularly at the higher temperature ranges. Internal structure and grain boundary differences

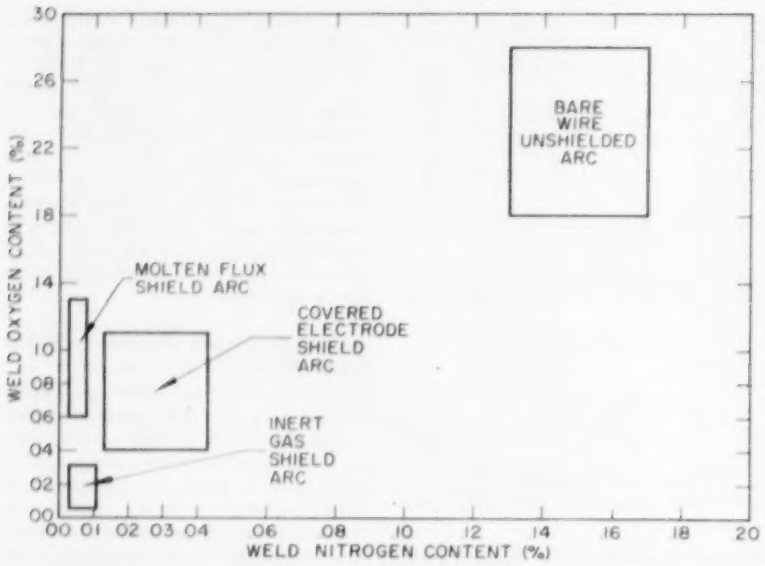
WELD OXYGEN CONTENT (%)
WELD NITROGEN CONTENT (%)
BARE WIRE UNSHIELDED ARC
MOLTEN FLUX SHIELD ARC
COVERED ELECTRODE SHIELD ARC
INERT GAS SHIELD ARC

Fig. 12 Graphical presentation of arc-shielding effects on carbon steel consumable electrode welds

not reflected in the conventional stress measurements, cause these wide variations. The solution to the high temperature ductility problem therefore lies in the attainment of a more thorough understanding of the reasons for such changes with the metals in question. Best results were secured with the Type 307, 4% Mn, 1% Mo grades. The relative changes found in reduction in area were of the same order as those of elongation and are not being shown in detail.

An effort was made to relate results secured from the tensile and impact tests for a representative weld. A plain Cr-Ni composition was chosen, Fig. 28. However, for such an austenitic matrix Cr-Ni steel weld the difference between true fracture stress and yield stress is still increasing rapidly at −300° F, the lower limit of the present tests.[7] Data

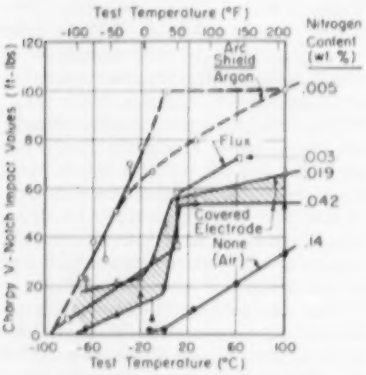

Fig. 13 Impact transition temperatures for shielded-arc low-carbon steel weld metals

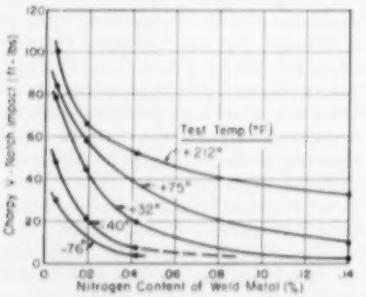

Fig. 14 Influence of nitrogen on low-carbon steel weld metal impact values

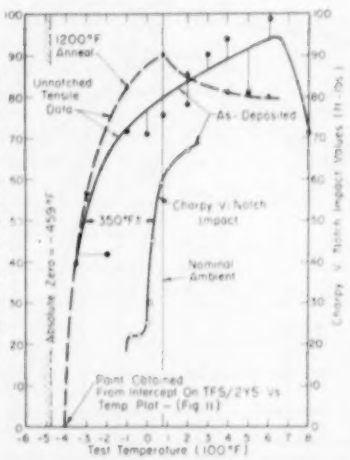

Fig. 15 Comparisons of impact and tensile results for covered electrode shielded (0.019 N) arc welds in low-carbon steels

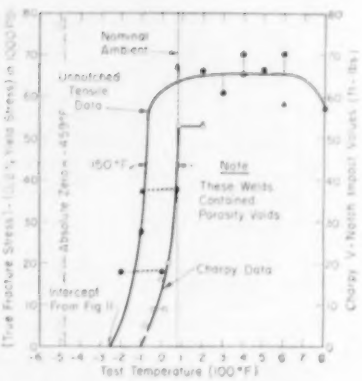

Fig. 16 Comparisons of impact and tensile results for covered electrode shielded (0.043 N) arc welds in low-carbon steels

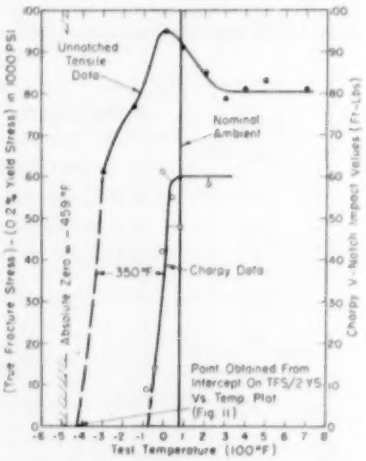

Fig. 17 Comparisons of impact and tensile results for as-deposited flux shielded arc welds in low-carbon steel

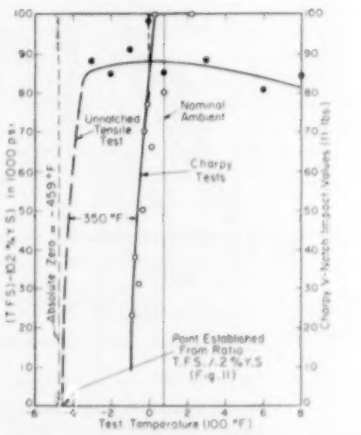

Fig. 18 Comparisons of impact and tensile results for argon shielded as-deposited arc welds in low-carbon steel

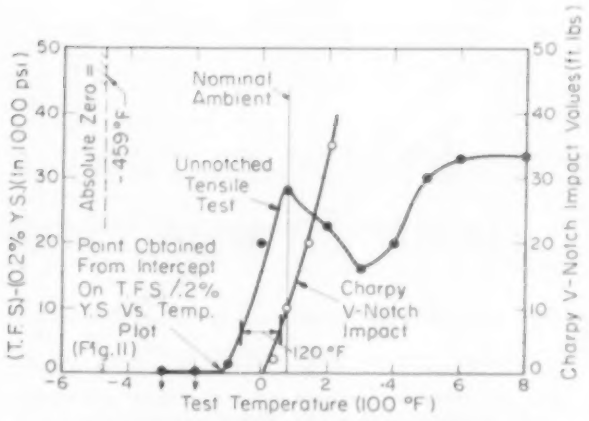
(T.F.S)-(0.2% Y.S)(in 1000 psi)
Charpy V-Notch Impact Values (ft lbs)
Absolute Zero = - 459°F
Nominal Ambient
Unnotched Tensile Test
Point Obtained From Intercept On T.F.S./.2% Y.S Vs. Temp. Plot (Fig. 11)
Charpy V-Notch Impact
+120 °F
Test Temperature (100 °F)

Fig. 19 Comparisons of impact and tensile results for as-deposited bare wire unshielded arc welds in low-carbon steels

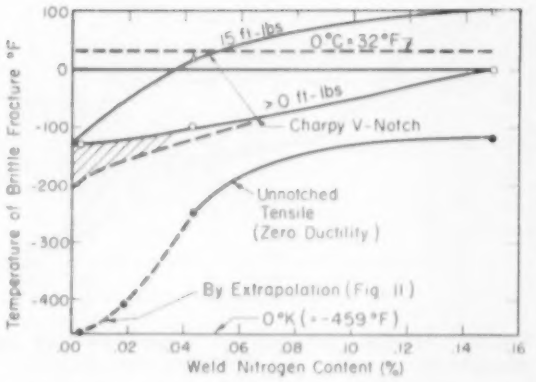

Fig. 20 Relations between weld metal nitrogen content and transition temperatures for low-carbon steels

already available[15] show that brittle fracture in the notched impact test for such welds does not occur even down to −320° F. For welds of both lattice structure forms, therefore, it is apparent that the subambient ductile-to-brittle fracture temperature can be depressed most readily by increasing the existing differential between yield stress and true stress at fracture. This can now be achieved in weld metals to varying degrees by using an alloy having an austenitic matrix of selected composition; by using body-centered-cubic structures with a minimum of interstitial impurities, carbon, nitrogen and oxygen, and by making welds wholly free of voids. High magnitudes of true fracture stress are not secured without substantial reductions in area at rupture. This criterion, too often ignored by the welding industry, becomes an item of controlling importance.

Summary

From the use of unnotched short-time tensile tests across a wide temperature range, it has been shown that the relative temperature response of low-carbon steel shielded-metal-arc weld metals is essentially independent of process, provided the deposits are sound and the nitrogen is not substantially greater than 0.02%. The basic characteristics of iron, a body-centered-cubic metal, are reflected across the temperature range more strongly than that of process characteristics or of minor variations in weld composition.

Unsoundness resulting from gas voids, slag or other inclusions and from mechanical and thermal laps or discontinuities seriously reduce the fracture stress and therefore promote brittle failure. The detrimental influence of such transient variables are not usually revealed in the yield and ultimate stress values but they are reflected in the ductility and true fracture stress data.

Low temperature impact characteristics are governed not only by the amounts of nitrogen and oxygen present but also by the lattice structure induced temperature dependence of the difference between the true fracture stress and the yield stress in tension. Best results for low-carbon steel welds were achieved from the use of inert gas shielding under conditions which produced sound welds, although good values were also secured with flux shielded and covered electrode shielded welds.

An excellent correlation has been found to exist between the subambient ductile-to-brittle fracture temperature in the unnotched tensile test and the V-notched Charpy test. For sound shielded-arc welds the transition temperatures are displaced 350° F upward in the impact test as a result of sensitivity to strain rate. Nitrogen content has a secondary effect on location of transition temperature, the lower the nitrogen content the lower the transition temperature.

The subambient temperature tensile stress characteristics of Cr-Ni steel weld metals are influenced predominantly by the presence of the face-centered-cubic austenitic matrix. The wide and often increasing divergence between the true fracture and the yield stresses at low temperatures assures the availability of good ductility at extremely low temperatures. Many of these welds, however, suffer from inability to flow plastically at the higher temperatures, a phenomenon which is related to internal phase changes and grain boundary variations. These undesirable characteristics are independent of normal lattice structure tendencies except as detrimentally influenced by the fact

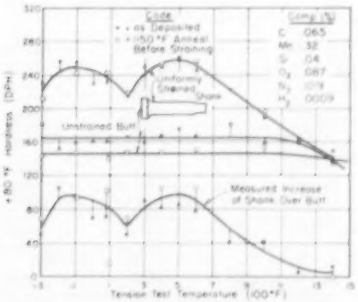

Fig. 21 Strain-temperature-hardness relations for 0.019 N covered electrode low-carbon steel weld metal

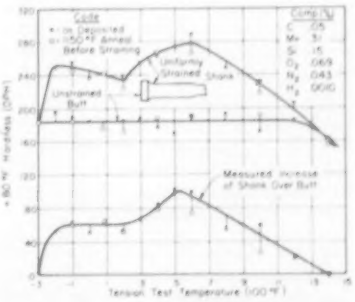

Fig. 22 Strain-temperature-hardness relations for 0.043 N covered electrode low-carbon steel weld metal

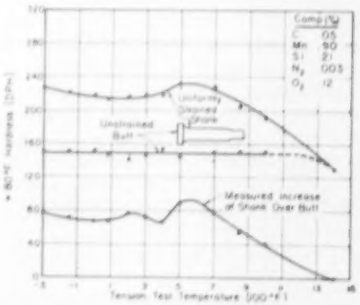

Fig. 23 Strain-temperature-hardness relations for 0.003 N flux shielded low-carbon steel weld metal

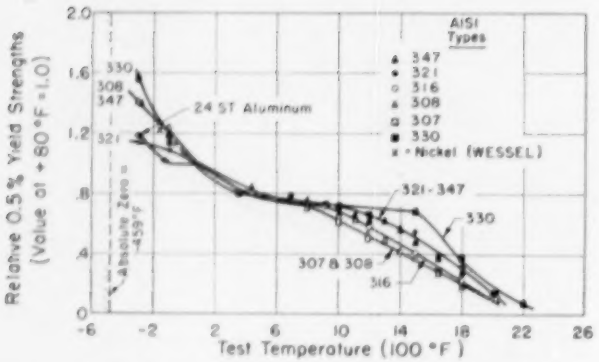

Fig. 24 Relations between test temperature and yield strengths for austenitic matrix Cr-Ni steel weld deposits

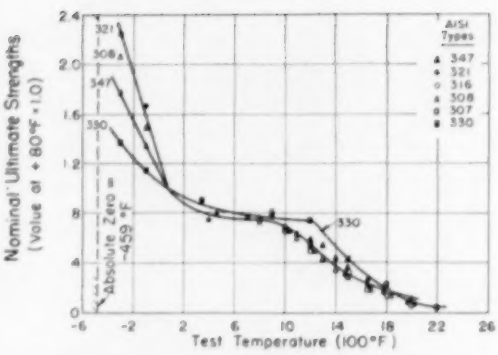

Fig. 25 Relations between test temperature and ultimate stress for austenitic matrix Cr-Ni steel weld deposits

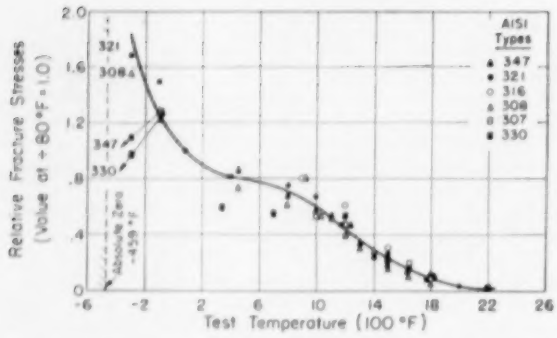

Fig. 26 Relations between test temperature and fracture stresses for austenitic matrix Cr-Ni steel weld deposits

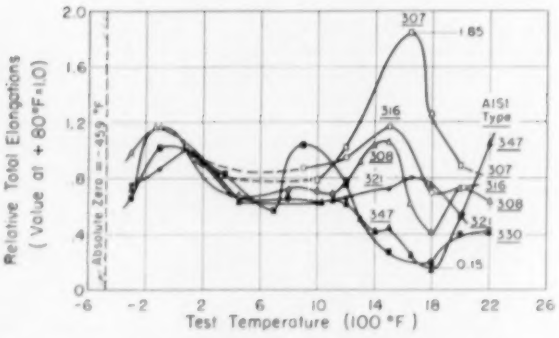

Fig. 27 Relations between test temperature and elongations for austenitic matrix Cr-Ni steel weld deposits

that fully austenitic structures tend to retain strength at the higher temperatures and therefore impose higher stresses upon the weakened grain boundaries.[7] Another example is that even low-carbon steel welds decrease in ductility when the crystal structure changes from body-centered-cubic to face-centered-cubic at and above 1600° F.

Acknowledgments

The additional data required for these studies were secured from tension tests made by E. T. Wessel and W. H. Pryle and hardness tests by R. J. Wurdack on welds made by P. T. Ehrhardt, all of the Metallurgy Department.

References

1. Jeffries, Z., and Archer, R. S., *The Science of Metals*, Chapter VI, McGraw-Hill Book Co., Inc. (1924).

2. Bechtold, J. H., "Effects of Temperature on the Flow and Fracture Characteristics of Molybdenum," *Jnl. Metals*, Trans. AIME, 1469–1476 (November 1953).

3. Eldin, A. S., and Collins, S. C., "Fracture and Yield Stress of 1020 Steel at Low Temperatures," *Jnl. Appl. Phys.*, **22**, 1296 (October 1951).

4. "Aging Phenomena in Iron and Steel After Rapid Cooling," *Philips Tech. Rev.*, **13**, 165–171, (December 1951).

5. Jenkins and Digges, "Effect of Temperature on the Tensile Properties of High Purity Nickel," *Jnl. Research*, Bureau of Standards, **48**, 313–324 (April 1952).

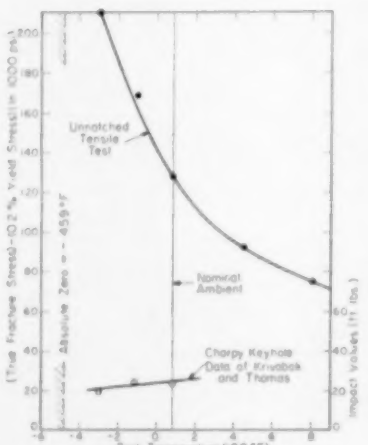

Fig. 28 Comparisons of impact and tensile results for as-deposited covered electrode shielded arc welds in type 308 Cr-Ni steel

6. Heuschkel, J., "Effects of Temperature on Weld Metal Properties," The Welding Journal, **33** (8), Research Suppl., 388-s to 397-s (1954).

7. Heuschkel, J., "Initial Characteristics of Chromium-Nickel Steel Weld Metals," *Ibid.*, **34** (10), Research Suppl., 484-s to 504-s (1955).

8. *Metals Handbook*, 1948 Edition, p. 1182, Carbon-Iron Constitution Diagram.

9. Ludwig, H. C., "Nitrogen Effects in Argon Arc Welding Atmospheres," The Welding Journal, **34** (9), Research Suppl., 409-s to 414-s (1955).

10. Lea, "The Effects of Temperature on Some of the Properties of Metals," *Engineering*, **113**, 829–832 (1922).

11. "Structure and Properties of Iron," *Metals Handbook*, 1948 Edition, pp. 423–443.

12. "Nickel and Nickel Alloys," Sections J & K, International Nickel Co., Inc.

13. Paxton, H. W., and Churchman, A. T., "The Effect of Temperature and Composition on the Deformation of Single Crystals of Iron, *ACTA Metallurgica*, **1**, 473–479 (1952).

14. Ball, J. G., and Winterdon, K., "Tensile Properties of Mild Steel Weld Metal at High Temperatures," *Trans.* The (British) Institute of Welding, *Welding Research*, **4**, No. 6, 104r–124r (December 1950).

15. Krisb, A., and Haupt, H., "Mechanical Properties of Alloy Steels at Sub-Zero Temperatures," *Arch Eisenhüttenw.*, **13**, 299–308 (1940).

16. Hadfield, R., and DeHaas, W. J., "On the Effects of Liquid Hydrogen on the Tensile Properties of Forty-One Specimens of Metals," *Phil. Trans. Roy. Soc.*, A232, 297–332 (1933).

17. Evans, E. B., and Klingler, L. J., "Heat Treatment Effects on Transition Temperature of a Ship Steel," The Welding Journal, **32** (9), Research Suppl., 417-s to 431-s (1953).

18. Krivobok, V. N., and Thomas, R. D., Jr., "Impact Tests of Welded Austenitic Stainless Steels," *Ibid.*, **29** (9), Research Suppl., 493-s to 495-s (1950).

A TEST BLOCK FOR WELDING GRAY AND NODULAR CAST IRONS

Simple test developed to discriminate between the many welding procedures and filler metals available for welding gray and nodular castings

BY WILLERD A. SCHUMBACKER AND ANTON L. SCHAEFFLER

ABSTRACT. The welding of gray iron castings has been an accepted practice for many years. With the inherent low strength and nil ductility of this material, not too much is expected of many weld repairs. Nodular or ductile cast iron has much higher strength and possesses a substantial amount of ductility. Nodular castings are replacing certain steel castings and hence more is expected of nodular iron castings than of gray iron castings. Weld repairs on nodular iron must also have better performance than repairs on gray iron.

Many processes and filler metals are available for welding gray and nodular castings. A simple test is therefore desirable to rate the various filler metals and welding procedures. A small test block for this purpose is described in this paper. The test results show that a specific procedure can be reproduced and hence the block can be used to discriminate between various procedures.

In the nickel base class of filler metals, the 55 Ni type is capable of producing a sound deposit whereas the 94 Ni type (popularly called 99 Ni) is not. Sound welds can be made in nodular iron with the 55 Ni electrode, but gray iron is susceptible to base metal cracking near the fusion line with this electrode.

Satisfactory results will be obtained if the gray or nodular cast blocks can be preheated to over 1100° F and a similar filler metal (gray or nodular iron) can be applied. It is possible to control the oxy-acetylene, inert-gas tungsten-arc and carbon-arc processes to give good results on casting repairs.

Introduction

Gray cast iron is probably the backbone of the foundry industry. Many papers have been written on its applications and on methods for the repair of casting defects and field failures. However, the applications for gray iron are limited because of its low ductility. Nodular, or ductile, cast iron is a fairly new material and new applications for its use are encountered daily. Nodular iron has much greater ductility than gray iron and usually has much higher strength. This new material will eventually find its proper place in engineering applications along with gray iron, malleable iron and cast steel.

The repair of defects in gray iron castings by oxy-acetylene welding with a similar filler metal, or by oxy-acetylene braze welding with a copper-zinc filler metal, is common practice. More recently, high nickel or nickel-iron metal-arc welding electrodes have been used for light fabrication, for maintenance welding and for the repair welding of casting defects.

Nodular iron has many metallurgical and mechanical characteristics which are different from those of gray iron, and therefore problems involved in the welding of nodular iron may not be the same as those encountered in welding gray iron. It is certain that problems which involve the repair welding of defects in castings and the fabrication of assemblies of nodular iron castings will be presented with greater frequency as this material is brought into more widespread use. Fundamental information is urgently needed to solve these problems.

The welding processes, filler metals and the different brands of materials for welding the various iron castings are so numerous that a simple weldability test is desirable for discriminating between welding procedures. A suitable weldability test must be reproducible, should use a relatively small amount of filler metal and should be economical. This paper describes a simple test coupon or block and the procedure for the evaluation of welding materials and processes for cast irons.

Materials and Procedure

Weld Test Block

The principal considerations in the design of the test block were that it should be easily prepared, afford considerable restraint to the weld, be reproducible and be representative of a groove prepared in an actual casting. With these considerations in mind, the test block shown in Figs. 1 and 2 was developed. This test block was cast to size, including the groove for the weld deposit. The cast blocks were tumbled and the groove was cleaned with a small grinding wheel or rotating burr before welding.

Fig. 1 Photograph of the test block which was used for the welding experiments. Magnification X 1/4

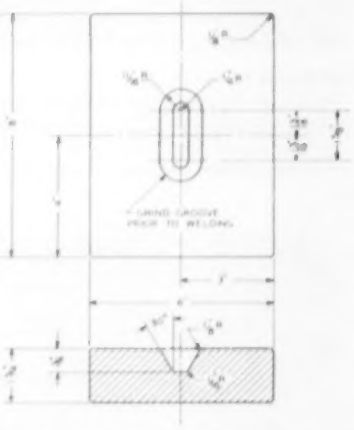

Fig. 2 Dimensions of test block

Willerd A. Schumbacker is Chief Technician-in-Charge, Welding Laboratory and **Anton L. Schaeffler** is Metallurgical Engineer, Welding Research, Allis-Chalmers Manufacturing Co., Research Laboratories, Milwaukee, Wis.

Presented at 1955 AWS National Fall Meeting held in Philadelphia, Pa., October 17-21.

Table 1A—Materials (Chemical Analyses, %)

	Type	Brand	Source*	T. C.	G. C.	Mn	P	S	Si	Ni	Cr	Mo	Cu	Al	Ti	Others
								Base metals								
1.	Gray	†	Base	3.36	2.39	0.84	0.176	0.114	2.07	0.10	0.12	0.04	0.24	0.00	0.03	<0.001 Mg
2.	Nodular	†	Base	3.45	3.12	0.40	0.022	0.007	2.84	<0.01	0.00	0.02	0.03	0.02	0.01	0.019 Mg
								Filler metals								
1.	55 Ni	A	Dep	1.66	1.40	0.50	0.011	0.001	0.35	50.46	0.01	0.01	0.11	0.05	0.39	...
		B	Dep	1.56	1.13	0.36	0.011	0.004	0.31	53.30	0.00	0.01	0.06	0.04	0.32	...
		C	Dep	1.02	0.69	0.49	0.007	0.004	0.69	49.73	0.06	0.01	0.09	0.17	0.69	...
		D	Dep	1.68	1.24	0.42	0.030	0.001	0.51	50.36	0.08	0.01	0.10	0.09	0.58	...
		E	Dep	0.77	0.34	1.20	0.008	0.005	0.20	52.40	...	...	...	...	0.16	...
2.	94 Ni	F	Dep	0.97	0.91	0.29	0.003	0.008	0.82	94.09‡	0.05	0.01	0.04	0.06	0.03	2.72 Fe
		G	Dep	0.80	0.54	0.26	0.003	0.006	0.58	94.38‡	0.07	0.01	0.08	0.13	0.43	2.91 Fe
		H	Dep	1.15	0.92	0.27	0.011	0.006	0.34	93.50‡	0.00	0.01	0.19	0.03	0.22	3.35 Fe
3.	Ni-Cu	J	Dep	0.45	0.18	1.06	0.031	0.003	1.22	55.65§	0.14	0.05	36.67	0.06	0.47	3.74 Fe
4.	Gray	K	Rod	3.65	2.96	0.77	0.710	0.077	2.79	0.01	0.04	0.01	0.12	0.00	0.08	<0.001 Mg
5.	Nodular	L	Rod	3.71	..	0.14	0.025	0.014	3.14	0.01	0.05	0.02	0.02	0.04	0.02	<0.001 Mg 0.15 Ce

* Indicates source of sample for chemical analysis: Base = base metal; Dep = undiluted deposit; Rod = bare rod.
† Specifications are given in Table 1B.
‡ Nickel by difference.
§ Ni by difference = 55.93.

Materials

Gray and nodular cast irons were used for the base materials. Typical chemical analyses of these irons are shown in Table 1A. The specified and the actual physical properties of these base materials are given in Table 1B. The filler metals used include various brands of 55 Ni and 94 Ni welding electrodes and gray and nodular iron gas welding rods. Table 1A shows the chemical analyses of these fillers and physical properties of some all-weld-metal samples are given in Table 1B. A few welds were made with various copper-base fillers.

Test Procedure

The test blocks were welded by the various welding procedures which were under investigation. The welding procedure variables included preheat and interpass temperature, welding process, types and brands of filler metals and heat treatment. The effect of peening was not investigated because it is difficult to specify and reproduce a peening procedure. After welding, each block was permitted to cool in air to room temperature.

Some blocks were tested in the as-welded condition whereas others were tested after heat treatment by one of the following methods:

1000° F—Heat with the furnace to 1000° F; hold for 2 hr and furnace cool. The cooling time from 1000 to 600° F was 10 hr.

1100° F—Heat with the furnace to 1100° F; hold for 4 hr and air cool.

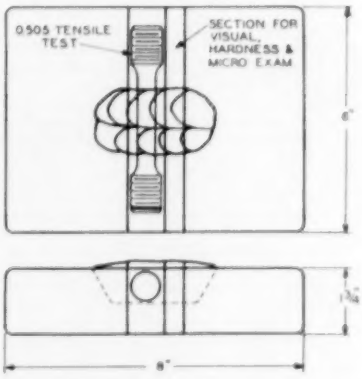

Fig. 3 Locations of macro slice and transverse 0.505 tensile test in welded test block

Table 1B—Materials (Physical Properties)

Type	Class or brand and diam, in.	Condition*	0.505 tensile test: Tensile strength, psi	Yield point, psi	Elongation % in 2 in.	Reduction of area, %
			Base metals			
Gray	ASTM A48-48	As-cast†	24,000–28,600			
	Class No. 25	1650‡	20,000–21,500			
	Specification	As-cast	25,000 min			
Nodular	ASTM A339-51T	As-cast§	69,750–72,500	51,000–55,000	9.0–14.0	
	Grade 60-45-10	1650§	71,000–72,250	54,000	20.5–23.0	21.0–24.0
	Specification	As-cast	60,000 min	45,000 min at 0.2% offset	10.0 min	
			Filler metals			
55 Ni	D, 5/32	As-welded	66,900	50,000	11.5	
	D, 3/16	As-welded	71,700	48,000	13.0	
	B, 1/8	As-welded	57,600	43,000	10.0	
	D, 1/8	1650	65,200	52,000	8.0	
	D, 5/32	1650	71,500	46,000	16.5	
	D, 3/16	1650	72,500	45,000	19.0	
94 Ni	F, 3/16	1650	46,800	36,000	5.0	6.0
	G, 3/16	1650	46,800	34,000	7.0	10.0
	H, 3/16	1650	49,000	37,000	7.0	6.0

* 1650 = 1650° F for 4 hr—furnace cooled. As-welded = All-weld-metal tensile test specimen per standard AWS procedure A298-55T except 400 to 600 preheat and interpass temperature was maintained.
† Range of ten tensile tests.
‡ Range of three tensile tests.
§ Range of four tensile tests.

1650° F—Heat with the furnace to 1650° F; hold for 4 hr and furnace cool. The average cooling rate through the critical zone (1550 to 1300° F) was 250° F per hour. In some cases the block was permitted to air cool after the block had reached 1250° F.

Fig. 4 Cross section of typical sound weld made with 55 Ni electrodes in nodular cast iron. Magnification X 3. (Reduced by $^2/_3$ upon reproduction.) Etchant: Ammonium persulfate

Examination

Each block was examined visually for weld and fusion zone cracks as welding progressed, after welding was completed and after the block had cooled to room temperature. This is reported in the various tables as "surface appearance." Visually sound blocks were then heat treated, if a heat treatment was specified. A cross section of the weld for macroexamination was then removed, as shown in Fig. 3. The visual examination of the etched cross section was recorded as "section appearance." Several representative sections were photographed and are shown in Figs. 4, 5 and 6. If the test block satisfactorily passed these surface and section inspections, a 0.505-in. diam transverse tensile test specimen was machined as indicated in Fig. 3. The results of the inspections and of the tensile tests for various material combinations and welding procedures are shown in Tables 2 to 8. Rockwell "A" hardness measurements were made on most of the macrosections. Some specimens were examined microscopically and the Knoop microhardness of various zones of the weldment were determined. Photomicrographs which show the microhardness impressions as well as the microstructures are given in Figs. 7 to 10. All hardness readings were converted to Brinell and the values are shown in Table 9. The hardness data may help to evaluate the machinability of the weldment as affected by various procedures.

Discussion of Results

Gray Iron

Under the test conditions described above, the 55 Ni and 94 Ni electrodes were of limited suitability for welding gray iron at preheat and interpass

Fig. 5 Cross section of deposit which contains weld cracks, typical of 94 Ni and 55–40 (Ni-Cu) electrodes, in gray or nodular iron, welded at a block temperature range of 250–350° F. Magnification X 3. (Reduced by $^1/_2$ upon reproduction.) Etchant: None

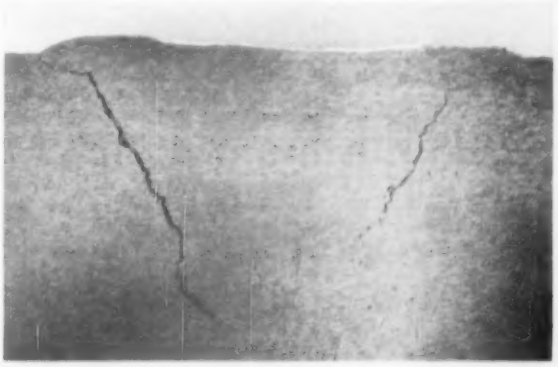

Fig. 6 Cross section of deposit in gray cast iron made with 55 Ni electrodes. The block temperature range of 70–125° F was too low, but this type of cracking was also observed at higher block temperatures. Magnification X 3. (Reduced by $^1/_2$ upon reproduction.) Etchant: None

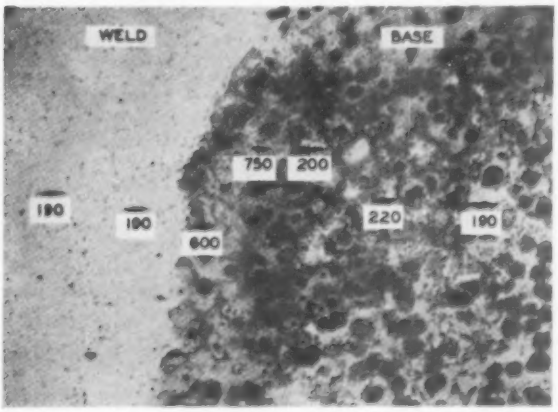

Fig. 7 Cross section of 55 Ni electrodes on nodular iron in the as-welded condition. The numbers above indicate the values of the microhardness (K_{100}) impressions shown on the photomicrograph. Magnification X 100. (Reduced by $^1/_2$ upon reproduction.) Etchant: Nital

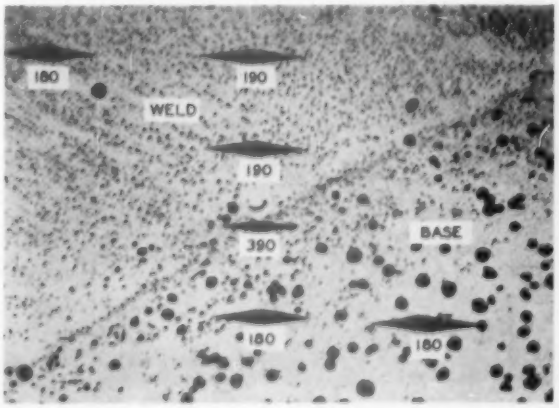

Fig. 8 Cross section of 55 Ni electrodes on nodular iron. After a graphitizing anneal at 1650° F (see Fig. 7 for the as-welded condition). The numbers above indicate the values of the microhardness (K_{1000}) impressions shown on the photomicrograph. Magnification X 100. (Reduced by $^1/_2$ upon reproduction.) Etchant: Nital

Table 2—Gray Cast-Iron Test Blocks Welded with 55 Ni Electrodes

Block temperature, ° F	Test No.	Electrode* Brand	Electrode* Size, in.	Heat† Treatment, ° F	Visual appearance‡ Surface	Visual appearance‡ Section	0.505 tensile test: Tensile strength, psi	0.505 tensile test: Elongation per cent in 2 in.	0.505 tensile test: Fracture‡
70–125	1	A	5/32	None	Sound	FLC		Not made	
	2	B	5/32	None	Sound	FLC		Not made	
	3	B	5/32	1100	Sound	FLC		Not made	
250–350	4	A	5/32	None	Sound	Sound	24,800	...	FL
	5	A	5/32	None	Sound	Sound	15,800	...	FL
	6	A	5/32	1100	Sound	FLC		Not made	
	7	B	5/32	None	Sound	Sound	14,800	...	FL
	8	B	5/32	1100	Sound	Sound	14,900	...	FL
	9	C	5/32	None	Sound	FLC		Not made	
	10	D	5/32	None	Sound	FLC		Not made	
	11	D	5/32	1100	Sound	FLC	10,600	...	FL
450–550	12	B-1	3/16	1650	Sound	Sound	14,700	1.0	B
	13	D-1	3/16	1650	Sound	Sound	19,100	...	FL and B

* "-1" after brand indicates different batch of same brand.
† 1000 = 1000° F for 2 hr; furnace cooled. 1100 = 1100° F for 4 hr; air cooled. 1650 = 1650° F for 4 hr; furnace cooled.
‡ FL = Fusion line. FLC = Fusion line crack. B = Base metal. Sl = Slight, e.g., slight amount of slag. Por = Porosity. W = Weld. WC = Weld crack. TWC = Transverse weld crack. LWC = Longitudinal weld crack.

Table 3—Gray Cast-Iron Test Blocks Welded with 94 Ni Electrodes

Block temperature, ° F	Test No.	Electrode* Brand	Electrode* Size, in.	Heat† treatment, ° F	Visual appearance‡ Surface	Visual appearance‡ Section	0.505 tensile test: Tensile strength psi	0.505 tensile test: Fracture‡
70–125	1	G	5/32	None	Sound	WC		Not made
	2	G	5/32	1100	Sound	WC		Not made
	3§	J	3/16	None	LWC	..		Not made
250–350	4	G	5/32	None	Sound	WC		Not made
	5	G	5/32	1100	Sound	WC		Not made
	6§	J	3/6	None	LWC	..		Not made
	7§	J	3/6	None	LWC	..		Not made
450–550	8	G-1	3/16	1650	LWC	..		Not made
650–750	9	G-1	3/16	1650	TWC	WC		Not made
	10	G-1	3/16	1650	Sound	Sl Por	18,800	FL and B
850–950	11	G-1	3/16	1650	Sound	WC		Not made
	12	G-1	3/16	1650	Sound	Sound	13,600	W, FL and B

* "-1" after brand indicates different batch of same brand.
† 1100 = 1100° F for 4 hr; air cooled. 1650 = 1650° F for 4 hr; furnace cooled.
‡ See footnotes, Table 2.
§ Brand J is a Ni-Cu filler.

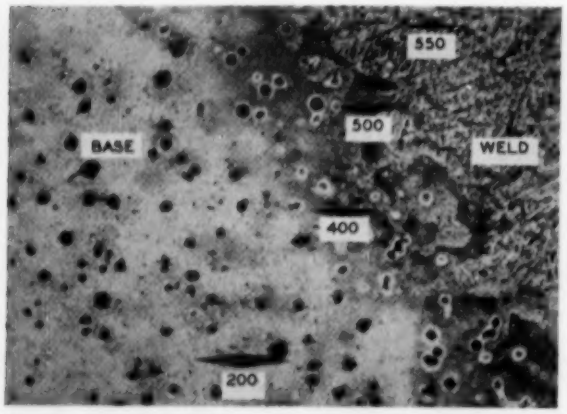

Fig. 9 Cross section of an as-welded nodular iron weld deposit using the inert-gas tungsten-arc process on nodular iron base metal. The numbers above indicate the values of the microhardness (K_{1000}) impressions shown on the photomicrograph. Compare with Fig. 10 for heat treated condition. Magnification X 100. (Reduced by 1/2 upon reproduction.) Etchant: Nital

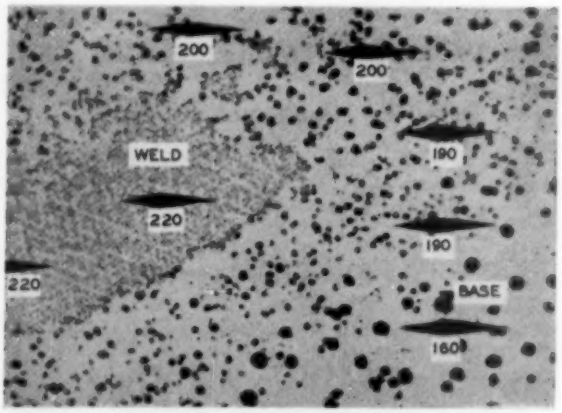

Fig. 10 Cross section of nodular iron weld deposit using the inert-gas tungsten-arc process on nodular iron base metal after a graphitizing anneal at 1650° F. The numbers above indicate the values of the microhardness (K_{1000}) impressions shown on the photomicrograph. Magnification X 100. (Reduced by 1/2 upon reproduction.) Etchant: Nital

temperatures as high as 550° F. Fusion line cracks occurred in weldments made with the 55 Ni electrode (Table 2). In the case of the 55 Ni electrode a higher preheat would undoubtedly prevent fusion line cracking. The 94 Ni electrode was found to be unsuitable because the weld itself cracked even with preheat temperatures as high as 950° F (Table 3).

With a high temperature preheat and subsequent anneal, sound welds with fairly good properties and color match can be made with gray iron filler deposited by the oxy-acetylene or the inert-gas tungsten arc processes. The test data for some welds made at the higher preheat temperatures are shown in Table 4. If color match is not important, a braze weld made with the oxy-acetylene process and a copper-zinc filler will give very satisfactory weldments as shown in Table 5.

Table 4—Gray Cast-Iron Test Blocks Welded with Gray Cast-Iron Filler Metal (Block Temperature 1100° F Minimum)

Test No.	Welding process*	Heat† treatment, ° F	Appearance of cross section‡	0.505 tensile test: Tensile strength, psi	0.505 tensile test: Fracture‡
1	Oxy-acetylene	None	S1 Por	22,000	FL
2	Oxy-acetylene	1100	Sound	23,700	FL
3	Oxy-acetylene	1100	Sound	26,250	B
4	Oxy-acetylene	1100	S1 Por	24,000	W
5	Oxy-acetylene	1100	Sound	24,750	B
6	Inert-gas tungsten Arc—A	None	Por	Not made	
7	Inert-gas tungsten Arc—A	None	Por	Not made	
8	Inert-gas tungsten Arc—A	None	Sound	29,200	B

* "A" after "inert-gas tungsten arc" indicates argon shielding.
† 1100 = 1100° F for 4 hr; air cooled.
‡ Surface appearance was sound in all specimens. See footnote ‡ in Table 2.

Nodular Iron

With a slight preheat of 250–350° F, and 55 Ni electrodes, fusion line cracking of nodular iron was not a problem. The greater ductility of nodular iron compared to that of gray iron was probably responsible for the improvement in weldability. Some satisfactory welds were produced with all brands of 55 Ni electrodes. Although the data are not conclusive, the welds produced by brand B seemed to be more variable than welds produced by the other brands, Table 6.

Very high preheats are required if the 94 Ni electrodes are used and even then the results are not consistently good (Table 7). Weld metal cracking is the major problem. One brand of nickel-

Table 5—Gray and Nodular Cast-Iron Test Blocks Welded with Copper Base Filler Metals

Test No.	Base metal	Welding process	Filler metal*	Block temperature, ° F	Heat† treatment, ° F	Visual appearance‡: Surface	Visual appearance‡: Section	0.505 tensile test: Tensile strength, psi	0.505 tensile test: Yield point, psi	0.505 tensile test: Elongation in 2 in., %	0.505 tensile test: Fracture‡
1	Gray	Oxy-acetylene	Cu-Zn	1100+	None	Sound	Sound	26,000			B
2	Gray	Oxy-acetylene	Cu-Zn	1100+	None	Sound	Sound	14,200			B
3	Gray	Oxy-acetylene	Cu-Zn	1100+	1100	Sound	Sound	25,000			B
4	Nod.	Oxy-acetylene	Cu-Zn	1100+	None	Sound	Sound	28,000			FL
5	Nod.	Oxy-acetylene	Cu-Zn	1100+	None	Sound	Sound	42,400	29,500	4.0	FL
6	Nod.	Oxy-acetylene	Cu-Zn	1100+	1100	Sound	S1 slag	23,000			FL
7	Gray	Arc	Al-5r	70–300	None	W and FLC		Not made			
8	Gray	Arc	Al-Br	600–700	None	W and FLC		Not made			
9	Gray	Arc	Ph-Br	70–300	None	WC		Not made			
10	Gray	Arc	Ph-Br	600–700	None	WC		Not made			

* Cu-Zn = Copper-zinc low-fuming bronze bare wire. ASTM B259–52T Class R CuZn-C. Al-Br = Aluminum bronze. ASTM B225–52T Class E Cu Al-A2. Ph-Br = Phosphor bronze. ASTM B225–53T Class E Cu Sn-A.
†, ‡ See footnotes in Table 2.

Table 6—Nodular Cast-Iron Test Blocks Welded with 55 Ni Electrodes

Block temperature, ° F	Test No.	Electrode*: Brand	Electrode*: Size, in.	Heat† treatment, ° F	Visual appearance‡: Surface	Visual appearance‡: Section	0.505 tensile test: Tensile strength, psi	0.505 tensile test: Yield point, psi	0.505 tensile test: Elongation in 2 in., %	0.505 tensile test: Reduction of area, %	0.505 tensile test: Fracture‡
70–125	1	B	5/32	None	Sound	FLC			Not made		
	2	B	5/32	1100	Sound	FLC			Not made		
	3	B-1	3/16	1650	Sound	Sound	50,000		2.0		W
	4	B-1	3/16	1650	Sound	S1 Por	35,400				FL and W
	5	D	3/16	1650	Sound	Sound	52,000	46,250	2.0		W
250–350	6	A	5/32	None	Sound	Sound	53,200		10.0		B
	7	A	5/32	None	Sound	Sound	53,000	40,000	12.0	28.0	B
	8	A	5/32	1100	Sound	Sound	55,200		10.0		FL
	9	B	5/32	None	Sound	WC	13,100				W
	10	B	5/32	1100	Sound	FLC	28,200				FL
	11	B-2	5/32	1650	Sound	Sound	57,500	51,250	4.5		B
	12	C	5/32	None	Sound	S1 Slag	58,900	45,800	9.0	21.0	B
	13	D-1	5/32	None	Sound	Sound	53,000	40,800	9.0	28.0	B
	14	D-1	5/32	1100	Sound	Sound	54,200	41,800	14.0	28.0	B
	15	D-1	5/32	1650	Sound	S1 Slag	52,000	39,000	5.0	6.0	W
	16	E	5/32	1650	Sound	Sound	55,700	49,500	4.5		W

* "-1" and "-2" after brand indicates different batch of same brand.
†, ‡ See footnotes in Table 2.

Table 7—Nodular Cast-Iron Test Blocks Welded with 94 Ni Electrodes

Block temperature, ° F	Test No.	Electrode* Brand	Size, in.	Heat† treatment, ° F	Visual appearance‡ Surface	Section	0.505 tensile test: Tensile strength, psi	Yield point, psi	Elongation in 2 in., %	Fracture‡
70–125	1	G	5/32	None	Sound	WC		Not made		
	2	G	5/32	1100	Sound	WC		Not made		
250–350	3	F	3/16	None	LWC	...		Not made		
	4	G	5/32	None	Sound	W and FLC		Not made		
	5	G	5/32	1100	Sound	W and FLC		Not made		
	6	G-1	3/16	None	LWC	...		Not made		
	7	H	3/16	None	WC	...		Not made		
	8§	J	3/16	None	LWC	...		Not made		
450–550	9	F	3/16	None	LWC	...		Not made		
	10	G-1	3/16	None	LWC	...		Not made		
	11	H	3/16	1650	Sound	Sound	37,500	...	3.0	W
	12	H	3/16	1650	Sound	WC	33,400	...	...	W and FL
	13§	J	3/16	None	LWC	...		Not made		
650–750	14	F	3/16	None	LWC	...		Not made		
	15	G-1	3/16	1650	Sound	WC	33,500	...	1.5	W
	16	G-1	3/16	1650	Sound	Sound	57,300	48,500	5.0	W and B
	17	H	3/16	1650	Sound	Sound	48,000	...	4.0	W and B
	18§	J	3/16	None	LWC	...		Not made		
850–950	19	F	3/16	1650	WC	WC		Not made		
	20§	J	3/16	None	LWC	...		Not made		

* "-1" after brand indicates different batch of same brand.
†, ‡ See footnotes in Table 2.
§ Brand J is a Ni-Cu alloy.

copper filler was tested. As shown in Table 7, brand J, a sound weld could not be made with preheat temperatures as high as 900° F.

Heat treatment of nodular iron welded with 55 Ni electrodes seems to be unnecessary if machinability is not a factor. Satisfactory tensile properties were obtained from as-welded specimens. Based on the hardness tests, the 1650° F heat treatment of the weldment appears to be desirable for good machinability of the heat-affected zone.

If nodular iron castings can be given a high preheat, at least 1100° F, a filler metal which deposits an iron with a nodular graphite structure can be used. As shown in Table 8, satisfactory weldments were produced with the commercially available cerium-bearing nodular filler by the oxy-acetylene, inert-gas tungsten arc and carbon arc processes.

A sound weld can be made with copper zinc filler metal in nodular iron, but this material is unsuitable if the base metal strength or color must be matched. The data in Table 5 show that failure occurred at the bond line.

Hardness Measurements

Fusion welding will produce a hard heat-affected zone in gray and nodular iron. Hardness measurements were made with the Rockwell tester or Knoop microhardness tester in order to determine the effect of welding and subsequent heat treatment on the hardness of the heat-affected zone. As shown in Table 9, a converted hardness of 616 Bhn was found in the heat-affected zone of an as-welded specimen. A stress relief, and especially an anneal heat treatment, reduced the hardness so that the weldment could be readily machined.

Metallography

Figure 7 shows that a 55 Ni weld deposit contained some graphite in the

Table 8—Nodular Cast-Iron Test Blocks Welded with Nodular Cast-Iron Filler Metals

Block temperature 1100° F minimum

Test No.	Welding process*	Heat† Treatment, ° F	Visual appearance‡ Surface	Section	0.505 tensile test: Tensile strength, psi	Yield point, psi	Elongation in 2 in., %	Fracture‡
1	Oxy-acetylene	1000	Sound	Sound	55,000	...	1.0	W and FL
2	Oxy-acetylene	1000	Sound	S1 Por	56,000	...	...	W and FL
3	Oxy-acetylene	1000	Sound	S1 Slag	51,000	...	...	W and FL
4	Oxy-acetylene	1650	Sound	Sound	56,000	48,000	2.0	W and B
5	Oxy-acetylene	1650	Sound	Sound	69,000	53,000	6.0	W and B
6	Oxy-acetylene	1650	Sound	Slag	46,350	45,000	1.5	W
7	Oxy-acetylene	1650	Sound	Por	41,500	...	1.0	W
8	Oxy-acetylene	1650	Sound	Slag and por	42,750	...	1.0	W
9	Inert-gas tungsten—A	None	Sound	Sound	54,700	...	8.0	B
10	Inert-gas tungsten—A	1100	Sound	Sound	53,700	...	5.0	FL
11	Inert-gas tungsten—A	1650	Sound	Sound	58,400	45,400	6.0	FL
12	Inert-gas tungsten—He	1650	Sound	Sound	61,000	56,000	2.5§	W and B
13	Inert-gas tungsten—A	1650	Sound	S1 por and slag	58,300	48,000	4.0	W
14	Carbon-arc	1650	Sound	Sound	64,000	52,000	13.5	B
15	Carbon-arc	1650	Sound	Sound	60,700	...	3.5	W
16	Carbon-arc	1650	Sound	S1 por	53,200	48,200	3.0	W

* "A" and "He" after "Inert-gas tungsten" indicates argon and helium shielding, respectively.
†, ‡ See footnotes in Table 2.
§ Weld not centered; broke outside gage length.

Table 9—Hardness of Welded Blocks

Test No.	Block temperature, ° F—avg	Heat treatment, ° F	Maximum hardness—Bhn: Base metal — Unaffected	Base metal — Heat-affected zone	Weld metal — First pass	Weld metal — Remainder	Converted from*
			Gray iron—55 Ni electrodes (see Table 2)				
12	500	1650	108	130	147	153	RA
13	500	1650	112	117	153	159	RA
			Gray iron—94 Ni electrodes (see Table 3)				
9	700	1650	112	121	153	147	RA
10	700	1650	117	135	139	150	RA
11	900	1650	106	108	153	147	RA
12	900	1650	108	121	141	147	RA
			Nodular iron—55 Ni electrodes (see Table 6)				
3	100	1650	162	176	147	153	RA
4	100	1650	147	159	162	169	RA
5	100	1650	141	153	162	169	RA
13	300	None	174	616	174	174	K_{100}
15	300	1650	145	362	174	174	K_{1000}
			Nodular iron—94 Ni electrodes (see Table 7)				
11	500	1650	108	125	147	135	RA
12	500	1650	153	147	153	139	RA
15	700	1650	141	169	159	159	RA
16	700	1650	147	147	159	153	RA
17	700	1650	140	135	155	150	RA
19	900	1650	153	162	153	153	RA
			Nodular iron—nodular filler (see Table 8)				
2	1100+	1000	180	265	210	210	RA
3	1100+	1000	176	305	210	210	RA
9	1100+	None	145	530	250	530	K_{1000}
10	1100+	1100	145	490	250	530	K_{1000}
11	1100+	1650	156	176	205	205	K_{1000}
12	1100+	1650	162	169	180	180	RA
13	1100+	1650	153	147	176	176	RA
14	1100+	1650	147	141	169	162	RA
15	1100+	1650	162	162	162	159	RA
16	1100+	1650	147	159	169	162	RA
			Nodular iron—copper-zinc filler (see Table 5)				
4	1100+	None	216	240	112	112	K_{100}

* RA = Rockwell "A." K_{100} = Knoop—100 g load. K_{1000} = Knoop—1000 g load.

as-welded state. The heat-affected zone even though hard, contained some spheroidal graphite. After a heat treatment at 1650° F, Fig. 8, the amount of graphite in the weld deposit increased and the heat-affected zone was softened. A somewhat hard constituent remained at the fusion line.

A nodular iron deposit had a dendritic appearance as shown in Fig. 9. A full anneal softened this carbide structure with the formation of ferrite and spheroidal graphite particles (Fig. 10).

Summary and Conclusions

A test block and an evaluation procedure have been developed to discriminate between filler metals and welding processes for welding gray and nodular cast irons. The test block is examined visually during and after welding for the presence of weld and base metal cracks. A transverse section of the block is examined for soundness and, if it is sound, a transverse 0.505-in. diam tensile specimen is machined and tested.

The following general conclusions can be drawn from the limited number of tests made:

In these tests, most brands of 55 Ni electrodes produced sound weld deposits whereas the 94 Ni electrodes produced cracked weld deposits.

With a preheat and interpass temperature range of 250–350° F, nodular iron was satisfactorily welded with 55 Ni electrodes. Good tensile properties were obtained from as-welded specimens, but annealing would be desirable to soften the heat-affected zone, if the weld must be machined. With a higher preheat temperature, 1100° F, nodular iron was satisfactorily welded by the oxy-acetylene, inert-gas tungsten-arc, and carbon-arc processes with nodular iron filler rod. These welds were annealed in order to soften them and to produce the nodular graphite structure in the weld deposit.

Gray iron was more difficult to weld than was nodular iron because the inherent low ductility of gray iron promotes the formation of fusion line and base metal cracks. Apparently sound gray iron weldments produced by the metal-arc process with nickel-base electrodes tended to fail at the fusion line at relatively low strength.

DISCUSSION BY L. M. PETRYCK AND G. R. PEASE

We have already commended the authors privately for a job well done and would like to do the same here publicly.

The test specimen is one which we, like the authors, have used for several years and upon which we have learned to depend for estimating crack resistance. In fact, it was on the basis of the performance in this sort of test that the arc welding of gray iron, and later ductile iron, progressed in stages, utilizing nickel-copper alloys, the 90–95% nickel alloys and finally the 60/40 nickel-iron alloys.

L. M. Petryck and G. R. Pease are Research Metallurgists, International Nickel Co., Research Laboratory, Bayonne, N. J.

It is perhaps appropriate at this time to attempt to correct a rather widespread impression; that the 60/40 nickel-iron alloy was primarily the result of efforts to downgrade the nickel type of electrode in compliance with government-ordered nickel conservations measures. The timing of the first announcement of the 60/40 electrode was inadvertently such as to create this impression, but actually the merits of the nickel-iron type of electrode, with respect to resistance to hot cracking, were well known when it was introduced to the industry.

The quantitative demonstration that nodular, or ductile iron is easier to weld than gray iron will be welcome news to those who are including the use of this new material in their engineering plans.

DISCUSSION BY HALLOCK C. CAMPBELL

This is a very stimulating paper. Perhaps that is only natural, for as soon as we develop means of measuring a phenomenon, the "art" has become a science, and it is characteristic of a science that each experiment proposes new experiments. I hope I will not ask the authors more questions than there is time to answer, but I do envisage many uses for their test method.

The small test block is very advantageous. It is simple, inexpensive, apparently reproducible. I judge that the reproducibility stems from the easy casting properties of the nodular and gray irons, because I recall a similar test clock made of 15Cr-35Ni (Type HT) alloy which was unsatisfactory. The trouble there was traced to shrinkage cracks at the base of the groove. The 15/35 test welds always cracked severely in the root pass, until the test block was redesigned as a slotted groove. No attempt was made to cast a thicker plate, which may be one of the factors in the success of the present test; to my memory the solid high alloy castings were only 1 in. thick.*

Would the authors comment on the correlation of their test with production experience? For example, has there been evidence from the field that the 55 Ni electrode performs better in production welding of nodular iron than the 94 Ni type? Does the test block show any advantage of the traditional intermittent string-bead "cold welding" techniques long used for cast irons? I note that there has been no attempt to prescribe a pass sequence, which may mean that the test is insensitive to that variation.

The nickel electrodes were not satisfactory in the tests on gray iron. Might they have been successful when given the same 1100° F preheat used with the gray iron electrodes? Would the base metal cracking have been avoided when using a "cold welding" technique?

The welding of nodular iron with cerium-bearing filler metal is an interesting achievement. I know the inoculating of castings is a delicate operation, because of the tendency to lose the inoculant through oxidation or volatilization. Does the test block indicate any evidence of difficulty in obtaining a nodular microstructure because of losses related to the use of high currents, high preheat, or a poorly adjusted oxy-acetylene flame? Possibly the hard constituent at the fusion line in Fig. 8 is an indication of the tendency of the nodular iron to revert to white or gray iron through loss or inactivation of the nodularizing material.

Hallock C. Campbell is Director of Research, Arcos Corp., Philadelphia, Pa.

* Thomas, R. David, Jr., "Welding of High-Alloy Castings," The Welding Journal, 31 (1), Research Suppl., 27-s to 32-s (1952).

AUTHORS' REPLY

A large number of questions, comments and helpful suggestions are always appreciated by the authors of a paper because they indicate that someone is really interested in the subject. We thank those who have discussed the paper orally at the meeting and the International Nickel Co. and Arcos Corp. for their written comments.

The comments of Messrs. Petryck and Pease do not require a reply. It is consoling to know that others have experienced hot cracking with the 94 Ni filler and that the 55 Ni filler was developed to overcome this trouble. We were glad to hear that Inco has used a similar test block, but were disappointed that they did not relate some of their experiences. For example, did they experience the same fusion line cracks when welding gray iron with the 55 Ni electrode?

Dr. Campbell has asked a number of very valuable questions which we felt would certainly be asked by a number of people. It is not possible to draw direct comparisons between the results obtained in the test block and the results obtained on production repairs. Repairs on defective castings can be either similar, more difficult, or less difficult to make than the weld in the groove in the test block. The soundness and the degree of restraint encountered in production castings may be different from that found in the simple test block. Our major objective was to obtain a comparison between various filler materials and welding processes. Naturally we have made use of the information we have obtained on the test block for improving casting repairs, but we realize that other factors may cause a change to be made in the welding procedure.

The difference in restraint between the test block and production castings may explain why many people have obtained satisfactory repairs with the 94 Ni and the 60Ni–40Cu fillers. On the other hand, how many times have repair welds been examined critically for defects through the cross section? A tensile test across the joint is seldom checked. Also, if cracks had been present, they may have been obliterated by peening. If the repair must hold water pressure we know immediately if the weld is satisfactory, but if the casting serves as a base for a piece of machinery, the repair need only have cosmetic effect, and sometimes not even that, to be called satisfactory.

In some of our initial tests on gray iron, we did try the "cold welding" technique mentioned by Dr. Campbell. A half inch of weld was made and was then peened. Those specimens contained fusion line cracks and the procedure was therefore discarded.

We did not attempt to prescribe a definite pass sequence, but permitted the welder to proceed as he judged best. A number of different welders were used for the tests and therefore we believe that pass sequence is not a significant factor.

It is possible that the 55 Ni electrodes would produce sound welds in gray iron if an 1100° F preheat could be used. This high a preheat is difficult to maintain with a metal arc electrode; auxiliary heating is required. If the part can be preheated to 1100° F we would prefer to use gray iron filler and the oxy-acetylene process.

A nodular iron filler rod should be applied with as little heat as possible. Prolonged heating or puddling with the oxy-acetylene torch will cause an excessive loss of the nodularizing element. Possibly that occurred even in the weld made with the inert-gas tungsten-arc process shown in Fig. 10. It appears that a portion of the weld has reverted to fine flake graphite, but the small amount of flake graphite was insufficient to affect the over-all efficiency of the joint.

The hard constituent observed at the fusion line (Fig. 8) of a weld made with 55 Ni electrodes is probably caused by a diffusion of nickel. This higher alloy zone may require a very slow furnace cool for maximum softening. The weld shown in Fig. 10 was made with the nodular iron filler rod and there is no evidence of the hard zone. Even if there had been a great loss of the nodularizing element, the loss could not cause the fusion line to be hard. If the fusion zone had reverted to gray iron this zone could still be completely softened by the heat treatment, provided that no nickel was present.

After the 1955 AWS National Fall Meeting, we decided to conduct a few

Table 10—Nodular Cast-Iron Test Blocks Welded with 15Cr–70Ni + MoCb Electrodes

Block temp., ° F	Test No.	Heat treatment,* ° F	0.505 tensile test: Tensile strength, psi	Yield point, psi	Elongation in 2 in., %	Fracture†
250–350	1	None	52,000	..	1.5	FL
	2	1650	65,000	52,000	6.0	FL
	3	1650	61,500	51,500	4.0	FL & B
	4	1650	62,750	50,500	4.0	FL

Chemical analysis of 15Cr–70Ni + MoCb electrode

C, %	Mn, %	P, %	S, %	Si, %	Ni, %	Ni, %	Mo, %	Cb + Ta, %	Cu, %	Fe, %
0.05	1.49	0.016	0.007	0.34	70.18	15.24	0.80	1.87	0.17	9.82

* See Table 2, footnote b.
† See Table 2, footnote c.

tests with a new electrode which is recommended for joining many combinations of dissimilar metals. The chemical analysis of the weld deposit is shown in Table 10. Four nodular iron blocks were welded at a preheat and interpass range of 250–350° F. One block was left in the as-welded state and the other three were heat treated at 1650° F for 4 hr. Transverse 0.505 tensile tests were made on each block and the results are given in Table 10.

It appears that this electrode may be better than the 55 Ni electrode for welding nodular iron. Additional tests with this electrode are in progress as well as tests with other brands of 14-Cr–75Ni electrodes and with 15Cr–35Ni electrodes.

TENSILE-IMPACT PROPERTIES OF COMMERCIALLY PURE TITANIUM AT VARIOUS TEMPERATURES

Welded and nonwelded specimens tested at −65, 70 and 600° F to determine tension-impact energy, elongation and reduction in cross-sectional area

BY O. H. HENRY AND B. Z. HYATT

SUMMARY. After designing the necessary jig and preparing the necessary equipment, the authors conducted tensile-impact tests with specimens of commercially pure titanium. Two types of titanium specimens were tested: welded and nonwelded. Of the former type, there were, first, those specimens with the welded bead intact and, second, those specimens with the welded bead removed. The welded and nonwelded specimens were tested at the following temperatures: at −65° F, with the use of a cold chamber; at 70° F, without the use of any chamber; and at 600° F, with the use of a hot chamber.

Three important values were measured and calculated: first, the tension-impact energy expressed in foot-pounds; second, the elongation expressed in percent; and third, the reduction in cross-sectional area expressed in percent.

Nonwelded Specimens. For the nonwelded specimens, it was found that at the three test temperatures the tension-impact energy did not markedly change. Therefore one may conclude that at the temperatures tested −65, 70 and 600° F, the energy-absorbing characteristics of commercially pure titanium are similar.

The percent reduction in cross-sectional area and the percent elongation showed

O. H. Henry is Professor of Metallurgical Engineering at the Polytechnic Institute of Brooklyn. B. Z. Hyatt is at present a Graduate Student in Metallurgy at the University of Illinois.

Paper is based on a Thesis presented by B. Z. Hyatt submitted in partial fulfillment for the degree of Bachelor of Metallurgical Engineering at the Polytechnic Institute of Brooklyn.

Fig. 1 Tensile-impact jig and pendulum head

similar increases with temperature. At 70° F both values were slightly higher than the values at −65° F. However, the values at 600° F were markedly above those at 70° F. Hence, one may state that the ductility of the titanium, as revealed by the percent elongation and the percent reduction in cross-sectional area, is much greater at 600° F than at 70° F and is slightly greater at 70° F than at −65° F, while the foot-pounds of energy required to fracture the specimens remained fairly constant at these same temperatures.

Welded Specimens. For the welded specimens, it was found that at the three test temperatures, the average foot-pound value for those specimens with the beads intact was higher than the average foot-pound value for those specimens with the beads removed. The average values were reported with the scatter above and below these values also indicated. The average foot-pound values for the specimens with the bead removed increased markedly from −65 to 70 to 600° F, while the average foot-pound value for the specimens with the bead intact does not increase from −65 to 70° F but does decrease from 70 to 600° F. Hence, one may observe the average foot-pound value for the specimens with the bead intact was better at −65 and 70° F than at 600° F, whereas the average foot-pound value for the specimens with the bead removed was best at 70° F.

The percent reduction in cross-sectional area and percent elongation in 2 in. increase with increasing temperature with the average values for the specimens with the bead intact being higher at each successively higher temperature.

Introduction

The physical properties of titanium and titanium alloys do not diminish to any great extent within a wide range of temperatures.

There is a lack of data on the tensile-impact properties of titanium.

Method of Testing

Tension-impact tests were performed using the Tinius Olsen Impact Machine of the pendulum type. A special jig which gripped and held in position the titanium sheet specimen was designed to facilitate tension-impact testing. The jig is shown in Fig. 1.

The pendulum when released from a fixed height will deliver an energy load to the cross-arm of the jig which instantaneously transmits the energy to the specimen, thus subjecting the specimen to tension and impact simultaneously. At the lowest position of its swing the pendulum will have the maximum kinetic energy. After the partial transmission of energy, the pendulum will rise to a specific height which is dependent upon the energy remaining. The difference in energy of the pendulum before and after impact is the energy absorbed by the specimen. When the pendulum rises, a pointer is pushed along a calibrated semicircular scale, and thus the tension-impact value in foot-pounds is indicated.

As the pendulum falls and delivers its blow, energy losses are incurred by vibration of frame and anvil, and by friction at the bearings. These energy losses could not be calculated but are thought to be negligible. There was an additional energy loss, which was the energy absorbed by the cross-arm. This energy was thought to be constant.

Selecting the Specimen

The titanium which was available to the authors was in sheet form of 0.093 in. gage. The chemical composition of the titanium sheet in the annealed condition is as follows: 99% titanium, 0.2% max. carbon, 0.8% all other elements. Since there was no standard form of tension-impact specimen for sheet material, the authors proposed the use of a standard rectangular tension test specimen with a 2-in. gage length. The specimens were cut and machined to shape with the longitudinal grain parallel to the length (see Fig. 2).

Preparing Special Environments

In addition to the room temperature or 70° F tests, the tension-impact test required two other environments: cold, −65° F and hot, 600° F. Previous researchers found that a mixture of dry ice and alcohol would provide an adequate medium for cooling the specimen and that a molten salt would be a suitable medium for heating the specimen. A cooling chamber, a copper-lined wooden tank with thick walls, and a heating chamber, a natural gas furnace lined with refractory bricks within which a steel pot, holding the salt, was placed, were available to use for the experiment.

During the test the cold bath was held at −70 ± 5° F to compensate for any heating of the specimen, and the hot salt was held at 620 ± 10° F to compensate for any cooling of the specimen during transference to the machine.

Testing

First, the dimensions of the specimens, minimum width, average thickness were recorded. Second, hardness readings were taken on the ends of the specimens. Third, a 2-in. gage mark was punched on the specimens. Fourth, the specimens were placed in the jig in the following manner.

One end was placed in the stationary base, fitting snugly against the shoulders of the base; then the top plate, whose under surface was serrated, was placed on the specimen which did not lie flush with the base but projected slightly above it; next the bolts were tightened.

The other end of the specimen was placed on the base of the cross-arm and positioned between the shoulders of the center plates, and then the cross-arm top plate was secured to the base.

The head of the pendulum was placed against the plate of the cross-arm and by sliding the wedges, exact contact was made between the head and the plate.

For tests at low or high temperature the above procedure was carried out, and then the jig was pivoted so that the entire assembly could be immersed in the cold or hot medium. When the specimen attained the proper temperature, the jig was quickly pivoted from the medium to the machine, clamped into position, and then the pendulum was released by a trigger mechanism. After several trials, the authors were able to transfer the jig, clamp it in position, and release the pendulum in 5 seconds.

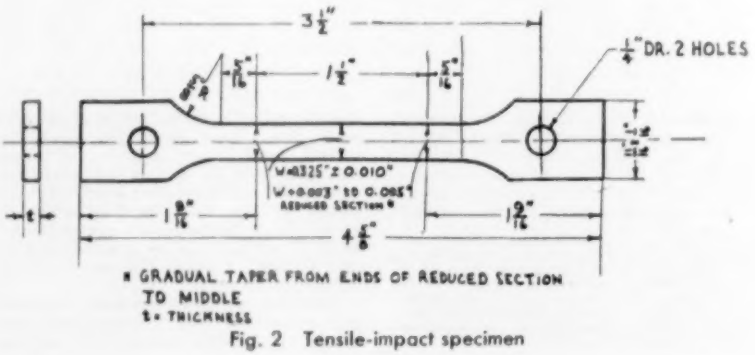

Fig. 2 Tensile-impact specimen

Table 1—Nonwelded Specimens Statistical Distribution Values

	Ft-Lb			Tensile-impact elongation in 2 in. (%)			Reduction in cross-sectional area (%)		
	−65° F	70° F	600° F	−65° F	70° F	600° F	−65° F	70° F	600° F
$\bar{X}$*	125.16	129.06	123.70	12.96	15.61	27.39	36.20	38.27	57.78
σ	7.8	8.7	10.1	1.1	1.1	3.0	1.7	2.3	3.7
C_v	6.2%	6.8%	8.2%	8.5%	7.2%	11%	4.7%	6.0%	6.4%

* $\bar{X}$, Arithmetic mean. σ, Standard deviation. C_v, Coefficient of variation.

Welding

Specimens of RC 70A, commercially pure titanium, were welded using the following procedure:

First, two 6-in. wide strips of titanium were beveled to form a double vee (although the welding was done from one side); second, the strips were placed on a steel backing plate; third, the arc was struck and the double-vee butt joint was formed.

Helium gas, flowing at the rate of 10 cfh, passed under the titanium joint, while argon gas, flowing at a rate of 18–20 cfh, passed over the upper surface of the welded joint. A thoriated tungsten electrode with a current of 100 amp was used, and the argon gas flowed around the electrode. To prevent contamination of the welded joint, a second argon following torch was used. Thin strips of the titanium were used for the filler metal.

The titanium was welded with the elongated grain (due to rolling) perpendicular to the joint. The specimens were neither preheat treated nor postheat treated.

Next the titanium was cut and tension-impact specimens were made. The beads of some of the specimens were removed, thus forming a flat surface.

Results

I. Nonwelded Specimens

There were approximately 28 tensile-impact specimens tested at each of the three temperatures −65, 70 and 600° F. In analyzing the results, the authors first calculated the arithmetic mean which is a measure of the central tendency.

Second, the authors calculated the standard deviation which is a measure of the dispersion of values.

Third, the authors calculated the coefficient of variation; which can be used to compare dispersions (see Table 1).

The authors ascertained the following information from frequency histograms.

1. Foot-Pounds. For −65, 70 and 600° F the values do not appear to differ by too much. They lie within 120 and 140 ft-lb. Thus one may conclude that the tensile-impact strength does not differ considerably at the temperatures −65, 70 and 600° F.

2. Reduction in Cross-Sectional Area (%). For −65° F the reduction in cross-sectional area was the least ($\bar{X}$ = 36%). At 70° F the value increased slightly, but for 600° F, the value ($\bar{X}$ = 58%) was almost twice as great as the value at −65° F and 1¾ times as great as the value at 70° F. Thus the reduction in cross-sectional area increases slightly from −65 to 70° F and increases considerably from 70 to 600° F.

3. Tensile-Impact Elongation in 2 In. (%). For −65° F the elongation in 2 in. was the least ($\bar{X}$ = 13%). At 70° F the value ($\bar{X}$ = 16%) increased slightly, but for 600° F, the value ($\bar{X}$ = 27%) was almost twice as great as the value at −65° F and almost 1½ times as great as the value at 70° F. Thus the elongation appears to respond similarly to the reduction in cross-sectional area, increasing slightly from −65 to 70° F, and increasing considerably from 70 to 600° F.

II. Welded Tensile-Impact Specimens

There were approximately 16 specimens, 8 with beads and 8 without beads, which were tested at each of the three temperatures, −65, 70 and 600° F.

Since the number of specimens tested was small, the authors deemed that the best manner to present the results would be in the form of average curves.

Foot-pounds, reduction in cross-sectional area (%) and tensile-impact elongation in 2 in. (%) were plotted against temperatures. These curves also indicate the scatter about the average.

The authors obtained the following information from these graphs.

1. Foot-Pounds. With Bead: For −65° F the average value is 113 with the scatter 18% above and 22% below. The average value remains the same at 70° F and decreases to 105 at 600° F with the scatter the same at both temperatures as that of −65° F.

Without Bead: At −65° F the average value is 80 with a scatter 18% above and 20% below; at 70° F the average value increases to 93 and at 600° F decreases to 64 with the scatter for both these temperatures about equal to the −65° F values.

By comparing the average values of the specimens with bead to those without bead, one can readily see that the former have the greater tensile-impact strength and the best values appear to be at the temperatures −65 and 70° F.

2. Reduction in Cross-Sectional Area (%). With Bead: At −65° F the average value was 13% with a 5% scatter above and below. The average value increased to 27% at 70° F and further increased to 53% at 600° F with the scatter remaining the same for both temperatures and equal to the −65° F value.

Without Bead: The average value for −65° F was 13% with a large scatter of 100% above and below. For 70° F the average value increased to 34% with 14% scatter above and 29% below. There was a further increase in the average to 56% at 600° F with a decrease in the scatter to 14% above and 11% below.

One may surmise the following: the percent reduction in cross-sectional area is greater at 600° F than at 70° F and greater at 70° F than at −65° F for both beaded and nonbeaded specimens. The percent reduction was greater for the beaded specimens than for the nonbeaded specimens.

3. Tensile-Impact Elongation in 2 In. (%). With Bead: For −65° F the average value was 11% while the scatter was 9% above and below. At 70° F the average increased to 13% with scatter 8% above and 12% below. The average sharply increased to 24% at 600° F with scatter 7% above and 10% below.

Without Bead: The average value was 7% at −65° F with scatter 16% above and 50% below. At 70° F the average increased to 10% with scatter 16% above and 38% below. There was a further increase in the average to 19% at 600° F with scatter 13% above and 13% below.

One may conclude that the tensile-impact elongation is greater at 600° F than at 70° F and greater at 70° F than at −65° F. Also the percent elongation is greater for beaded than for nonbeaded specimens.

In the total analysis one may conclude that the specimens with the bead had properties which were better than the specimens without the bead.

In removing the bead, and filing the adjacent area, the machinist effectively made the cross-sectional area smaller and thus the volume within the gage length was smaller. Hence, the foot-pounds of energy which could be absorbed by the specimen without the bead was less.

Acknowledgment

The authors wish to express their appreciation to the Republic Aviation Corporation for supplying the titanium specimens to be tested at specific temperatures to obtain data that would be of value to the aircraft industry.

RESISTANCE OF LOW-ALLOY STEEL PLATES TO BIAXIAL FATIGUE

The relative resistance to repeated loading of several low-alloy steels and a carbon steel are compared; also, the effect of notches and welds upon the fatigue properties of each material is reported

BY C. E. BOWMAN AND T. J. DOLAN

SYNOPSIS. The resistance of plate specimens of several low-alloy steels to repeated loading under a state of biaxial stress was studied and compared to similarly loaded specimens of a carbon steel commonly used in pressure vessels. Tensile stresses were developed in the top surface of the plate, the ratio of the principal stresses simulating that in the shell of a cylindrical pressure vessel. In general three types of specimen representing various degrees of fabrication were studied for each of the eight steels. They were: plain or unnotched plates, notched plates and plates with a hand-deposited weld bead along their longitudinal centerline. A few random tests were made of plates with simulated fittings or with transverse welds for some of the steels.

This paper compares the relative resistance to repeated loading of the various steels and reports the effect of notches and welds upon the fatigue properties of each material. The steels having the highest static tensile strength demonstrated the greatest resistance to repeated loading, but their superiority over plain carbon steel plates was not as large as might be indicated by comparing the ratio of their yield or ultimate strengths to those of the carbon steel. The fatigue strengths of welded specimens were comparable to those for the unnotched plate, but the data showed more scatter. The increased scatter might be attributed to two factors: (*a*) grinding the weld bead flush polished the weld and adjacent plate in the most highly stressed region which improved the fatigue life; (*b*) fatigue cracks developed out of minute flaws in the weld in certain plates thus reducing their fatigue life.

A small notch (having a depth of 0.01 in., a root radius of 0.01 in. and a length of 3/8 in. perpendicular to the direction of the maximum stress) was sufficient to reduce the allowable cyclic strain range by a factor of 1.25 or more. The studies emphasize the importance of eliminating flaws such as rolling marks, punchmarks, stamped numbers and chisel marks from the surface of a high-quality pressure vessel that is subjected to repeated loading. All welds should be ground flush and inspected for blowholes or undercutting as those conditions may nucleate a fatigue crack. It should be emphasized that all of the steels studied demonstrated a remarkable resistance to progressive fracture under repeated loading at high strain levels. A pressure vessel designed and built *eliminating obvious flaws or severe stress raisers* could be operated at stress levels well in excess of current code limitations without fear of fatigue failure.

C. E. Bowman is Associate Professor and **T. J. Dolan** is Head, Department of Theoretical and Applied Mechanics, University of Illinois, Urbana, Ill.

Presented at AWS 1955 National Fall Meeting held in Philadelphia, Pa., October 17–21.

Introduction

Current design codes for pressure vessels have made it impractical to use low-alloy high-strength steels in preference to carbon steels for most applications because little or no advantage may be taken of the improved mechanical properties of the alloy steel. New demands, however, are being made upon the industry which virtually require that codes be revised to permit an increase in the allowable design stresses for certain classes of vessels. It has been proposed that an increase in the allowable stress should be accompanied by a requirement that the fabricated vessel be of highest quality, reducing all stress raisers to a minimum, and by the introduction of low-alloy high-strength steels that have yield strengths two or three times that of the carbon steels.

While in the past few failures of pressure vessels have been attributed to fatigue, the proposed increase in allowable design stresses and the use of new steels has made it imperative that their fatigue properties be given careful consideration. A coordinated study of the suitability of the low-alloy steels for pressure vessel applications including a study of the effect of various design details and fabrication operations upon their fatigue resistance has been undertaken by the Pressure Vessel Research Committee. A comparison is being made in all cases between the higher strength steels and a carbon steel, A201, with which manufacturers and users of pressure vessels have had long experience. This paper is the third report[1, 2] on one phase of that program conducted at the University of Illinois in cooperation with the PVRC.

The research was designed to determine the relative resistance to repeated loading for the various steels when subjected to loads that would cause failure in a relatively small number of cycles. To accomplish that goal all plates were subjected to loads sufficient to develop strains in the central region of their top surface which were near or above the yield point strain for the material; the studies were aimed primarily at surveying the relative fatigue strengths for repetitions of less than 5×10^5 cycles of loading. The hydraulic loading was applied from zero to maximum pressure at a frequency of about 100 cpm.

A detailed description of the design of the rectangular plate specimens, of the loading fixtures and of the hydraulically operated testing machine was given in the previous papers. Briefly, the specimen (similar to that used by Blaser, Tucker and Kooistra[3]) was designed to develop a state of biaxial tension in the central region of its top surface, the ratio of the principal stresses being approximately 2 to 1. The design not only permitted a comparison of the relative fatigue properties of various grades of steel plate, but it was also well adapted for comparing the effects of various types or degrees of fabrication such as welding or notches upon the resistance of a material to withstand repeated cycling.

The two previous papers describe the results obtained for A201 Grade A and A302 Grade B as well as more limited studies of A225 Grade A and 90B* steels. The previous studies covered unnotched and notched plates, and effect of a longi-

* The code used by Gross and Stout[2] to designate these materials has been adopted for this paper.

Table 1—Nominal Chemical Analysis and Mechanical Properties

Steel	Condition	C	Mn	P	S	Si	Ni	Cr	Mo	V	Ti	Cu	B
		%											
A201	Normalized	0.13	0.40	0.013	0.029	0.20	...	...	...	...	...	...	...
A225	Normalized	0.20	1.28	0.023	0.035	0.15	...	...	...	...	...	...	...
4885 HT	Normalized	0.15	1.12	0.034	0.031	0.18	0.06	0.05	0.017	0.085	0.007	0.11	...
A302	Normalized	0.21	1.31	0.022	0.027	0.25	...	...	0.41	...	...	...	...
70A	Normalized and tempered	0.13	0.48	...	...	0.21	2.17	...	0.39	0.11	...	0.73	...
70B	As-rolled and tempered	0.21	0.75	0.017	0.033	...	2.04	...	0.22	...	...	0.95	...
90A	Quenched and tempered	0.31	1.45	...	...	0.25	...	...	0.12	...	...	...	...
90B	Quenched and tempered	0.16	0.93	0.014	0.023	0.26	0.87	0.50	0.45	0.06	...	...	0.0031

Tensile properties of the high-strength steels

Steel	Yield strength, 0.2%, psi	Tensile strength, psi	Elongation, %	Reduction of area, %
A201	38,500	60,500	35.5	68.2
A225	52,500	76,100	29.2	65.0
4885	48,400	70,600	31.7	70.0
A302	51,800	87,300	23.8	59.3
70A	79,200	95,200	25.5	71.0
70B	84,800	101,800	19.5	56.2
90A	113,000	129,500	17.5	61.5
905B	123,400	130,000	15.5	50.2

tudinal submerged-arc weld, a hand-deposited weld, or a fitting welded to the plate, to simulate a pressure vessel attachment such as a nozzle. Limited studies were also made to observe the effect of polishing the surface, of other types of notches, and of a modified design to simulate the stress raising effect of openings in a vessel.

The results of the earlier research were used to plan the additional study of five low-alloy high-strength steels, and the program was conducted in cooperation with the Committee on High-Strength Steels of the PVRC. Three types of specimens, an unnotched, a notched and a plate with a longitudinal hand-deposited weld were studied for each of these steels.

Materials and Specimens Investigated

All materials were received and tested as $^3/_4$-in. steel plates. The nominal values of the chemical analysis and mechanical properties are listed in Table 1. In the previous work plates of A201, A225 and A302 steel were normalized at 1650° F, pickled to remove the scale and stress relieved at 1150° F. The unnotched and notched specimens of the new steels 4885, 70A, 90A and 90B steels were pickled to clean the surface, but otherwise they were tested in the as-received condition as outlined in Table 1. The above procedure was also followed for the 70B steel except that it was first tempered at 1100° F for 4 hr.

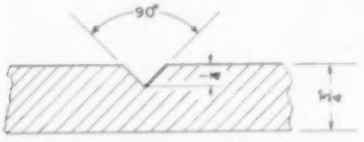

Fig. 1 Notch detail for hand-deposited weld

The welded specimens of high-strength steel were fabricated by machining a longitudinal V-groove along the center of the top surface of the plate as shown in Fig. 1. A multipass hand-deposited weld was laid in the groove by a qualified welder following the procedure outlined in Table 2. The specimens were cold-straightened to remove the small bow caused by welding (the straightening operation was necessary to adapt the specimen to the close tolerances of the loading fixture). The excess weld metal was removed and the welded surface was ground flush with the adjacent plate, the final grind marks being aligned parallel to the direction of maximum stress. The five high-strength steel plates were tested in the as-welded and straightened condition, whereas the welded specimens of A201 and A302 were stress relieved at 1150° F after the welding and straightening operations. A few studies were also made of plates with the weld bead aligned parallel to the direction of maximum stress.

All specimens were cut from the plate stock so that the direction of rolling was parallel to the direction of the maximum principal stress. The specimens were pickled to remove the mill scale, but otherwise the plate surface was in the as-rolled condition.

The notched specimens were fabricated by milling a plunge cut into the geometric center of the test surface of the specimen using a $2^3/_4$-in. diam milling cutter of the type normally used to notch Charpy impact specimens. The resulting notch (aligned perpendicular to the direction of maximum stress) had a depth of 0.01 in., a root radius of 0.01 in. and a length of about $^3/_8$ in. The theoretical stress concentration factor for the notch was about 2.8 as determined by Neuber's method.[6]

Further studies were made with plates containing 1-in. diam counterbored

Table 2—Welding Procedure

Steel	Plate temperature, ° F	Electrode, $^3/_{16}$ in.	Current, amp, and travel, ipm
4885	Room	E7016	200 at 6
70A	Room	E10015	200 at 6
70B	Room	E9015	200 at 6
90B	Room	E12015	200 at 6
90A	200	E12015	200 at 6

holes in the center of their top surface. These were designed to simulate an opening in a pressure vessel where the state of stress at the junction between the edge of the hole and the top surface of the plate compares to that existing at the entrance to a nozzle or fitting on the inside surface of a pressure vessel.

Test Procedure

The maximum strain, the maximum variation in strain during each loading cycle (hereafter referred to as strain range per cycle), the deflection, the hydraulic pressure, and the number of cycles necessary to cause failure were recorded for each specimen.

The total strain range per cycle (measured in the center of the top surface of the specimen) was chosen as the most suitable parameter for determining the severity of the test condition to which each specimen was subjected and for comparing the data for the various steels. This criterion also gave a valid comparison of the severity of cyclic loading between the biaxial fatigue studies, the bending specimens studied by Gross and Stout,[3-5] and the pressure vessel models studied by Welter.[12] The commonly used parameter of stress was unsatisfactory for comparison of data; the stress was not a simple or a linear function of the total strain because of the plastic deformation which occurred in most of the tests. Similarly, when the *cyclic* strain exceeds

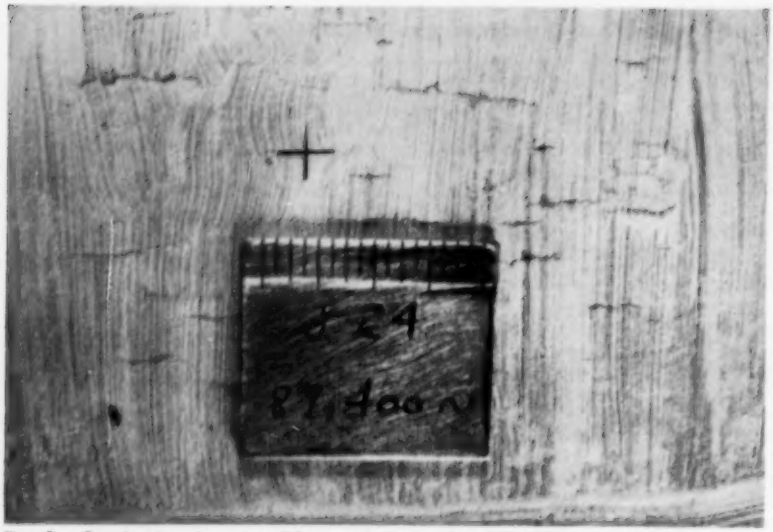

Fig. 2 Cracks developed in 90A steel plate after 87,400 cycles of 3135 micro-in./in. strain (the (+) indicates geometric center of specimen)

the yield point strain, the stress range is no longer linearly related to the strain range because of the hysteresis effect.[8] In the plastic region, *stress* concentration tends to decrease with load while *strain* concentration increases with load.[9] In order to eliminate confusion only the measured values of maximum strain and of strain range are reported in this paper.

The criterion for failure was chosen as a crack having a length of $^{3}/_{16}$ in. This length was chosen because it was a crack long enough to be readily detected at any point in the 30 to 50 sq in. area in which initial failure normally occurred but yet was short enough so as not to seriously disturb the stress distribution in the surface of the specimen. To aid in the detection of cracks a thin coating of white lead cut with machine oil was brushed over the surface of the specimen. As a crack developed, a dark stain appeared in the white lead which

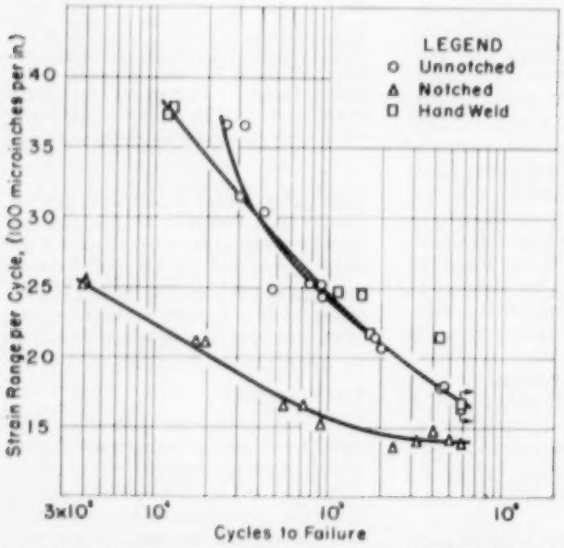

Fig. 3 Relation between strain range and fatigue life for 48S5 steel plate

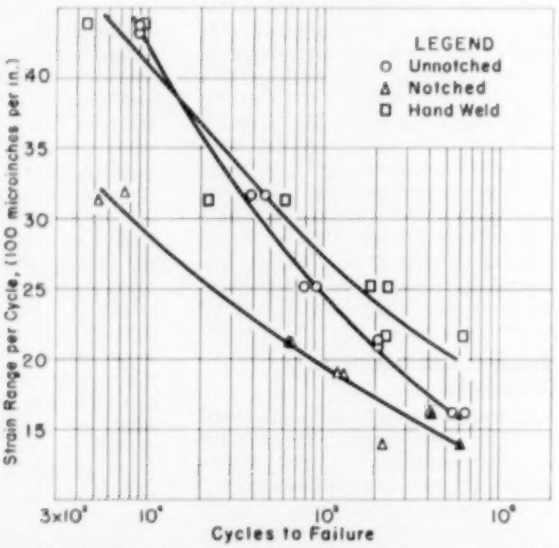

Fig. 5 Relation between strain range and fatigue life for 70A steel plate

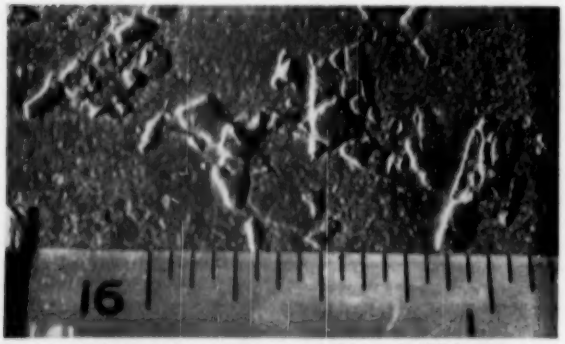

Fig. 4 Mill scale impressions in surface of 48S5 plate

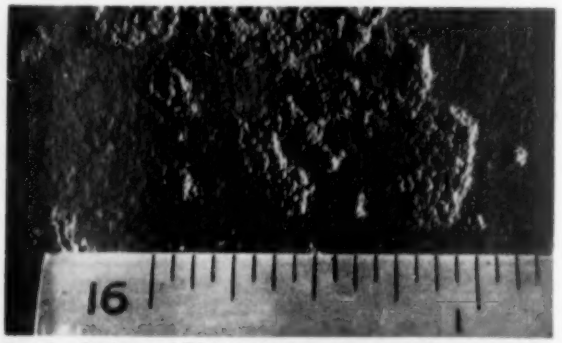

Fig. 6 Surface of 70A steel plate showing pitted condition

facilitated detection of initial failure and outlined the crack growth. At the highest cyclic strains, a failure occurred in as few as 4000 cycles while at the lowest strain range some specimens did not fail after 1,000,000 cycles; at no time were the tests conducted beyond 1,000,000 cycles of strain.

Cracks were, without exception, aligned perpendicular to the direction of the maximum principal stress for all types of plate specimen. Initial failure in unnotched specimens usually occurred within 2 in. of the longitudinal centerline and within 4 in. of the transverse centerline. However, surface defects in some plates were occasionally so severe as to cause failure to initiate at a point more remote from the region of maximum cyclic strain. In general, many cracks developed in a random fashion in the specimen as shown in Fig. 2; as the initial crack developed, it would often join one or two other cracks before it reached a length of 1 in.

Discussion of Results

Figure 3 is a plot of the maximum strain range to which the top surface of the plate specimen was subjected during each loading cycle versus the number of cycles necessary to cause failure for the three types of 4885 steel specimens. Data for the unnotched and notched plates show little scatter even though the surface of several samples contained mill scale impressions which were as deep as 0.010 to 0.020 in. as shown in Fig. 4. The fact that the smoothest plates were selected for the unnotched specimens probably minimized the harmful effect of the rough surface. The plates containing welds had approximately the same resistance to repeated loading as the unnotched plates, but showed somewhat greater scatter.

There were two general characteristics of all welded specimens that explain in part the greater scatter of data. In grinding the surface of the weld bead some of the area of the adjacent plate was also ground, thus improving the fatigue resistance relative to the unnotched plates. On the other hand, while visual examination of the various plates showed the welds to be of good quality, it did reveal three types of flaws that resulted from the welding operation and which had a deleterious effect upon their fatigue resistance. The most serious were holes or pipes having a diameter of 0.010 to 0.030 in. and which were frequently so deep that it was not feasible to remove them by grinding. The other two types of flaw were undercutting along the edge of the weld and chisel marks in the plate adjacent to the weld. These latter imperfections were removed using a small diameter grinding wheel. A study of the original data sheets for the welded plates revealed that for a majority of the specimens, initial failure occurred in an area of sound weld metal or in the adjacent plate. For about one-fifth of the plates, the initial failure started at a small diameter blow hole or flaw in the weld metal; however, this type failure seldom caused a significant reduction in the fatigue life as compared to unnotched plate.

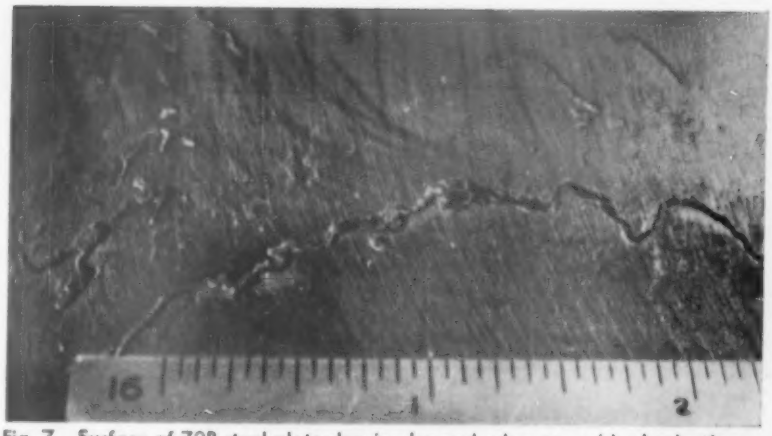

Fig. 7 Surface of 70B steel plate showing lapped edge caused by laminations

The unnotched specimens of 70A steel demonstrated consistent experimental results as shown in Fig. 5 even though it had a severely pitted surface, shown in Fig. 6, which appeared to have the same texture as that of a corrosive attack. In fact, areas of the surface were so severely pitted that four notched specimens failed from the pitted area rather than from the machined notch; thus in these instances the stress concentration in the pitted area exceeded that of the machined notch. The data for the specimens which failed in an area away from the notch are indicated by the solid triangles in Fig. 5. These specimens were sorted according to surface condition, as were the 4885 plates; the plates with the least pitting were used for unnotched specimens while those more severely pitted were used for the notched specimens.

Of the several steels studied, the 70A steel showed the least reduction in cyclic strain due to the introduction of a machined notch in the plate. Thus, it seems probable that surface defects in the unnotched specimens developed stress concentrations that resulted in lower fatigue strength of the plate than that which might be expected as a "par" value for the steel.

The 70B steel had a relatively smooth surface, but the plate contained some laminations which caused a very rough pattern on the surface of a few samples as shown in Fig. 7. The subsurface laminations such as shown in Fig. 8 did not appear to have deleterious effect on the fatigue life of the specimens (the light colored area indicated by the arrow represents the penetration of a fatigue crack from the surface down to the lamination in the plate). The machined notch penetrated a small subsurface lamination on one specimen with the result that failure occurred very prematurely during testing. However, the other notched specimens behaved in a normal manner. A study of the original data plotted in Fig. 9 indicated that the slight increase of scatter for the unnotched specimens of this steel was attributable to lamina-

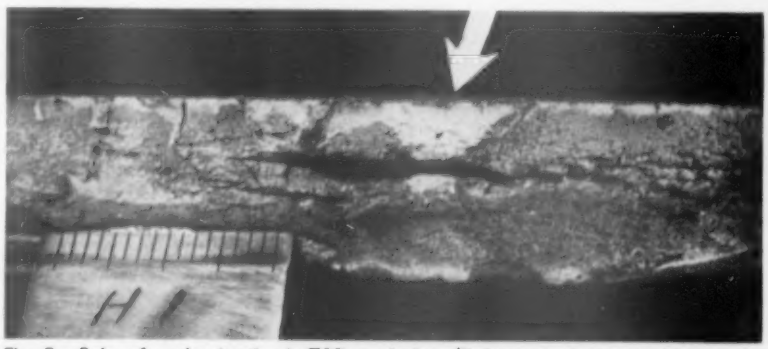
Fig. 8 Subsurface lamination in 70B steel plate (light area, designated by arrow, outlines penetration of fatigue crack)

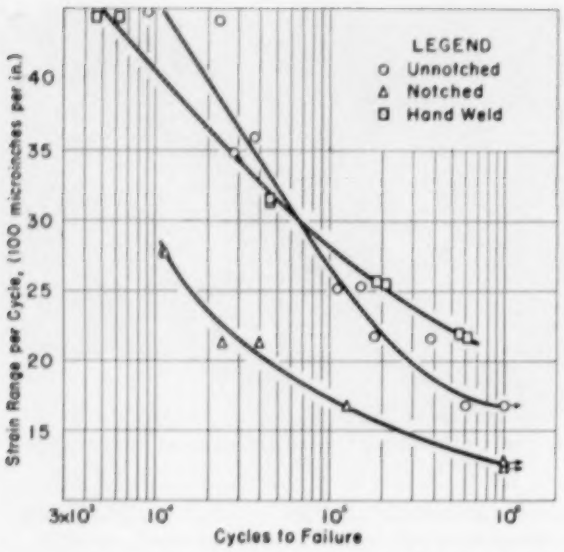

Fig. 9 Relation between strain range and fatigue life for 70B steel plate

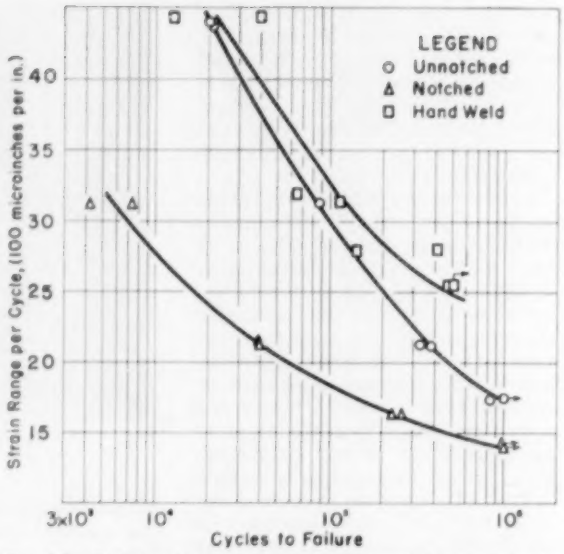

Fig. 10 Relation between strain range and fatigue life for 90A steel plate

tions in the surface. The welded specimens appeared to be slightly weaker in fatigue at high cyclic strains and somewhat stronger at lower levels of cyclic strain than the unnotched steel plate.

The surface condition of the 90A and 90B steels was relatively good, and the experimental data for both materials shown in Figs. 10 and 11, had little scatter. Of the eight steels studied these two materials showed the greatest reduction in cyclic strain from unnotched to notched specimens. It is probable that this was due in part to the fact that the unnotched specimens were relatively smooth and approached a higher par value of fatigue strength as compared to those containing the machined notch. Thus the effective stress concentration of any surface roughness in the plate was low compared to several of the other unnotched materials that were studied.

In general, it may be stated that plates with welds had approximately the same (or in some instances slightly greater) resistance to repeated loading than unnotched plate of the same material. On the other hand, the machined notch in the center of the specimen decreased the allowable strain range to which the plate could be subjected for a life of 10^5 cycles to a level of 0.58 to 0.80 of that of the unnotched plate. If the theoretical stress concentration factor for the machined notch was fully effective, however, the allowable strain range for those plates would be 0.36 of that for unnotched plates.

Five of the welded plates were radiographed before testing; each was of different material and four of the five tested at different pressures. One of these plates was cycled at a low pressure and did not fail, while the other four were cycled at intermediate pressures and each failed in the weld. Three of the failures occurred in sound weld metal while the fourth failure developed out of a small blowhole which was barely detectable in the radiograph upon re-examination. However, none of these failures in the weld or from a blowhole exhibited abnormally low fatigue life.

Tests of the six plate specimens containing transverse welds (that is weld beads oriented *along* the direction of maximum stress) indicated that they were as resistant to fatigue as unnotched plates and plates containing longitudinal welds. Therefore, the different orientation of residual stresses resulting from welding did not produce an observable difference in cyclic life for these limited studies. The work of Wilson[10, 11] would indicate that with this orientation of the weld the data should show less scatter than with the weld perpendicular to the maximum stress as was the case for the other welded plates. However, an accurate check of this theory could not be obtained with only six specimens.

Four plates each of A201 and A302 steels containing a counterbored hole having a sharp lip were found to be slightly less resistant to fatigue than notched plates of the same material. However, two similar specimens with a lip radius of $^1/_{16}$ in. were much more resistant to fatigue than notched plates. These findings are in good agreement with those of Welter[12] who found that a sharp-lipped nozzle was a more severe

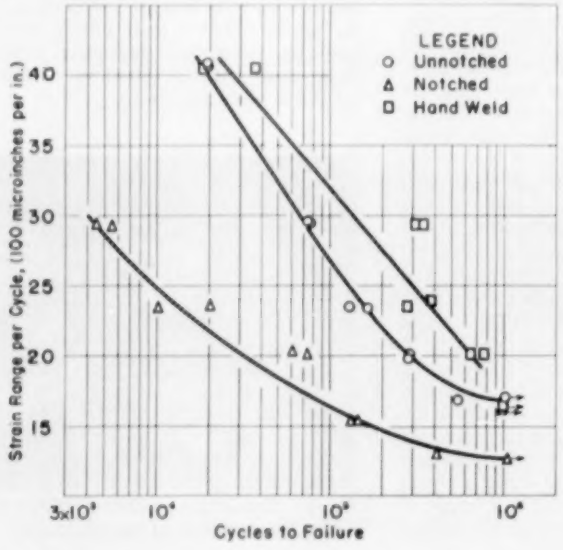

Fig. 11 Relation between strain range and fatigue life for 90B steel plate

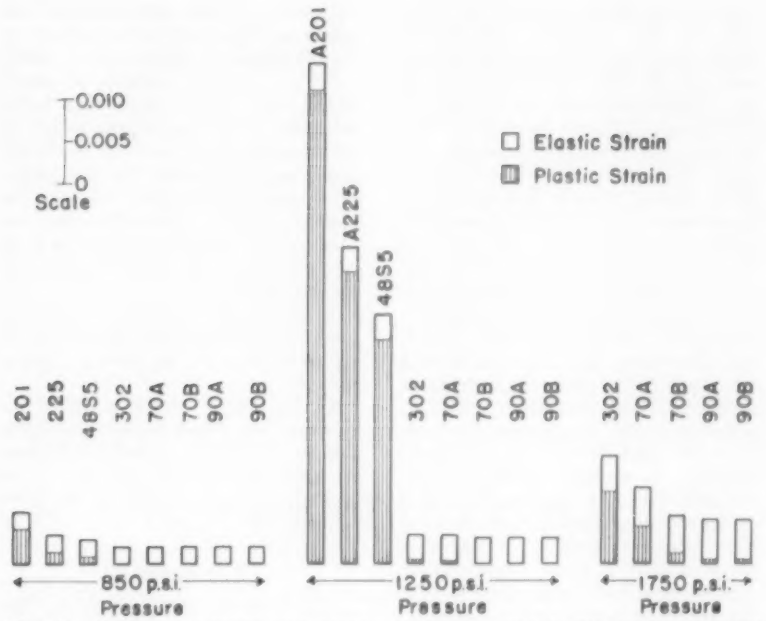

Fig. 12 Cyclic strain range and accompanying permanent strain in tests of plate specimens

stress raiser than the machined notches.

One characteristic of the hydraulically loaded plate fixture was that there was no physical limitation to the plastic deflection of the specimen except for limit stops that would halt the test if the total deflection exceeded a safe value. Thus, if the hydraulic pressure on the bottom surface of the plate was sufficient to cause the stress level in the plate to exceed the yield strength of the material, the specimen would yield during the first few loading cycles until a state of equilibrium was reached between the applied load and the deformation stresses. The elastic or cyclic strain remained constant for a given thickness of plate and cyclic pressure and was independent of the material as shown by the open bars in Fig. 12. Inelastic strain occurred in the weaker materials such as A201 at a relatively low pressure as shown by the shaded bars in the same figure. At a pressure of 1250 psi, the A201 material developed an inelastic strain of over 5% and it was found that large plastic deformations in the A201 steel were accompanied by strain hardening.[9] It seems probable that the strain hardening thus developed had a favorable influence upon the fatigue properties of the material. However, the excessively large plastic deformations encountered in the A201 steel at pressures exceeding 850 psi (for which the cyclic strain was about 2100 micro-in./in.) would cause severe deformation of a pressure vessel that probably could not be tolerated in actual design. It will be noted that the highest strength steels sustained a relatively small amount of inelastic deformation when cycled at pressures even up to 1750 psi.

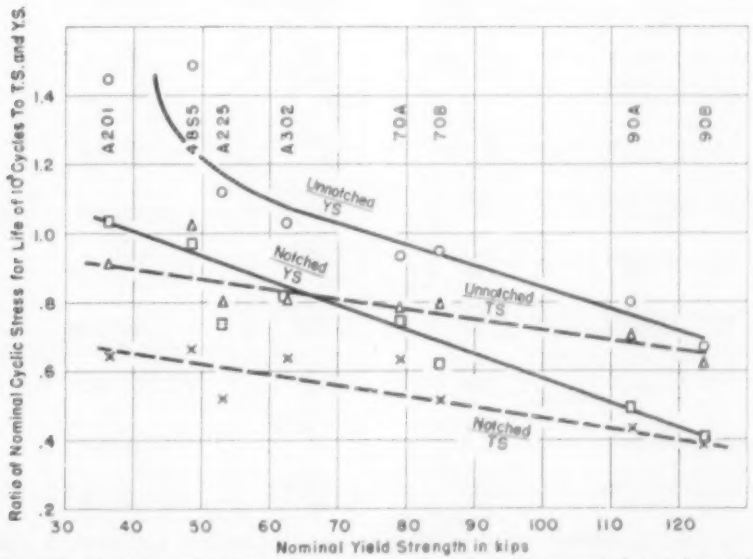

Fig. 13 Variation of relative fatigue strength with yield strength for eight steels

In Fig. 13 the ratios of the nominal cyclic stress* corresponding to a life of 10^5 cycles divided by the yield strength (and the same values divided by the tensile strength) are plotted as a function of the yield strength. The two solid curves representing the unnotched and the notched data for each steel divided by the yield strength are approximately parallel and their slope indicates that the cyclic stress for a life of 10^5 cycles becomes a smaller fraction of the yield strength as the yield strength increases. The two dashed curves representing the unnotched and the notched data for each material divided by the tensile strength are also parallel, but have less slope than that of the solid lines. Thus, it indicates that the allowable cyclic strain also becomes a smaller proportion of the tensile strength as the yield strength increases. However, this latter proportion decreases at a smaller rate than the ratio based on the yield strength. Probably the most significant trend indicated by the curves was that the allowable cyclic strain for *unnotched* specimens and for *notched* specimens was influenced to about the same degree as the strengths of the steels increased. It will also be observed in Fig. 13 that all of the steels were able to withstand a cyclic strain ranging from 0.7 to 1.4 times the yield point strain in the unnotched plate for a life of 10^5 cycles. (These cyclic strains corresponded to approximately 0.6 to 0.9 of the tensile strengths of the steels tested.) Thus all of the steels showed surprisingly high resistance to progressive fracture under repeated biaxial stressing.) A similar set of curves to those in Fig. 13, except with the abscissas equal to the static tensile strengths of the steels, were plotted but are not reproduced here since they showed almost identical trends to those illustrated.

The first column of the bar chart in Fig. 14 compares the ratio of allowable strain range for unnotched and notched plate of each of the steels with that of A201 for three different cyclic lives. A study of the data reveals that in general the low-alloy higher strength steels are more resistant to fatigue than in the A201. However, the increased resistance of those steels is not as great as might be anticipated from their yield

* The nominal cyclic stress is defined as the strain range per cycle multiplied by the modulus of elasticity for steel, 30×10^6.

or tensile strengths. Their improved performance was usually greatest for a life of 10^5 cycles. These ratios are very similar to those reported for these same steels by Gross and Stout.[5] The second bar chart in Fig. 14 shows the allowable cyclic strain that unnotched and notched specimens withstood for three values of cyclic life. Without exception, the allowable cyclic strain decreased with increased cyclic life. In general, the allowable cyclic strain increased with increased yield and tensile strength. The most pronounced exception was the unnotched A201 which had a relatively large allowable cyclic strain for a life of 5×10^4 cycles. This was attributed, however, to the favorable effect of strain hardening that resulted from the large plastic deformation developed in the plate at the higher test pressures. The third set of bar graphs gives the ratio between the strain ranges for notched and unnotched plate for the three values of cyclic life. This ratio was relatively constant for each of the eight steels, indicating only moderate variation in the fatigue sensitivity of any of the materials to the machined notch. For a life of 10^5 cycles the 70A steel sustained the smallest reduction in allowable cyclic strain while the 90A and 90B materials sustained the greatest reduction. Each steel was most notch sensitive at the highest values of cyclic strain and least notch sensitive at the lowest values of cyclic strain.

To date, there is no evidence that the values of allowable strain range for a given cyclic life obtained from the plate specimen studies may be translated quantitatively to pressure vessel design practice. Rather, this research has compared various materials and the relative or qualitative effect of various surface conditions and typical fabrication operations.

The data reported are in good qualitative agreement with those reported by Gross and Stout;[3-5] however, the allowable cyclic strain that the plate specimens withstood for a given life was much lower than for the cantilever beam specimens studied at Lehigh University. The lack of quantitative agreement would, however, be expected because of the difference in the size and type of specimen and because the cantilever beam specimens had a machined surface while the plate specimens were tested with the as-rolled surface. Some deoxidation of the surface of the plate as well as surface roughness may also have also been present to lower their fatigue strengths. Welter[12] found that in a few tests the allowable cyclic strain for pressure vessel models containing machined notches and welded attachments was somewhat lower than for the plate specimens at about the same cyclic life. The fabricated vessel models had a more uniform distribution of tensile stress throughout the thickness of the plate and thus probably developed a higher effective stress at the root of the notch (in the plate specimens the root of the notch penetrated to a region of lower stress than that measured on the top surface). Also the simulated nozzles in the vessel models had a sharp lip at the edge of the hole that was shown to be a severe stress raiser by the limited studies on plates. The fact that the vessel models were cycled at a very slow rate would also account for about a 15% reduction in strength based on the data reported by Gross and Stout.[5] Thus it is felt that a fairly good agreement exists between the data reported on the same steels by the three coordinated programs.

As a result of this research program, much has been learned concerning the resistance to repeated loading of high-strength, low-alloy steels and the effect of various fabrication operations upon their fatigue resistance. It has been observed that a rough plate surface, whether obtained artificially (such as the machined notch) or whether it exists in the as-received plate (as in the case of the 70A steel) will cause a significant reduction in the resistance of the plate to repeated loading. On the other hand, high-quality welds with the reinforcement removed should have no deleterious effect upon the fatigue life.

Conclusions

1. Hand-deposited welds of good quality ground flush with the plate surface did not reduce the resistance of the plate to repeated biaxial stressing.

2. The fatigue resistance of unnotched and of notched plate specimens increased with the static strength but not as rapidly as the rate of increase of yield or tensile strengths.

3. The fatigue strength reduction of the eight steels caused by a notch machined in the plate was relatively constant, their fatigue notch sensitivity being slightly greater for the higher cyclic strains (short life studies). The strength reduction due to the notch was roughly half that predicted by the theoretical stress concentration factor of 2.8 for the notch.

4. The surface condition of the plate may have a significant influence upon the resistance of the steel to fatigue failure.

5. Unnotched plates of *all* of the steels exhibited great resistance to plastic fatigue; they were able to withstand cyclic strains greater than 0.6 of the yield point strain for 10^5 cycles before failure.

Acknowledgment

This work was sponsored by the Pressure Vessel Research Committee of the Welding Research Council, of which F. L. Plummer is Chairman and J. H. Drucker is Executive Secretary. This work was under the general supervision of the Fabrication Division of which E. I. Boberg is Chairman. The research was conducted in Talbot Laboratory by personnel of the Department of Theoretical and Applied Mechanics of the University of Illinois. The execution of the work was made possible by the cooperation of J. M. Robertson and H. T. Musgrove, Laboratory Mechanics of the Department Staff.

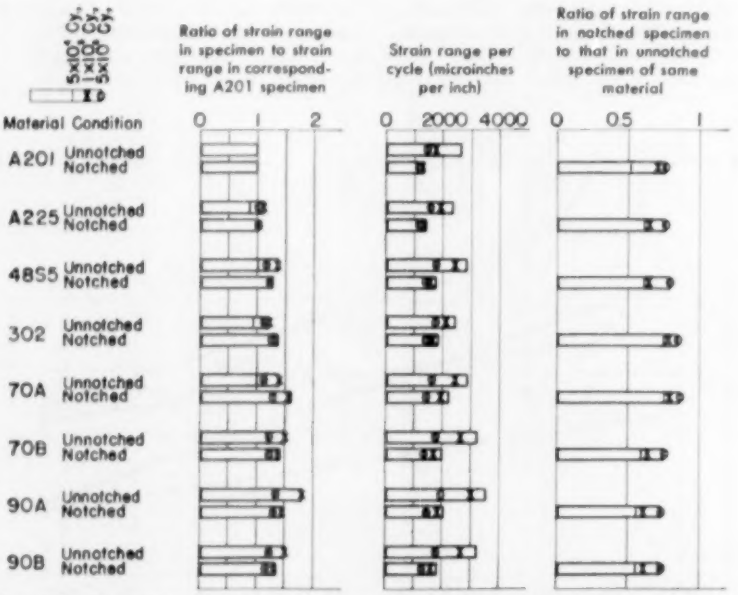
5x1x1/2
Material Condition
A201 Unnotched Notched
A225 Unnotched Notched
4855 Unnotched Notched
302 Unnotched Notched
70A Unnotched Notched
70B Unnotched Notched
90A Unnotched Notched
90B Unnotched Notched
Ratio of strain range in specimen to strain range in corresponding A201 specimen
0 1 2
Strain range per cycle (microinches per inch)
0 2000 4000
Ratio of strain range in notched specimen to that in unnotched specimen of same material
0 0.5 1

Fig. 14 Comparisons of data for unnotched and notched specimens of eight steels

References

1. Bowman, C. E., and Dolan, T. J., "Biaxial Fatigue Properties of Pressure Vessel Steels," THE WELDING JOURNAL, **32** (11) Research Suppl., 529-s to 537-s (1953).

2. Bowman, C. E., and Dolan, T. J., "Further Studies of the Biaxial Fatigue Properties of Pressure Vessel Steels," *Ibid.*, **34** (1), Research Suppl., 51-s to 591-s (1955).

3. Gross, J. H., Tsang, S., and Stout, R. D., "Factors Affecting Resistance of Pressure Vessel Steels to Repeated Overloading," *Ibid.*, **32** (1), Research Suppl., 23-s to 29-s (1953).

4. Gross, J. H., Gucer, D. E., and Stout, R. D., "The Plastic Fatigue Strength of Pressure Vessel Steels," *Ibid.*, **33** (1), Research Suppl., 31-s to 39-s (1954).

5. Gross, J. H., and Stout, R. D., "Plastic Fatigue Properties of High-Strength Pressure-Vessel Steels," *Ibid.*, **34** (4) Research Suppl., 161-s to 166-s (1955).

6. Neuber, H., *Theory of Notch Stress-Principles for Exact Stress Calculation*, J. W. Edwards Bros., Inc., Ann Arbor, Mich. (1946).

7. Blaser, R. V., Tucker, J. T., Jr., and Kooistra, L. F., "Biaxial Fatigue Tests on Flat-Plate Specimens," *Ibid.*, **31** (3) Research Suppl., 161-s to 168-s (1952).

8. O'Reilly, H. R., "Range of Stress Accompanying Cyclic Plastic Loading of Steel," M.S. Thesis, Department of Theoretical and Applied Mechanics, University of Illinois, 1954.

9. Box, W. A., "The Effect of Plastic Strains on Stress Concentrators," *Proc. Soc. Exptl. Stress Analysis*, **8** (2), pp 99–110 (1951).

10. Wilson, W. M., and Thomas, F. P., "Fatigue Tests of Riveted Joints," *Univ. of Ill. Eng. Expt. Sta., Bull.* **302** (1938).

11. Wilson, W. M., Bruckner, W. H., McCrackin, T. H., and Beedle, H. C., "Fatigue Tests of Commercial Butt Welds in Structural Steel Plates," *Ibid., Bull.* **344** (1943).

12. Welter, G., Unpublished progress reports to Pressure Vessel Research Committee, Fabrication Division.

EFFECT OF CURRENT AND ATMOSPHERES ON ARC TEMPERATURES

Authors discuss the problems involved in measuring and mapping the temperatures in the arc stream and report early progress made on this project

BY G. M. GORDON, OLGA A. COTTER AND E. R. PARKER

Introduction

The properties of deposited weld metal depend upon the reactions that occur in the arc. These in turn are affected by the composition of the flux and gas used to shield the metal during its transit from the electrode to the work. At the present time there is no way in which the nature or extent of the chemical reactions occurring in the arc can be predicted. It was with this in mind that the present investigation was started, with the hope that quantitative data could be obtained which would make accurate correlations and predictions possible.

The first, and one of the major, problems under attack is that of measuring and mapping the temperatures in the arc stream. This is a difficult task but one that must be mastered before progress can be made. Temperature measurements are of prime importance because all reactions are temperature dependent, with equilibrium constants and reaction rates of the multitudinous potential reactions varying in a presently undetermined manner.

The purpose of this paper is to discuss the problems involved in the measurement of arc temperatures and to report the early progress made on this project.

G. M. Gordon is a Research Engineer, Olga A. Cotter is a Research Engineer, and E. R. Parker is a Professor of Metallurgy, Minerals Research Laboratory, University of California, Berkeley, Calif.

Presented at AWS 1955 National Fall Meeting held in Philadelphia, Pa., Oct. 17–21.

Temperature

The term temperature is used to define the thermal energy existing in a system. At low temperatures, the problem of temperature measurement is relatively simple but at the high temperatures of the electric arc, which reach thousands and even tens of thousands of degrees, the problem is far from simple. Old and standard measuring devices are useless and temperature must even be defined in new and different ways. A few of the considerations involved in arriving at an arc "temperature" are listed below:

A. Extrapolation of physical properties, such as thermal expansion and the thermocouple effect, density and velocity of sound.

B. Extrapolation of thermodynamic properties.

C. Relating energy forms such as velocity or potential to kinetic energy.

D. Determination of the degree of ionization such as is used by astronomers which is obtained from the Saha ionization equation.

E. Application of various laws or rules that have been developed such as Plank's Radiation laws and the Wein's Displacement Law which are the basis of radiation meters and optical pyrometers.

F. Deduction from other physical properties or combinations of these other factors. For example, the Ornstein formula which relates the intensity of spectral lines to temperature.

The positive column of a carbon arc is considered a good example of thermal equilibrium. Ornstein[1] and Finkelnberg[2] have demonstrated mathematically that equilibrium does exist and that thermal kinetic energy relationships may be applied. However, in a welding arc, equilibrium in the true sense of the word cannot exist. The temperature of the gas, ions, electrons, etc., as determined from measurement of ionization, velocity of sound, absorption and spectral line intensities has been reported to be between 4000 and 30,000° C. However, high-speed movies have shown that the metal is transferred across the arc as drops of liquid. Since iron has a boiling point of about 3000° C, at least two temperature ranges must be present in a welding arc, that of the liquid metal and that of the surrounding gas.

It appears from a thermodynamic view that the reactions between the gas and the metal drops is controlled by the surface temperature of the liquid metal. The kinetic temperature of the vapors, electrons and ions will also play an important role since this is the source of the energy that melts the electrode and its coating (if one is present).

Table 1—Temperatures Obtained From Spectral Line Intensities

Line pair	ΔE, v	Temperature at current, ° K — 1.0 amp	2.5 amp	4.0 amp
Sn 3264 / 3034	0.57	5020	6580	9450
Fe 3402 / 3415.5	1.02	5020*	5410	5700
Fe 3425 / 3415	0.81	5020*	5190	5310
Fe 3323.7 / 3298	0.57	5020*	5300	5460
Fe 3292.0 / 3292.6	1.03	5020*	5490	6280
Fe 3016.2 / 3232.6	1.21†	4230	4068	3910

* From temperature assumed at 5020° K.
† From King and King data.[5]

Reactions may, of course, take place in the pool of deposited metal. Such reactions will be studied later. The present research is concerned with events that occur in the arc plasma; the anode and cathode regions, with their extreme temperature gradients, are not presently under investigation.

Initial experiments utilized a low current arc because these have been studied and used by spectroscopists; consequently there was considerable background information available. Also, since no liquid metal transfer takes place, conditions are relatively simple.

The studies to date fall into three categories. The initial experiments involved studies of the plasma of low-current arcs by means of spectrographic techniques. The first step was to evaluate the various techniques which had been reported in the literature. The second phase consisted of utilizing one particular method to determine the effects of various atmospheres upon the arc temperature. The third portion is just beginning. It consists of an attempt to measure the temperatures present in a high current-constant potential welding arc. A discussion of the problems involved in the measurement of the arc plasma temperature is presented below.

Spectral Line Intensity Methods

Several methods have been developed in the past for determining arc temperatures using relationships between ionization potentials or spectral line densities, and temperature. One such relationship has been demonstrated by Semenova[2] and is shown in Fig. 1. From this it is apparent that elements which comprise the electrode coating, as well as the electrode metal, will largely determine the temperature of the arc. Saha[4] subsequently developed a relationship between the temperature and degree of ionization for a material having a given ionization potential. A third approach to the problem has been made by Ornstein which utilizes the application of Boltzmann's statistics to relate the intensity of a spectral line to the temperature. A variation of this technique, which utilizes the ratio of intensities of two lines of the same element, was used in the present investigation. This equation takes the form of:

$$\frac{I_a}{I_b} = Ke^{-(\Delta E/kT)}$$

where

I = intensity.
ΔE = difference in energy state of two lines.
k = Boltzmann's constant.
T = temperature.
K = probability constant of emission

Since the intensity ratio of two lines may be measured with a fair degree of accuracy, and the energy levels are known precisely, the temperature and constant K remain as the only unknowns. Three different methods were employed to evaluate the value of K for the present case. These are:

1. Direct calculation from published values of oscillator strengths.[5]
2. Determination of the temperature of the arc by using spectral lines of an impurity element in the electrode for which the values of K have previously been determined. From these data it is then possible to calculate K values for various pairs of iron lines.
3. Mathematically approximate K from a series of lines from arcs operated at different currents using assumed temperatures.

All of these methods are approximations and have inherent errors or difficulties which will be discussed in detail.

Experimental Procedure and Results

An Applied Research Laboratories, 1½ meter grating spectrograph and accessory equipment were used for the experiments. The electrodes were ³/₃₂ and ¹/₈ in. diam iron welding rods with a light copper coating. They were cut into ³/₄ in. lengths and placed into holes drilled in ¹/₄-in. copper rods.

Exposures were made at 1, 2.5 and 4 amp. The standard deviation for four pairs of lines were in the range of 2 to 2½%. The distribution of line intensities across the arc gap were studied by focusing an image of the arc on the secondary slit. The resulting image showed that the distribution varied from very low intensity close to the

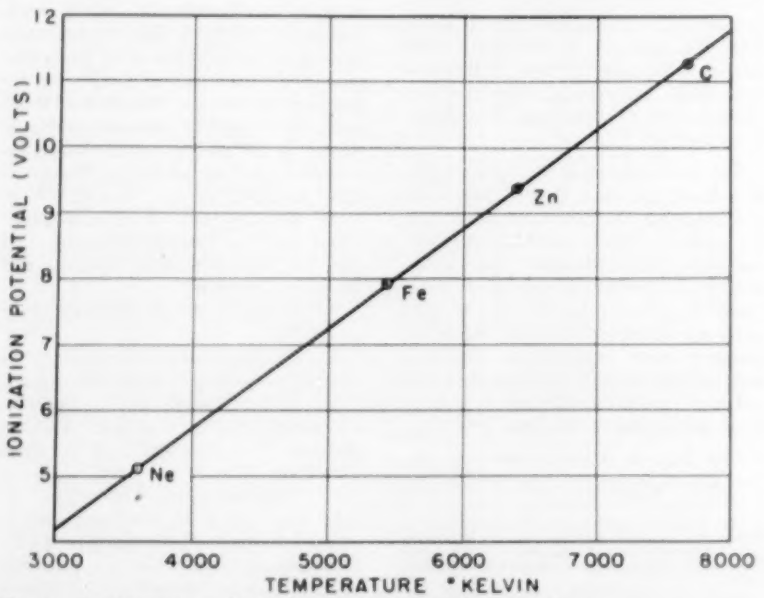

Fig. 1 Temperature vs. ionization potential (ref. Semenova)

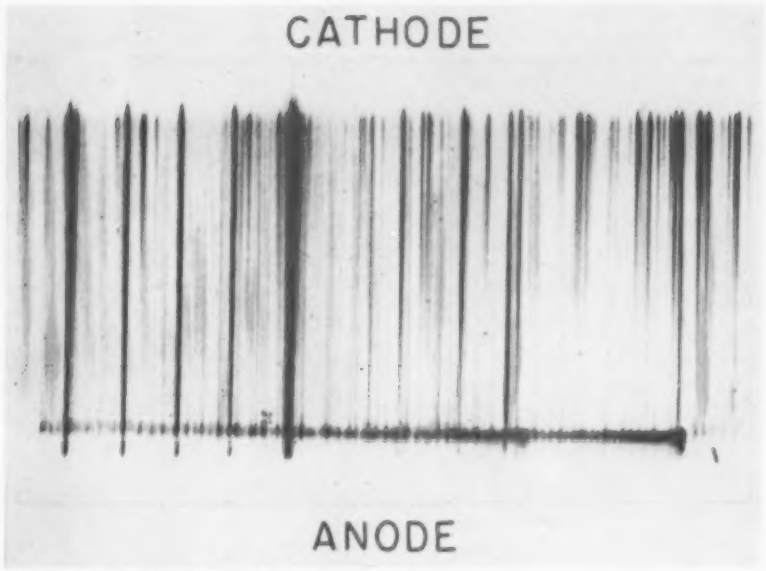

Fig. 2 Distribution of line intensities across the arc plasma

anode to high intensity near the cathode and a rather continuous gradation between the two electrodes. Although ionized and high energy lines were observed to some extent at both electrodes, there was a much higher concentration of such lines at the cathode. On the other hand, continuum spectra from the molten metal and band structure were observed at the anode. A typical image of this type is shown in Fig. 2.

Quantitative studies made across the gap showed line intensity ratios from the region close to the anode and from the center of the arc were in fair agreement, while ratios from measurements close to the cathode were larger. (Throughout this work, all line ratios were detemined by dividing the high energy line by the low energy line so that an increase in intensity ratio will represent an increase in temperature.)

It is essential, if any degree of accuracy is to be expected at all from such measurements, that the self-absorption of the particular lines chosen be almost negligible. Dieke and Crosswhite[6] have discussed absorption in detail and have shown that the greater the intensity of the lines, the greater the self-absorption. Therefore, all of the lines selected for this study were subjected to a test for self-absorption by comparing the intensity of the lines at two different current values. Only lines showing low self-absorption were used.

Langstroth and McRae[7] have reported the K value for two tin lines to be 3.06. The equation is as follows:

$$\frac{I\ \text{Sn}\ 3264}{I\ \text{Sn}\ 3034.1} = 3.06e^{-\frac{6600}{T}}$$

Since tin was an impurity in the copper coating of the electrode, it was possible to use this equation to obtain the temperatures shown in the first line of Table 1.

Using the temperature of 5020° K obtained in this manner for a 1-amp arc, calculations were made to determine arc temperature from iron lines which had been carefully selected to be free from interference, self-absorption and to have ΔE values of about 1 v. (At ΔE equal to 1 v, a 10% error in line ratios will result in about a 10% error in temperature).

The K values obtained were then used to calculate the temperature at the higher currents. These values along with those obtained from K values calculated from the work of King and King[8] are shown in Table 1.

The increase of temperature with current obtained from the tin ratios seems out of line since Mason[5] reports an increase of only 10% in temperature when the current is increased from 1 to 13 amp. However, the temperature of 5020° K appears reasonable and is in agreement with results reported by other workers. The (K) values were calculated from this temperature and they, in turn, were used in calculating temperatures for the 2.5- and 4-amp arcs. The resulting temperature increase seems more reasonable but considerable discrepancy is evident between results obtained from different line pairs.

The last temperatures reported in the table were determined from King's oscillator strength values. The lower state for both of these lines is less than 1 v above the ground state and as a consequence they are subject to considerable self-absorption. This is reflected in the decrease in temperature with current and, although the results are not considered valid, they have been included to illustrate the difficulty in attempting to use transition probabilities that have been determined in absorption studies.

Although the results of the above studies were somewhat inconclusive in so far as determining which of the attempted methods of measuring the arc temperature is concerned, the authors believe that the results produced by the intensity ratios of Fe 3425/Fe 3415 are probably the best. Consequently, the intensity ratio of these two lines was used in the next study concerning the effect of various arc atmospheres on temperature.

Effect of Gas Atmospheres

The arc was enclosed in a quartz chamber and the spectra observed in atmospheres of different gases. Line intensity ratios were calculated using the Fe 3425/Fe 3415 pair with the results shown in Table 2. Although it

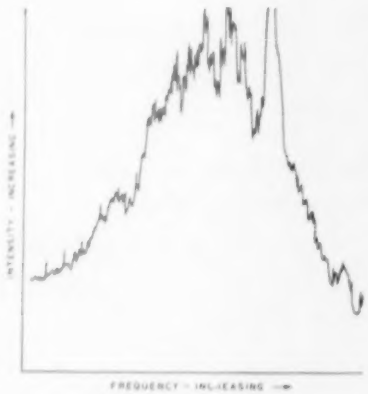

Fig. 3 Infrared energy distribution curve

Table 2—Influence of Gas Atmosphere on Arc Temperature

Atmosphere	*Voltage drop across electrodes*	*Intensity ratios of a 4 amp arc*	*Temperature, ° K*
Carbon dioxide	43	1.62	5900
Nitrogen	35	1.45	5520
Air	35	1.41	5490
Argon	20	1.31	5200
Helium	50	(1.16)	(4900)

was expected that the ionization potential of inert gases would increase the arc temperature over that of air and the dissociation of carbon dioxide would have a quenching effect which would reduce the temperature, it may be seen from the line intensity ratios of Table 2 that the results are exactly the reverse of those anticipated. These studies indicate, on the other hand, that carbon dioxide atmospheres surrounding the arc produce the highest temperature whereas argon (and possibly helium) produce the coolest arc. Air and nitrogen, both of which are polyatomic, seem to fall in an intermediate atmosphere range. The line intensity ratio shown for helium is in considerable doubt since a satisfactory arc could not be maintained in pure helium.

Infrared Studies

With this background information regarding arcs, the investigation has been extended to include study of high-current constant potential welding arcs. Emphasis is presently being placed on determination of the liquid drop temperatures. An infrared spectrometer has been set up to evaluate the radiation from the arc. The premise is made that only the liquid or solid material in the arc will emit a black body type of radiation. The wave length versus intensity curve that is obtained from such an arc can be corrected for the emissivity of liquid iron and Wien's displacement law applied. This law states that the wave length at which a maximum intensity is obtained on the Plankian curve is simply related to the temperature. Therefore, determining the wave length at the peak of the radiation curve permits a determination of the temperature of the liquid iron. Figure 3 shows one of the first curves obtained directly from the spectrometer. (This curve has not been corrected for emissivity of iron or for absorption of the optics). In this run, most of the radiation came from the deposited metal and not from the drops in the arc stream. In future experiments, various portions of the arc will be examined.

As stated initially, this paper must be regarded as a progress report only. Further studies are continuing, particularly in the infrared range. It is hoped that this research will lead to a better understanding of the physical characteristics of the arc and will disclose information about regions therein that are important in welding.

Acknowledgment

The authors wish to express their appreciation to the Office of Ordnance Research for their financial support of this research program. They also wish to thank Ronald Henley for his analyses and suggestions and Thomas H. Hazlett for his technical and administrative assistance throughout this work.

References

1. Ornstein, L. S., *Physik. Z.*, **32**, 517 (1931).
2. Buss, G., and Finkelnberg, *Zeit. fur phy.*, **138**, 212 (1954).
3. Semenova, O. P., *Compt. rend. Acad. Sci.* (URSS), **51**, 683 (1946).
4. Saha, M. M., *Treatise on Modern Physics*, Vol. 1, Indian press, Allahabad, p. 632 (1934).
5. King, R. B., and King, A. S., *Astrophysics Jnl.*, **87**, 24 (1938).
6. Dieke and Crosswhite, *Journal of the Optical Society of America*, **33**, 425 (1943).
7. Langstroth and McRae, *Can. Jnl. Res.*, **16A**, 17 (1938).
8. Mason, R. C., ASTM STP No. 76, 29 (1948).

RESEARCH NEWS

Malleable Iron Committee Organized by WRC

At the request of the Malleable Founders' Society, the Welding Research Council has organized a committee to deal with malleable iron under the chairmanship of S. E. Kelly, Eberhard Mfg. Co.

Some of the questions which face this committee are: Shall engineers and the malleable industry sanction the welding of malleable iron and, if so, what is the recommended procedure? What rods can be used? What temperatures are safe?

At present the welding of malleable iron is generally thought to be confined to unstressed parts or to the repairs of surface defects where that surface is not subject to machining. Pronounced differences of opinion exist on this problem. Welding is successfully accomplished on nodular iron which is basically similar to malleable iron.

Acting on its own initiative the Malleable Founders' Society has launched a preliminary test program to determine the present state of the art in the welding of malleable cast iron. At a meeting of the committee to be held shortly, suggestions for future research work will be considered.

Madrid Meeting of IIW Devoted to Productivity by Welding

The public session to be held in Madrid during the annual assembly of the IIW, July 1–8, 1956, will be devoted to the subject of productivity by welding, covering such topics as welders' training, factory organization, techniques and methods of work, equipment, inspection during production, etc.

The papers will show the advantages of welded construction from the point of view of productivity but will not make any comparison of the respective advantages of the various welding processes or of the different types of equipment used in fabrication.

Because of the short time available for the public session, only a limited number of papers can be presented; provisionally the maximum number of papers to be presented by each member country has been fixed at four; however, if some countries have not submitted this number of papers by the closing date given below, it will be possible for further papers from other countries to be presented instead.

All papers submitted will be examined by a Selection Committee composed of Spanish experts who will decide on the papers to be presented and may also limit the number of those to be discussed at the public session. Authors will be informed as early as possible whether their papers have been accepted.

It has been decided that the papers shall not be read at the public session but only discussed; they will be printed before the meeting and distributed to all those who attend it.

A simultaneous interpreting service into the three languages will be available at the session.

In order to facilitate the arrangements, prospective authors are asked to send in three copies of their papers before March 15, 1956.

Further information may be obtained from, and papers should be sent to: Comision Organizadora Asamblea IIS Instituto de la Soldadura, Goya 58, Madrid.